Novel hybrid PET/MRI applications in neurocognitive disorders

Franceschi, Ana M.

UNIVERSITY OF SPLIT
SCHOOL OF MEDICINE

ANA M. FRANCESCHI, M.D.

NOVEL HYBRID PET/MRI APPLICATIONS IN NEUROCOGNITIVE DISORDERS

DOCTORAL THESIS

Split, 2021

UNIVERSITY OF SPLIT
SCHOOL OF MEDICINE

ANA M. FRANCESCHI, M.D.

NOVEL HYBRID PET/MRI APPLICATIONS IN NEUROCOGNITIVE DISORDERS

DOCTORAL THESIS

Mentor: Boris Brkljačić, M.D., Ph.D.

Split, 2021

TABLE OF CONTENTS

2. ABBREVIATIONS

PET	Positron emission tomography
FDG	Fluorodeoxyglucose
PET/CT	Positron emission tomography / computed tomography
PET/MRI	Positron emission tomography / magnetic resonance imaging
T	Tesla
VIBE	Volumetric interpolated breath-hold examination
HASTE	Half-Fourier acquisition single-shot turbo spin echo
TSE	Turbo spin echo
DWI	Diffusion weighted imaging
ADC	Apparent diffusion coefficient
STIR	Short T1 inversion recovery
MPRAGE	Magnetization Prepared Rapid Acquisition Gradient Echo
SWI	Susceptibility-weighted imaging
CCD	Crossed cerebellar diaschisis
FTD	Frontotemporal dementia
bvFTD	Behavioral variant frontotemporal dementia
svPPA	Semantic variant primary progressive aphasia
lvPPA	Logopenic variant primary progressive aphasia
agPPA	Agrammatic (nonfluent) variant primary progressive aphasia
AD	Alzheimer's disease
DLB	Dementia with Lewy bodies
CBD	Corticobasal degeneration
PSP	Progressive supranuclear palsy
k	Cohen's kappa coefficient
DBS	Deep brain stimulation
SAR	Specific absorption rate
PD	Parkinson's disease
ET	Essential tremor
STN	Subthalamic nucleus
AC-PC	Anterior commissure-posterior commissure
RF	Radiofrequency
SNR	Signal-to-noise ratio

W/kg	Watts per kilogram
DICOM	Digital Imaging and Communications in Medicine

3. OVERVIEW OF DOCTORAL THESIS RESEARCH

This doctoral thesis is based on three scientific publications:

1. **Franceschi AM**, Matthews R, Bangiyev L, Relan N, Chaudhry A, Franceschi D. Added Value of Including Entire Brain on FDG PET/MRI Body Imaging. AJR Am J Roentgenol. 2018;24:1-9. doi: 10.2214/AJR.17.18858. PMID: 29792727.

2. **Franceschi AM**, Clifton M, Naser-Tavakolian K, Ahmed O, Bangiyev L, Clouston S, Franceschi D. FDG PET/MRI for Visual Detection of Crossed Cerebellar Diaschisis in Patients With Dementia. AJR Am J Roentgenol. 2021;216(1):165-171. doi: 10.2214/AJR.19.22617. PMID: 33170738

3. **Franceschi AM**, Wiggins GC, Mogilner AY, Shepherd TM, Chung S, Lui YW. Optimized, Minimal Specific Absorption Rate MRI for High-Resolution Imaging in Patients with Implanted Deep Brain Stimulation Electrodes. AJNR Am J Neuroradiol. 2016;37(11):1996-2000. doi: 10.3174/ajnr.A4865. PMID: 27418467

3.1. INTRODUCTION

3.1.1. PET Imaging

Positron Emission Tomography (PET) is a well-established modality in the evaluation of oncology patients. The most common radiotracer used in malignancy work-up is the glucose analogy ^{18}F-fluorodeoxyglucose (FDG) which is a positron emitter with a 110-minute half-life.[1] However, PET imaging alone has several limitations including low spatial resolution and difficulty in localizing and characterizing foci of increased uptake in the setting of normal physiological uptake of in different organs. Although PET imaging detects sites of malignancy and metastatic spread, other pathological processes such as inflammation and infection can also have prominent increased FDG uptake.[2] Computed tomography (CT) was added to the PET scanner to aid in the interpretation of whole-body PET imaging, greatly improving sensitivity and specificity. There are some drawbacks of PET/CT imaging such as higher radiation exposure level and the lack of anatomic definition related to inherited low tissue resolution of CT in the head and neck, pelvis, liver, and bone marrow.[3]

3.1.2. Hybrid PET/MRI

More recently PET/MRI has emerged as another hybrid imaging modality used in the detection of malignancy. The introduction of this hybrid scanner combined the molecular and functional tissue characterization of PET scanning with the superior tissue resolution of MR imaging without added radiation. The addition of MRI was particularly useful for assessing neoplastic diseases in the brain, head and neck, musculoskeletal system, abdominal organs especially the liver, and pelvis.[4] Because of the complexities of MR imaging, different protocols are established for imaging different parts of the body, with much variation between institutions and camera manufacturers. MRI also requires organ specific radiofrequency coils used in the transmission and receiving of signal.[5] Routine FDG PET/CT imaging for oncology is performed from the base of the skull to the mid thighs, with the exception of melanoma and some other malignancies, when imaging area is from the top of the head to the feet. This was established to limit scanning timing and reduce the amount of radiation exposure.[6] Brain metastases are difficult to diagnose by both PET and CT imaging especially without dedicated PET/CT brain protocols and intravenous contrast, so imaging of the entire

brain during PET/CT scanning was not considered valuable. On the contrary, with the introduction of the PET/MRI scanner both benign and malignant brain pathology can be detected by the MR portion of the scanner that would typically not be conspicuous with the use of PET/CT, even with dedicated brain protocols.[7]

3.1.3. Brain PET in Neurocognitive Disorders

Dedicated brain PET/MRI is a relatively novel imaging modality which offers great advantages over PET/CT in the evaluation of cognitively impaired patients with suspected underlying dementia and neurodegenerative disease. Specifically, the structural MRI component offers superior soft tissue contrast, lack of radiation exposure, and more information regarding intrinsic tissue characteristics when compared to CT, therefore improving anatomic accuracy. Furthermore, PET/MR scanners with simultaneous imaging capabilities allow for PET and MR to be obtained in a single, convenient session, which allows for precise image coregistration and improved anatomic localization. Additionally, hybrid imaging such as brain PET/MRI inherently promotes a more collaborative interpretation effort among radiologists, nuclear medicine physicians, and our sub-specialized clinical colleagues due to the inherent complexity of the imaging modality and associated pathology. This collaboration encourages a multidisciplinary team approach to complex cases, especially in patients with multiple comorbidities and complex differential diagnoses.

Crossed cerebellar diaschisis (CCD) is an imaging artefact present in patients with various supratentorial insults, including cerebral infracts, traumatic brain injury, and prior surgery. These insults may result in destruction of the corticobulbar, corticopontine, and/or corticocerebellar fiber tracts. Subsequent transneural degeneration of the aforementioned white matter tracts, specifically the corticocerebellar fibers results in cerebellar parenchymal changes that are best visualized by functional PET imaging and are typically occult on structural imaging studies.[8-11] Traditionally, CCD was considered to be associated with a degree of hemiparesis on clinical exam, however, Pantano et al illustrated that CCD may also be present in patients without any hemiparetic symptoms, suggesting that destruction of the pyramidal tract alone is not sufficient for the development of CCD, nor conversely, is it its sole clinical manifestation. Furthermore, in certain cases imaging

findings of CCD were present in patients' images hours after stroke, and subsequently resolved, suggesting that in certain etiologies, there exists a window of reversibility for cerebellar diaschisis.[8]

3.1.4. Deep Brain Stimulation

Deep brain stimulation (DBS) is an effective treatment for medically refractory movement disorders including Parkinson's disease (PD), essential tremor (ET) and dystonia. Imaging plays a critical role in stereotactic targeting and long-term assessment. Preoperative MR sequences routinely used for DBS placement guidance include a high-resolution T1-weighted sequence, used to identify standard anatomical landmarks such as the anterior and posterior commissures, as well as high-resolution T2-weighted MR imaging routinely used to target the subthalamic nucleus (STN), the most common structure targeted in DBS for PD. For reasons of patient safety and to judge treatment efficacy, it can be advantageous to place bilateral leads in staged unilateral procedures. Due to the precision required for stereotaxis and the size of the anatomic structures, immediate pre-operative imaging is the standard of care. When staged procedures are employed, this necessitates imaging with one electrode in place for subsequent placement of the second electrode. Additionally, electrode-in imaging may be required to assess lead placement. Manufacturer guidelines for performing MRI with DBS in situ are extremely conservative making it challenging to acquire diagnostic and therapeutic imaging in these cases.

The recommended head specific absorption rate (SAR) limit for Medtronic DBS Systems (Medtronic USA Neuromodulation, Minneapolis, MN) is 0.1 W/kg (compared with usual normal mode which calls for SAR<3.2 W/kg). These devices are rated conditional at 1.5 Tesla. The main safety concern is heating of the electrode due to energy deposition and a few prior complications have been reported in the literature[12-14], however, Larson et al described 405 patients imaged with implanted DBS systems using a variety of different scanning protocols and their review suggests that head SAR up to 3.0 W/kg may be applied without untoward incidents.[15] Other potential interactions between MRI and implantable neuromodulators include magnetic field interactions, induced stimulation, effects on neurostimulator function and artifacts from device. In a single published paper, Sakar et al reported being able to achieve diagnostic quality within manufacturer SAR

limit using research 3D spin-echo sequences.[16] The research sequences used in that study are not universally available, and the method they used most likely underestimated the loss of signal-to-noise (SNR). There is no clear consensus in the literature as to optimal SAR and MRI parameters for safe imaging of patients with DBS electrodes.[17-20]

3.1.5. Goals of Thesis Research

At our institution, when performing whole body PET/MRI for oncology patients, we routinely include the entire head. Therefore, the aim of the first study was to characterize both PET and MRI brain findings incidentally detected on the included head portion of the study.

There is limited data evaluating the prevalence of crossed cerebellar diaschisis (CCD) in patients presenting with cognitive impairment due to suspected underlying dementia and neurodegenerative disease, and its potential impact on progression of neurodegeneration and associated symptoms, in cases when CCD is present. Hence, the second study employed hybrid ^{18}F-FDG PET/MR brain imaging to detect differences in cerebellar metabolism as well as patterns of asymmetric hypometabolism in the cerebral cortex in patients undergoing neuroimaging evaluation for clinically symptomatic cognitive impairment. We conducted a retrospective, prevalence-based assessment for crossed cerebellar diaschisis, which may further our understanding of its potential contribution to underlying neuronal demise in the various dementia subtypes.

Obtaining high-resolution brain MRI in patients with previously implanted deep brain stimulator (DBS) has been challenging and avoided by many centers due to safety concerns relating to implantable devices. Consequently, in the third study, we present our experience using a practical clinical protocol at 1.5T using two magnet systems capable of achieving pre-surgical quality imaging in patients undergoing bilateral, staged DBS insertion.

3.2. MATERIALS AND METHODS

3.2.1. Article 1. Added Value of Including Entire Brain on FDG PET/MRI Body Imaging

We identified 269 adult patients (aged 18 years or older) from September 2013 until December 2016 referred for base of skull to mid-thigh FDG PET/MRI imaging that included the entire head. PET/MR studies were performed using a 3 Tesla Biograph mMR scanner (Siemens Healthcare). PET and MRI data were acquired simultaneously using mMR body radiofrequency coils. Simultaneous PET-MR imaging was obtained about 1 hour after administration of FDG. For diagnostic MRI body sequences, we performed T1 radial VIBE with fat suppression or T1 VIBE with fat suppression in the axial orientation, followed by T2 HASTE without fat suppression in the axial plane, T2 turbo spin echo (TSE) in the coronal plane, and either diffusion weighted imaging (DWI) with apparent diffusion coefficient (ADC) maps in the axial plane or short T1 inversion recovery sequence (STIR) of the spine in the sagittal plane. All PET/MRI images of the head were reviewed by a board-certified nuclear medicine physician and a board certified neuroradiologist first individually, and then concurrently. MIM version 6.1 (MIM Software, Inc., Cleveland, Ohio) was used to perform the visual assessment of PET/MRI images. Both PET and MRI findings were noted including abnormal FDG uptake, standardized uptake value, lesion size, and MRI signal characteristics. The Student's *t*-test was used in the statistical analysis of the results. The final data are reported with the mean ± standard error and corresponding *P*-values that represent statistical significance.

3.2.2. Article 2. Visual Detection of Crossed Cerebellar Diaschisis in Dementia Patients Utilizing FDG PET/MRI

A total of 75 subjects with clinically symptomatic neurodegenerative disorders were enrolled from January 2015 to February 2019. Subjects underwent brain [F18]-FDG PET/MR imaging as part of their routine clinical work-up for cognitive impairment with standard 12-channel head coil. Emission data was collected for 20 minutes during the time in which the dedicated brain MR sequences were acquired. 3D MPRAGE image data were additionally post-processed by NeuroQuant (2019 CorTechs Labs, Inc San Diego, California) for semi-

quantitative volumetric analysis. Two neuroradiology fellowship trained board-certified radiologists independently reviewed fused PET/MRI sequences and classified each case according to subtype of neurodegenerative disease. One nuclear medicine physician with 25 years of experience in brain PET imaging reviewed the PET portion of the study with additional cortical surface map reconstructions. All three readers separately scored the supratentorial brain parenchymal FDG uptake as follows: symmetrical, asymmetrical L>R, asymmetrical R>L FDG uptake. Following supratentorial analysis, the cerebellar FDG uptake was also independently scored as symmetric versus asymmetric cerebellar uptake, and specifically, evaluated for the presence of crossed cerebellar diaschisis. Inter-reader agreement was also evaluated with Cohen's Kappa coefficient for reader 1 vs. 2, reader 1 vs. 3, and reader 2 vs. 3.

3.2.3. Article 3. Optimized, Minimal SAR MRI for High-resolution Imaging in Patients with Implanted Deep Brain Stimulation Electrodes

We retrospectively reviewed the institutional database of patients who underwent implantation of DBS electrodes between 2/1/2012-8/1/2015 using the optimized low-SAR protocol. MRI scans were obtained 1-4 weeks prior to surgery. Patients with abnormal impedance readings, broken leads or electrodes not connected to the pacemaker were excluded as free wires are potentially more hazardous. DBS devices were deactivated prior to imaging. Imaging was performed on a Siemens Avanto or Aera 1.5 Tesla magnet with circularly polarized transmit-receive head coils under general anesthesia to minimize motion. Following imaging, devices were reprogrammed and inspected by trained neuromodulation staff. The day of surgery, a stereotactic headframe (Leksell, Elekta AB, Sweden) was affixed to the head under local anesthesia and a high-resolution CT scan was performed (kV 120, mAs 325, detector configuration of 128 at 0.6mm collimation). The CT data was then fused via standard stereotactic neurosurgical software (Brainlab AG, Germany) to the MRI scans for surgical targeting. All MR images were reviewed by a board-certified neuroradiologist and a neurosurgeon specializing in neuromodulation. Images were aligned parallel to the anterior commissure-posterior commissure (AC-PC) plane; the subthalamic nucleus was assessed on the T2 images on an axial slice 4 mm below AC-PC plane (z=-4). The globus pallidus was assessed on the axial T2 slice containing the anterior and posterior commissures (z=0). Overall image quality was graded as either acceptable or not acceptable for stereotactic

surgical guidance based on consensus review. The presence of device-related artifact and any other artifacts were noted, and a comment made as to the impact on image quality. Data were extracted from the DICOM header for each patient scan regarding SAR deposition for each sequence. Comparison of SAR between magnets was made using Student's t-test with a significance level $\alpha=0.05$.

3.3. RESULTS

3.3.1. Article 1. Added Value of Including Entire Brain on FDG PET/MRI Body Imaging

Of the 269 FDG PET/MRI body imaging studies that included the entire head, there were 173 females (64%) and 96 males (36%) with a mean age of 57.4 ± 1.1 years (age range 18-89). 250 studies were for cancer assessment (91 staging, 159 restaging). There were 72 patients with breast cancer, 50 with lymphoma, 31 cervical cancers, 16 other gyneco-urological cancers, 16 colorectal cancers, 12 head and neck cancers, 9 sarcomas, 8 pancreatic cancers, 6 lung cancers, 5 multiple myelomas, and 25 other cancer assessment scans with less than 5 patients per type of cancer (Table 1). Nineteen studies were performed for non-oncologic assessment (Table2). Thirty-seven patients (13.8%) had positive brain pathology on FDG PET/MRI body sequences, with 39 total intracranial findings identified (Table 3). Males had over 3 times the number of brain findings than females (male n=23 vs. female n=14) with $p<0.001$. Two patients had two brain abnormalities, one patient with brain metastases and a chronic infarct and the second patient with radiation changes and a subacute bleed. Sixteen subjects (5.9 %) had vascular disease (average age 71±3.2 years): 8 patients had findings compatible with chronic microvascular changes, while 6 had brain infarcts in various stages (Figure 1). One patient had a chronic subdural hematoma and another patient had a partially thrombosed aneurysm (Figure 2). Nine subjects (3.3%) had post-therapy changes in the brain due to prior radiation treatment (n=2), craniotomy unrelated to cancer assessment (n=3), craniotomy with radiation therapy (n=1) and chemotherapy (n=3). Two subjects had benign cystic lesions in the brain. Twelve subjects (4.5%) had serious non-vascular brain pathology including 5 of the patients imaged for paraneoplastic syndrome evaluation which revealed leptomeningeal metastases, metabolic encephalopathy, Creutzfeldt-Jakob disease, primary cerebral lymphoma, and encephalitis. There were 5 other patients with parenchymal cerebral metastases: 3 of these patients were diagnosed more than a year prior to the PET/MRI examination, 2 patients were diagnosed 1-3 days prior to the PET/MRI, and 1 patient had quiescent brain metastatic disease initially detected on his whole-body PET/MRI examination (Figure 3). In addition, there were 2 newly diagnosed pituitary adenomas (Figure 4). Only nine subjects (3.3%) had a new neurological or cognitive symptom suggestive of brain pathology. Of these patients, 1 patient had a positive brain finding that was chronic in nature (post-craniotomy changes) that did not explain the acute symptoms while the others had either

new or recently diagnosed brain abnormalities on PET/MRI. Furthermore, 11 patients (4.1%) had a change in treatment or management as a result of the brain findings on whole-body PET/MRI, including one of the two asymptomatic pituitary tumors who was referred for neurosurgical evaluation. Of the 7 patients with malignant brain lesions (leptomeningeal metastases, cerebral metastases, and primary cerebral lymphoma), 5 had neurological symptoms although malignancy with the primary cerebral lymphoma was previously unknown. The patients with Creutzfeldt-Jakob disease, metabolic encephalopathy, and encephalitis had new neurological or cognitive symptoms with dedicated brain MRI being obtained several hours after the PET/MRI. When comparing PET with MRI findings, 38 of the 39 brain findings (97.4%) could be detected on the MR images alone. Eight of the 39 brain findings (20.5%) had abnormal areas of increased FDG uptake on the PET images indicating underlying metabolic brain abnormality. Both pituitary adenomas had intense radiotracer uptake on PET images while only one had a lesion detectable on the MRI body sequences. Three of the 5 cerebral metastases had markedly increased FDG uptake, as did the primary cerebral lymphoma case, while the leptomeningeal metastases had only subtle PET abnormalities that were difficult to detect without the fusion images. The encephalitis case had intense temporal lobe FDG uptake. Two patients had cortical hypometabolism on the PET images not related to post therapy changes, including the Creutzfeldt-Jakob case which demonstrated markedly abnormal cortical and basal ganglia uptake on the PET images with increased signal on T2 weighted images within the basal ganglia. Also, the patient with metabolic encephalopathy had globally decreased cortical FDG uptake on PET with subcortical T2 hyperintensities on the corresponding MR images. The two patients with benign cystic brain lesions and the patient with the subdural hematoma had areas of absent FDG uptake corresponding to their respective lesions on the PET portion of the study.

Table 1. PET-MRI Performed for Cancer Evaluation

Cancer Type	**N**
Breast	72
Lymphoma	50
Cervical	31

Gyneco-Urological	16
Colorectal	16
Head and Neck	12
Sarcoma	9
Pancreatic	8
Lung	6
Multiple Myeloma	5
Other Cancers	25
Total	**250**

Table 2. PET-MRI Performed for Non-Cancer Pathology

Pathology	**N**
Paraneoplastic	6
Lymphadenopathy or Soft Tissue Mass	6
Lung Nodules	4
Monoclonal Gammopathy	2
Vasculitis	1
Total	**19**

Table 3. Categories of Brain Findings

Categories of Brain Findings	**N**
Vascular	16
Post Therapy Changes	9
Parenchymal Metastases	5
Benign Cystic Lesions	2
Pituitary Adenomas	2
Creutzfeldt-Jakob disease	1
Metabolic Encephalopathy	1
Encephalitis	1
Primary CNS Lymphoma	1
Leptomeningeal Metastases	1
Total	**39**

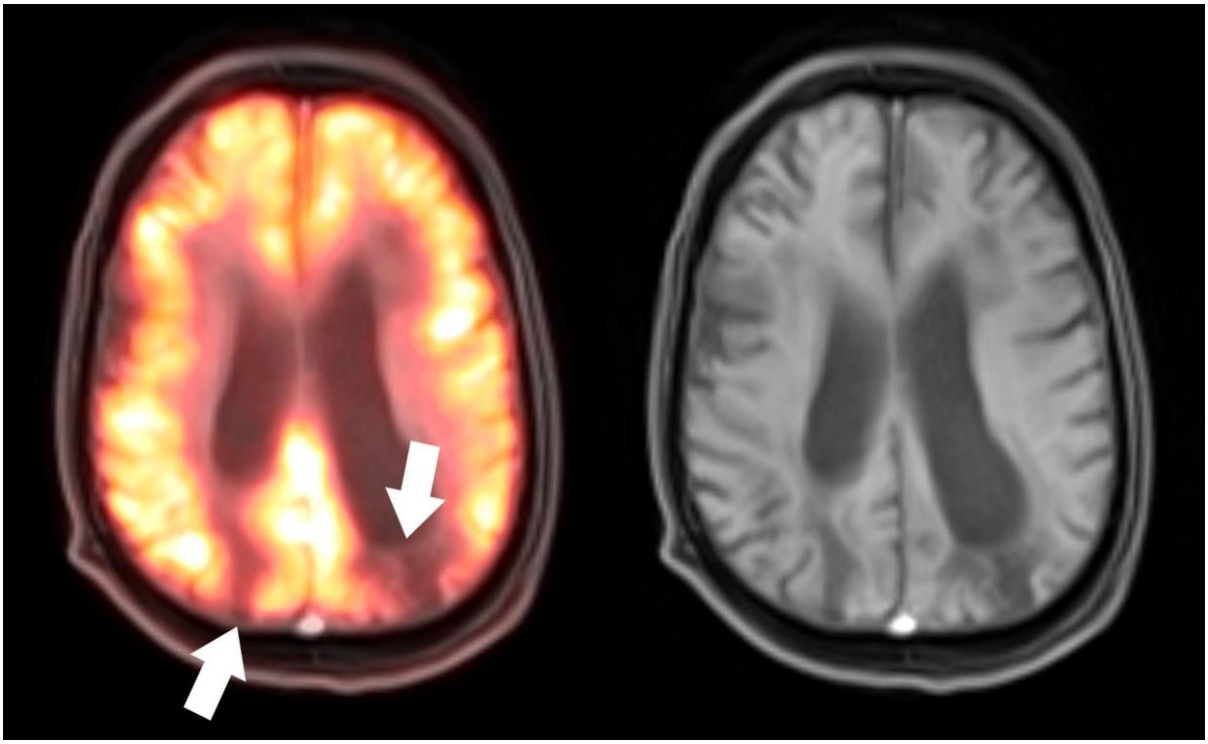

Figure 1. 55-year-old male for staging of multiple myeloma. PET/MR axial fusion image (left image) show metabolic cortical defects in the parieto-occipital region (arrows). T1 radial VIBE axial with fat suppression image (right image) show chronic middle cerebral artery / posterior cerebral artery border zone (watershed) infarcts.

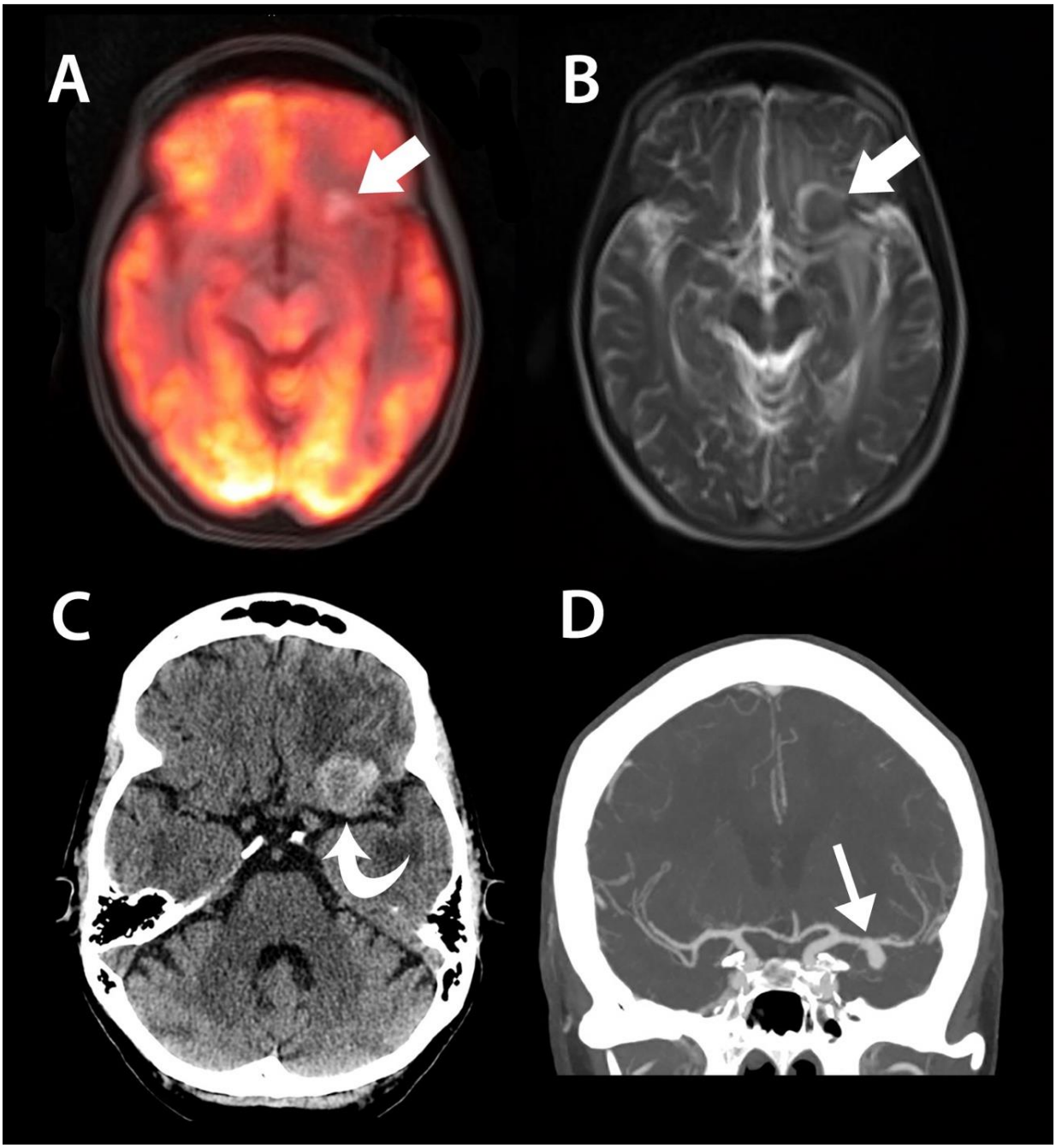

Figure 2. 64-year-old female with breast cancer and no neurological symptoms. A. PET/MR T1 fat saturated axial fusion. B. Axial T2 HASTE. C. Axial non-contrast CT head. D. CT angiogram (CTA) coronal maximum intensity projection image (MIP). There is T1 hyperintense and T2 hypointense signal within thrombosed part of the of the left middle cerebral artery aneurysm which is hyperdense on non-contrast CT head. CTA coronal MIP shows patent part of the inferiorly oriented saccular aneurysm.

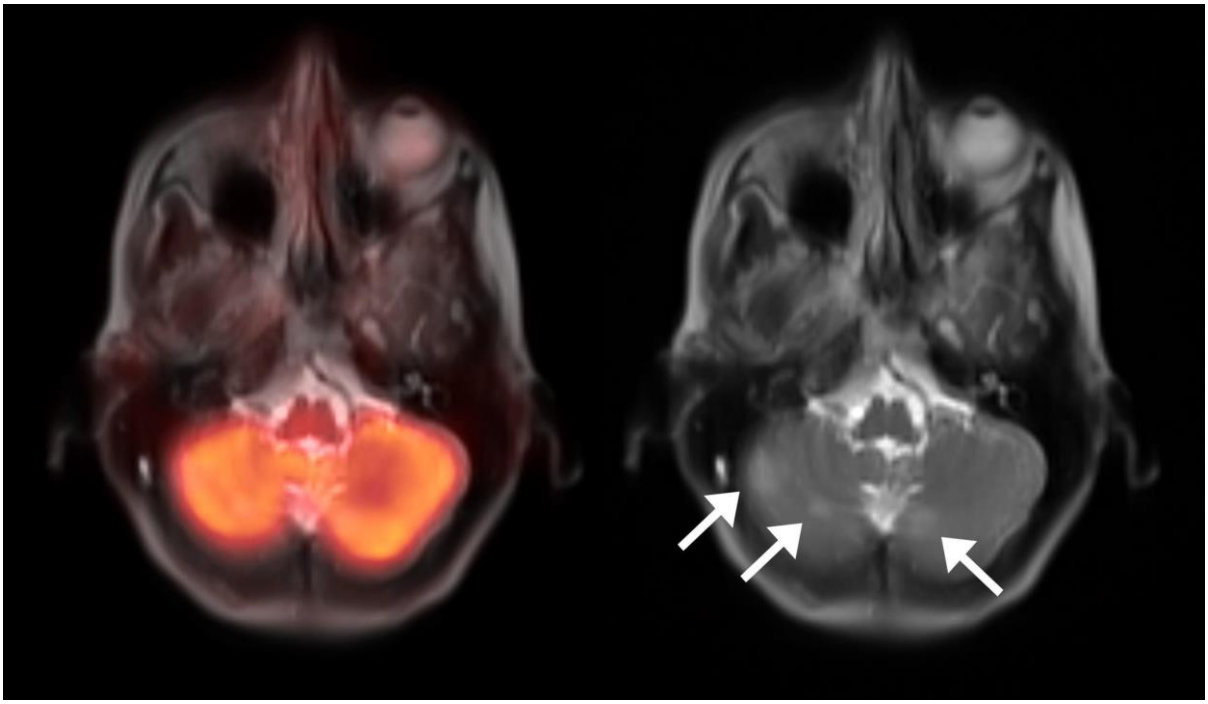

Figure 3. 54-year-old female with breast cancer with no neurological symptoms. PET/MR axial fusion image (left image) shows no abnormal focal FDG uptake within the cerebellum. T2 haste axial demonstrates 3 new foci of hyperintensity within the cerebellar hemispheres that were suspicious for metastases (thin arrows). Other cerebral suspicious lesions were seen. Follow up dedicated brain MRI confirmed multiple cerebral metastases.

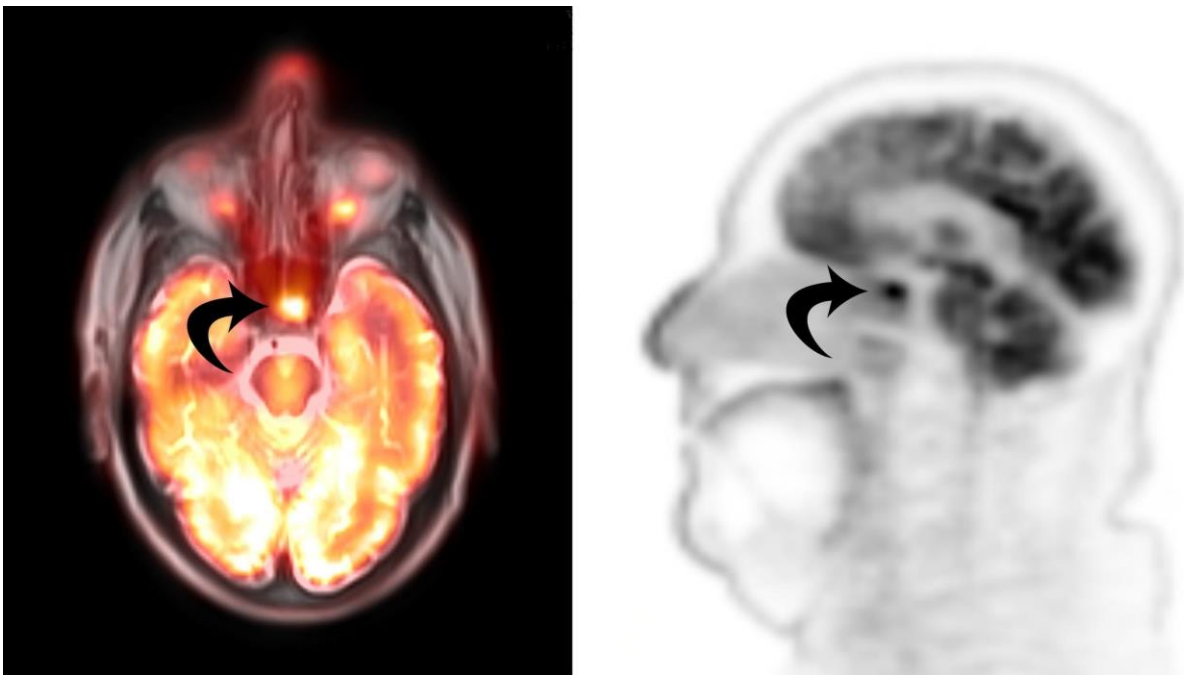

Figure 4. 79-year-old male with head and neck cancer. PET/MR fusion axial fusion image with T1 radial VIBE fat suppression (left image) and PET sagittal (right image) show an intense hypermetabolic focus representing a pituitary adenoma (curved arrows).

3.3.2. Article 2. Visual Detection of Crossed Cerebellar Diaschisis in Dementia Patients Utilizing FDG PET/MRI

Of the 75 subjects enrolled, the average age was 74 years, with 31 males and 44 females. Qualitative assessment of brain PET/MRI images revealed 19 subjects with imaging findings typical for frontotemporal dementia (FTD) as follows: 9 behavioral variant (bvFTD), 6 semantic variant primary progressive aphasia (svPPA), 3 logopenic variant primary progressive aphasia (lvPPA), and 1 agrammatic variant primary progressive aphasia (agPPA); 12 subjects with Alzheimer's disease (AD); 10 subjects with dementia with Lewy bodies (DLB); 12 subjects with corticobasal degeneration (CBD); and 2 subjects with progressive supranuclear palsy (PSP). Characteristic patterns of hypometabolism on FDG-PET and associated structural imaging findings for these dementia subtypes are outlined in Table 4. Initial inter-reader agreement in detection of asymmetric supratentorial hypometabolism in these cases is depicted in Table 5 with Cohen's Kappa coefficient for inter-reader reliability noted to be perfect agreement ($k = 1$) for all combinations of readers (1 vs. 2, 1 vs. 3, and 2 vs. 3). Ten of 75 (7.5%) subjects demonstrated hypometabolism within the cerebellar hemisphere contralateral to the side of supratentorial cortical hypometabolism, findings compatible with associated crossed cerebellar diaschisis. The underlying neurodegenerative disorders within the 10 subjects with crossed cerebellar diaschisis were as follows: 6 subjects with suspected frontotemporal dementia (specifically, three bvFTD [Figure 5], two semantic PPA, and one logopenic PPA), 3 subjects with corticobasal degeneration [Figure 6], and 1 subject with Alzheimer's disease. Initial inter-reader agreement in detection of CCD is depicted in Table 6. Inter-reader reliability was also assessed for detection of asymmetric supratentorial hypometabolism using Cohen's Kappa coefficient [Table 7].

Table 4. Brain FDG-PET Hypometabolism and Structural MRI Findings

Dementia Subtype	Regions of hypometabolism with FDG-PET	Structural MRI Findings
Behavioral Variant Frontotemporal Dementia (bvFTD)	• Frontal and anterior temporal lobes • Anterior cingulate gyrus	• Volume loss in the frontal and to a lesser degree in the temporal lobes
Semantic Variant Primary Progressive Aphasia (PPA)	• Asymmetric involvement of the temporal poles • Predilection for the left temporal lobe/pole	• Volume loss in the left > right temporal lobe (anterior > posterior) • Hippocampal atrophy (left > right)
Logopenic Variant PPA	• Left lateral temporoparietal regions • Supramarginal and angular gyri of the parietal lobe and superior temporal gyrus/temporal operculum	• Volume loss in the left temporal and parietal lobes
Agrammatic Variant PPA	• Predominant left dorsal frontal and fronto-insular	• Volume loss in the left posterior fronto-insular cortex
Alzheimer's Disease	• Bilateral parietotemporal (including precuneus) • Posterior cingulate gyrus • Mesial temporal lobe (hippocampus and entorhinal cortex)	• Volume loss in the parietotemporal (precuneus) and mesial temporal lobe
Lewy Body Dementia	• Bilateral parietotemporal and occipital • +/- basal ganglia • Symmetric mesial occipital lobe (cuneus and primary visual cortex)	• Overlap with Alzheimer's • Volume loss involving the parietotemporal and also in the occipital lobes • Highly specific sign is the Absent Swallow Tail Sign (loss of expected hyperintensity in nigrosome-1 of the substantia nigra) seen on SWI - susceptibility weighted imaging
Corticobasal Degeneration	• Asymmetric frontal, parietotemporal and occipital lobes of a single cerebral hemisphere • Asymmetric subcortical structures (ipsilateral basal ganglia, thalamus) • Asymmetric primary sensorimotor cortex	• Pronounced asymmetric volume loss in posterior frontal/parietal region of a single cerebral hemisphere (superior parietal lobule) • Asymmetric ipsilateral primary sensorimotor cortex
Progressive Supranuclear Palsy	• Paramedian frontal lobes • Anterior cingulate gyrus • Basal ganglia and midbrain	• Midbrain atrophy (Hummingbird/penguin sign, Mickey Mouse

		appearance, Morning Glory sign) • May have absent swallow tail on SWI (seen in atypical parkinsonian syndromes)

Table 5. Inter-reader agreement in detection of crossed cerebellar diaschisis

Outcome	Reader 1	Reader 2	Reader 3
Symmetric Cerebellar FDG Uptake	65	65	65
Cerebellar Diaschisis	10	10	10

Table 6. Inter-reader agreement in detection of asymmetric supratentorial hypometabolism

Outcome	Reader 1	Reader 2	Reader 3
No Asymmetry in Cortical FDG Uptake	51	37	40
L>R Hypometabolism	20	33	30
R>L Hypometabolism	4	5	5

Table 7. Inter-Reader Reliability (Cohen's Kappa Coefficient)

	Reader Agreement (%)	Cohen's Kappa Coefficient (k)
Reader 1 vs. Reader 2	81.3	0.62
Reader 1 vs. Reader 3	85.3	0.70
Reader 2 vs. Reader 3	96	0.92

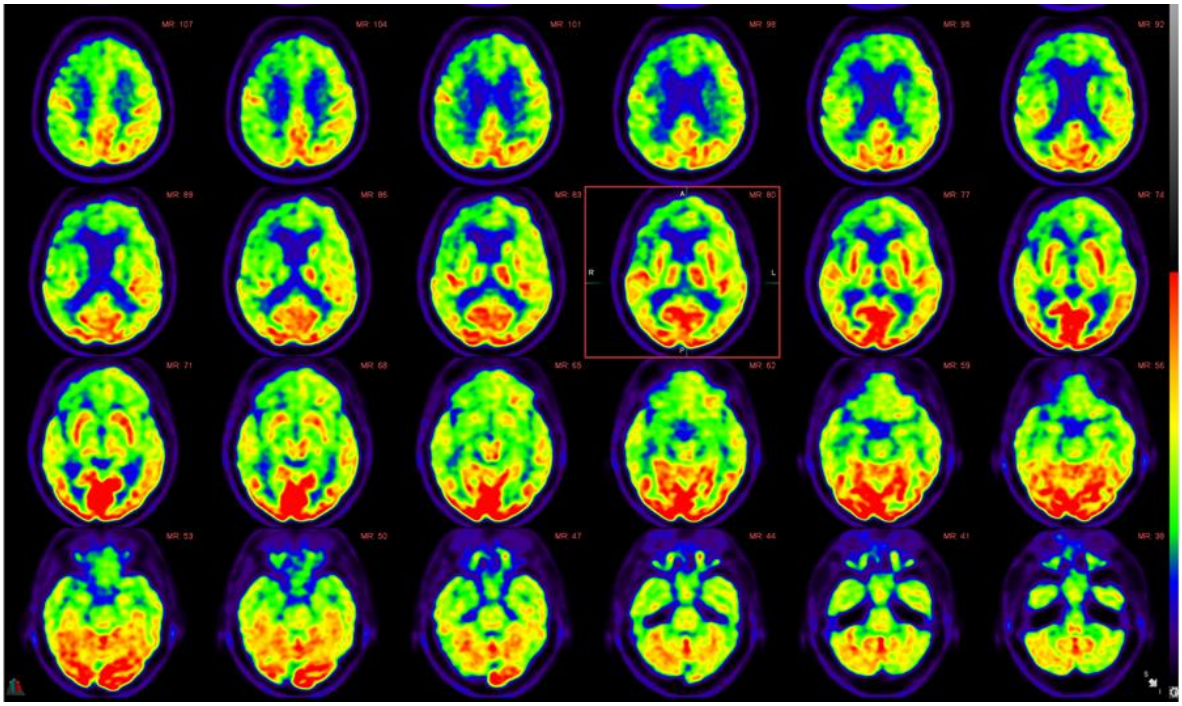

Figure 5. Serial fusion FDG-PET and FLAIR axial views of a 73-year-old female with metabolic and structural imaging findings suggestive of underlying behavioral variant frontotemporal dementia, with associated crossed cerebellar diaschisis. Specifically, there is abnormal FDG distribution pattern with significantly decreased radiotracer uptake primarily in the right frontal lobe and to a lesser degree in the right temporal lobe, including the anterior cingulate gyrus, with corresponding striking hypometabolism in the contralateral left cerebellar hemisphere, findings consistent with crossed cerebellar diaschisis.

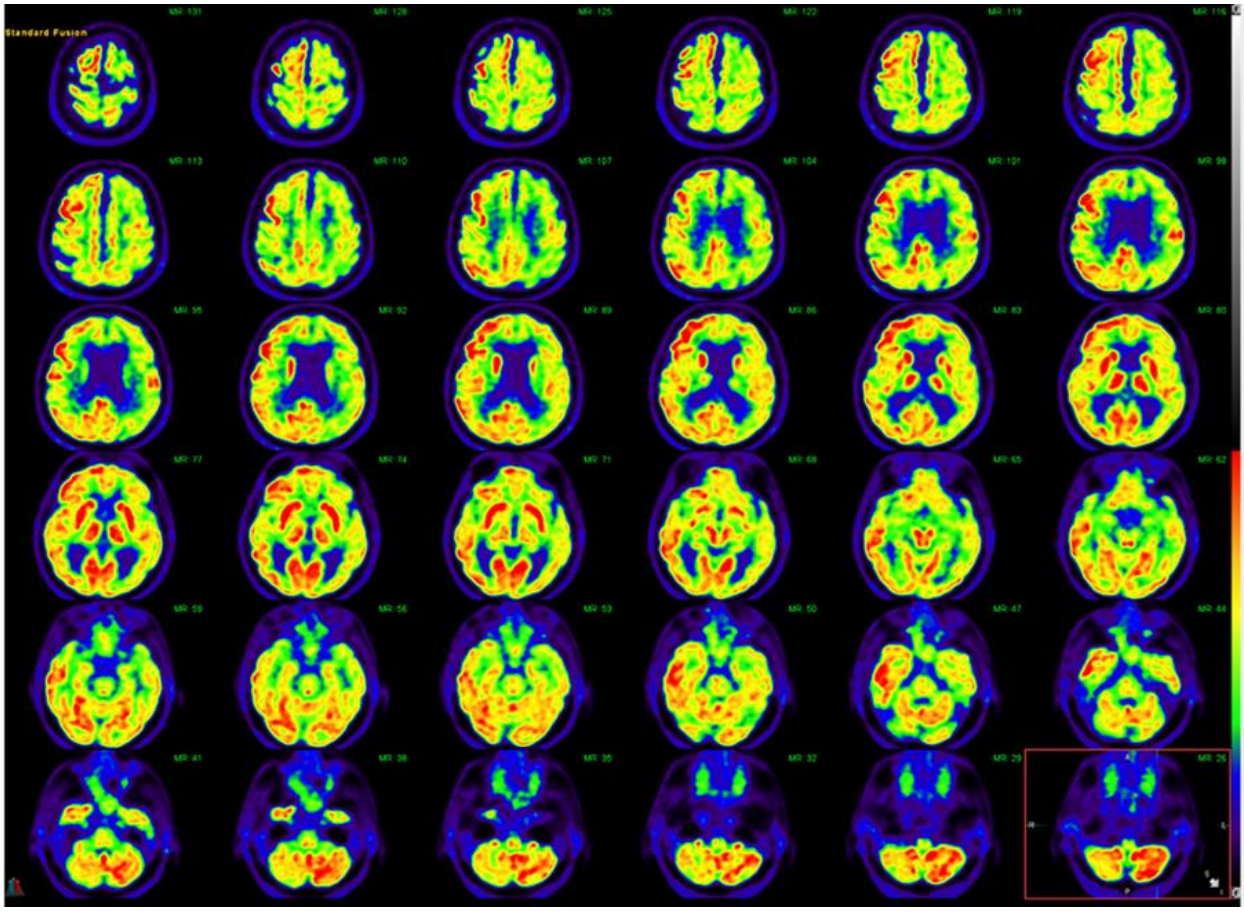

Figure 6. Serial fusion FDG-PET and FLAIR axial views of a 75-year-old male with metabolic and structural imaging findings suggestive of underlying corticobasal degeneration, with associated crossed cerebellar diaschisis. Specifically, there is abnormal FDG distribution pattern with striking supratentorial asymmetry and decreased radiotracer uptake in nearly the entire left cerebral hemisphere. Marked hypometabolism is evident particularly in the left frontoparietal region including in the left sensorimotor cortex with decreased uptake also noted in the ipsilateral left basal ganglia and left thalamus. There is corresponding hypometabolism in the contralateral right cerebellar hemisphere, findings compatible with crossed cerebellar diaschisis.

3.3.3. Article 3. Optimized, Minimal SAR MRI for High-resolution Imaging in Patients with Implanted Deep Brain Stimulation Electrodes

Twenty-nine patients (23 male / 6 female) were included in the study. Mean age was 58 (range 16-75, standard deviation 14). All subjects (22 Parkinson's disease, 6 dystonia, 1

essential tremor) had Medtronic (Minneapolis, MN) neuromodulation implants in situ (Activia PC Models No. 37601 and 37603). There were 25 subthalamic nucleus [Figure 7 and 8] and 4 globus pallidus implants; 10 patients had bilateral electrodes. Of the 29 patients, five were scanned on the Aera system and 24 on the Avanto. Average imaging time was 6 minutes 17 seconds for MPRAGE and 12 minutes and 16 seconds for T2. Average SAR deposition for MPRAGE was 0.114 ±0.021 for the Avanto system, 0.090±0.001 for the Aera system and 0.109±0.021 overall. Average SAR deposition for T2 weighted sequence was 1.037±0.214 for the Avanto system, 0.828±0.091 for the Aera system and 0.987±0.210 overall. SAR deposition for both MPRAGE and T2 weighted sequences were significantly lower on the Aera system; p=0.012 and p=0.03, respectively [Figure 9]. Four patients underwent MPRAGE imaging only, for reasons not specified upon retrospective review. All patients tolerated imaging well with successful completion of MR imaging. No clinical adverse effects were reported during or immediately after imaging. All images were deemed by consensus review to be adequate for surgical stereotaxis and were used for subsequent surgical guidance. At average follow-up time of 553 days ~ 1.5 years (range 2 – 1251 days; standard deviation 374 days), there were no adverse patient outcomes and no cases requiring lead replacement resulting directly from MRI complication. Consensus review of imaging revealed mild device-related local susceptibility artifact present in all studies and judged not to affect overall image quality required for subsequent stereotaxis [Figure 10]. Mild aliasing artifact (seen only on T1-weighted images) was present in 6/29 (21%) cases and apparent motion artifact was seen in 4/29 (14%) cases, all seen on MPRAGE sequence. No such artifacts were present on T2-weighted images.

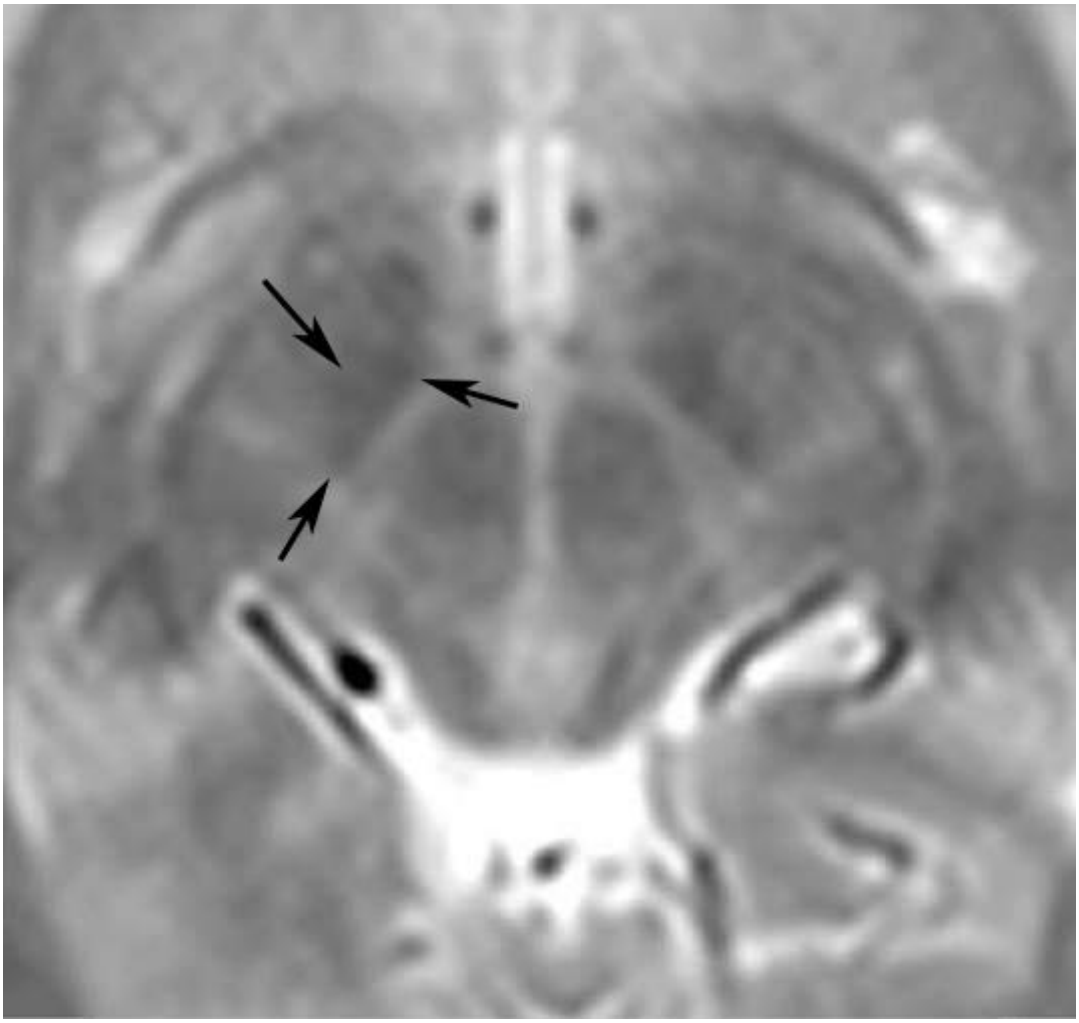

Figure 7. The smallest of the basal ganglia nuclei can be delineated on appropriate T2 weighted imaging through a region just cephalad to the midbrain. The subthalamic nucleus, a frequent target for deep brain stimulation, is outlined by arrows on the patient's right.

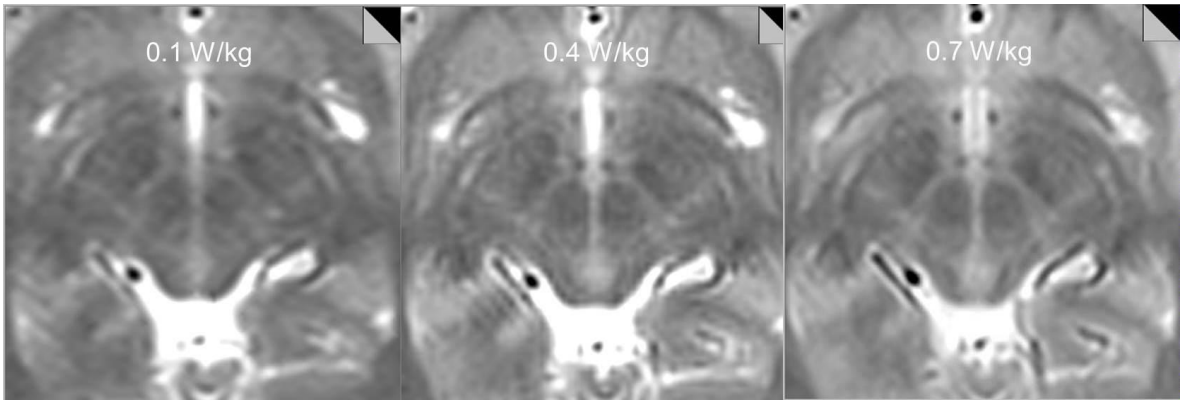

Figure 8. Tests on a volunteer subject show decreasing anatomic detail of the subthalamic region with decreasing SAR. T2-weighted images obtained with a SAR=0.1W/kg and 0.4 W/kg were deemed insufficient for stereotaxis by consensus view between neuromodulation neurosurgeon and neuroradiologist while images obtained with a SAR of 0.7W/kg were adequate for intraoperative stereotaxis.

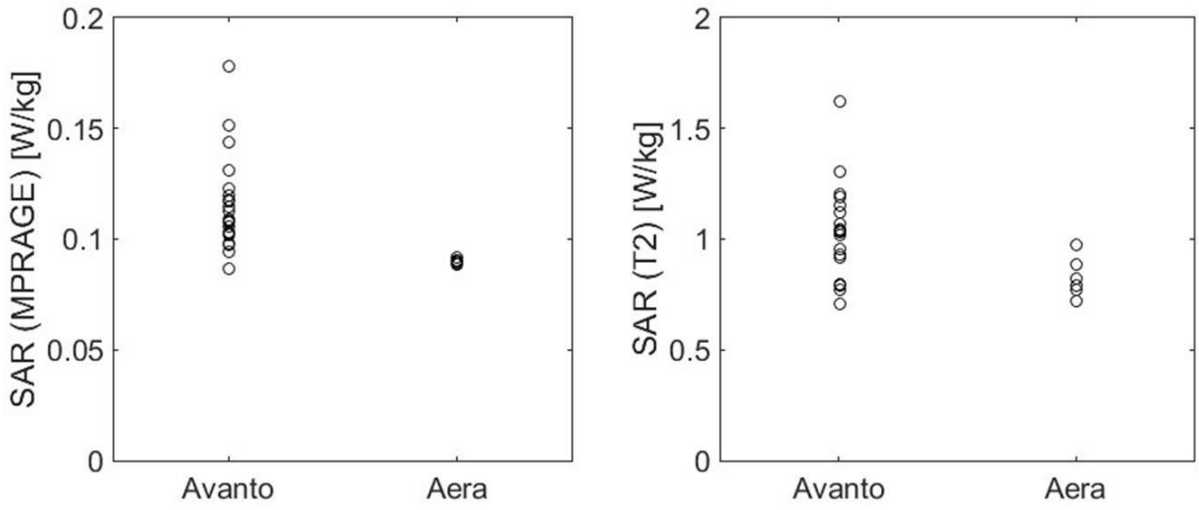

Figure 9. SAR deposition was significantly lower on the Aera system for both MPRAGE (p=0.01) (A) and T2 weighted images (p=0.03) (B). On the Aera system, all patients were imaged using SAR <1 W/kg and the SAR standard deviation was small: 0.02 and 0.09 W/kg for MPRAGE and T2 weighted images, respectively.

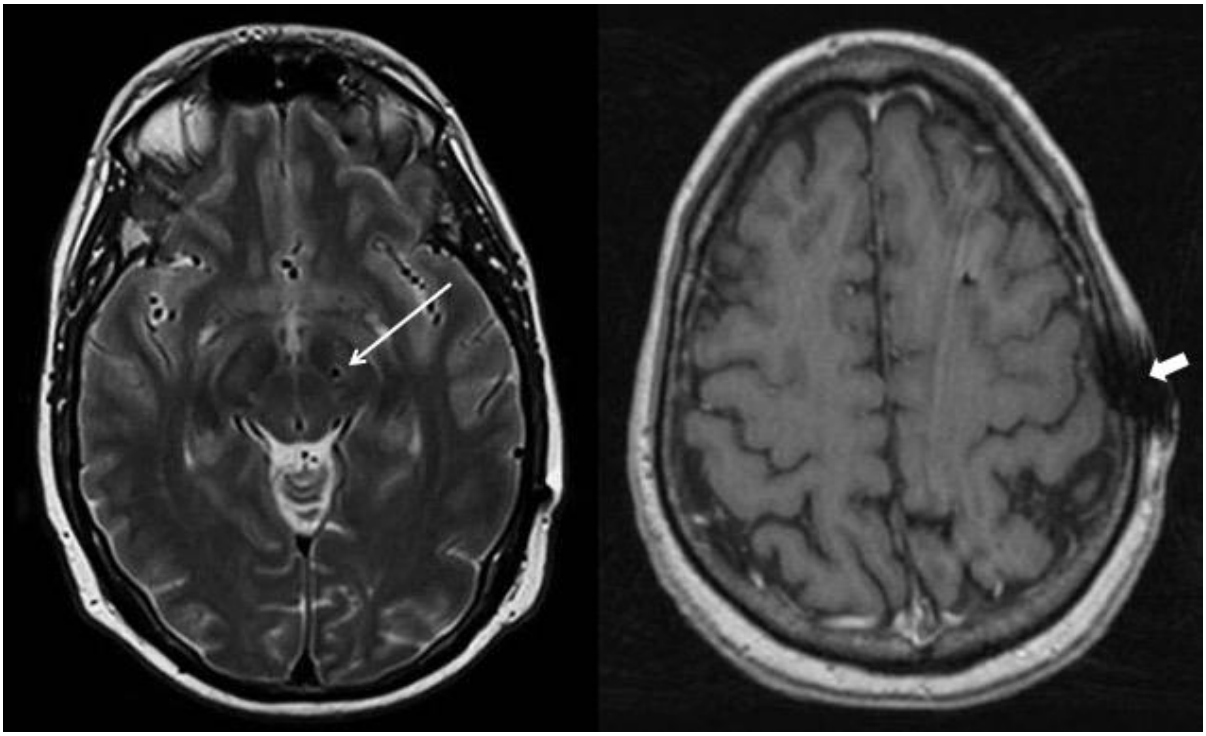

Figure 10. (A) Susceptibility from the electrode was very minimal within the adjacent brain parenchyma on T2 weighted images (arrow). (B) Device-related local susceptibility in the scalp at the site of electrode entry was seen in most cases on the MPRAGE and was felt not to affect image quality. Additionally, a minority of cases showed artifacts likely attributable to stimulated echos arising from peripheral fat on MPRAGE images only (arrowhead). Overall, all images were judged to be adequate for presurgical guidance.

3.4. SCIENTIFIC CONTRIBUTION OF THESIS RESEARCH

3.4.1. Scientific Contribution

These studies highlight the potential of hybrid PET/MRI in neuroimaging, with a special emphasis on neurocognitive disorders. Whole-body PET/MRI imaging is a rapidly evolving modality that is most commonly employed for cancer evaluation. The standardized base of skull to mid-thigh imaging may miss many important brain pathologies that are discovered incidentally using MRI body sequences. These pathologies could change patient management or alter patient prognosis. The amount of time required for the acquisition is only an additional 3-5 minutes of imaging time for the base of skull to mid-thigh scan. FDG PET/MRI whole-body scan that includes the head may show added value in the management of patients.

Furthermore, brain PET/MRI has become an indispensable tool in the assessment of dementia. Little is known about crossed cerebellar diaschisis in the context of geriatric cognitive impairment due to underlying neurodegenerative disease. Our study addresses the potential of routine assessment of cerebellar metabolism patterns as well as asymmetry in supratentorial tracer uptake in the evaluation of cognitively impaired patients undergoing hybrid PET/MR as part of dementia diagnostic efforts.

Finally, our results also demonstrate the effective use of an optimized imaging protocol balancing image quality and low SAR to scan patients with DBS implants for surgical planning. Relatively low SAR imaging is accomplished with longer imaging times, use of a low SAR radiofrequency pulse and adjustment of image resolution and is well tolerated by patients without complications.

3.4.2. Limitations

Article 1. Added Value of Including Entire Brain on FDG PET/MRI Body Imaging

In our study, the shorter 5-minute acquisition time during PET-MR imaging limits the number and quality of MRI sequences that can potentially be obtained as compared to a dedicated brain MRI study. In addition, with dedicated PET imaging of the brain there is a higher resolution matrix often 344 x 344 x 127 with longer imaging time leading to better quality images compared to 172 × 172 x 515 used on the typical body PET acquisition. Of all the cerebral lesions identified on the PET/MRI body sequences, there was a predominance of MRI findings over PET findings. In fact, all of the PET findings with the exception of the Creutzfeldt-Jakob case had corresponding abnormalities on the body MRI sequences. The MRI findings were best identified on the T2 haste sequence which had 5 mm slice thickness and was not optimized for evaluation of the brain parenchyma. The most clinically relevant findings were identified on both the PET and MRI portions of the examination. Of limitation to this study, we had a higher proportion of female patients compared to male patients. In addition, the types of indications for obtaining whole-body PET/MRI studies, especially the types of cancers imaged, vary depending on the institution and referring clinicians. Our study had a predominance of cervical cancer, breast cancer, and lymphoma which may not be reflective of cases in other institutions.

Article 2. Visual Detection of Crossed Cerebellar Diaschisis in Dementia Patients Utilizing FDG PET/MRI

In our study, the key finding in cognitively impaired patients undergoing clinical [F18]-FDG PET/MR neuroimaging as part of their routine dementia workup is an expected association of asymmetric supratentorial hypometabolism in cases with crossed cerebellar diaschisis. Previously, this imaging finding has been well documented in patients with supratentorial cerebral infarcts, traumatic brain injury and prior surgery, however, our findings indicate that crossed cerebellar diaschisis may be oftentimes present in patients presenting with underlying neurodegenerative disease. While this is the first study to effectively examine findings of crossed cerebellar diaschisis in the context of neurodegenerative disorders in a clinical setting, limitations include a relatively heterogeneous dataset, retrospective nature, and limited availability of long-term patient follow up to assess for morbidity and mortality, including

potential clinical impact of CCD-type pathology. Therefore, our future work will focus on further elucidating the impact of cerebellar diaschisis and hemispheric asymmetry on clinical presentation, neurologic and neurocognitive assessment, and disease progression in patients with neurodegenerative disease, with a special focus on the FTD subtypes and patients with corticobasal degeneration.

Article 3. Optimized, Minimal SAR MRI for High-resolution Imaging in Patients with Implanted Deep Brain Stimulation Electrodes

Of note, our results indicate significantly lower SAR for both pulse sequences on the Aera scanner compared with the Avanto scanner with lower standard deviation of SAR values which could be due to a variety of factors including coil selection. The two magnet systems have a number of differences including bore diameter, software version and coil. In our clinical practice, specifications for the Aera and Avanto magnet systems are as follows: D13 DHHS, 70cm diameter bore, CP send/receive AERA head coil with integrated Pre-amplifier: 315 mm x 475 mm x 360 mm (L x W x H) and B17, 60cm diameter bore, CP Avanto head coil with 2 integrated preamplifiers: 480mm x 330mm x 270 mm (L x W x H), respectively. SAR levels reported by different scanners can also vary for the same actual delivered energy, and this has motivated the manufacturer recent shift to using B1+rms as the safety metric for DBS implants. It is important to note that different magnets and magnet systems can effect SAR and individualized phantom scanning and testing should be done prior to clinical implementation. The primary indication for our subjects was pre-surgical targeting and electrode placement / location confirmation. One limitation of this protocol is that it may not be suitable for other indications such as assessing new or additional pathology. In fact, the protocol does not include whole brain coverage which would result in higher SAR. Furthermore, all of our scans were performed with the patient under general anesthesia thereby allowing for slightly longer scan time without motion. Scan time would certainly be a limitation for awake subjects.

3.5. SUMMARY

Novel Hybrid PET/MRI Applications in Neurocognitive Disorders

Introduction: Hybrid brain PET/MRI is a novel imaging modality which offers great advantages over PET/CT in the evaluation of neurocognitive disorders. Specifically, the structural MRI component offers superior soft tissue contrast, lack of radiation exposure, and more information regarding intrinsic tissue characteristics when compared to CT, therefore improving anatomic localization and increasing diagnostic accuracy.

Methods: We performed three retrospective studies to analyze: a) added value of including entire brain on FDG PET/MRI body imaging; b) brain FDG PET/MRI for visual detection of crossed cerebellar diaschisis in dementia patients; and c) an optimized, minimal specific absorption rate MRI for high-resolution imaging in parkinsonian patients with implanted deep brain stimulation electrodes.

Results: Of the 269 FDG PET/MRI whole-body studies, 37 patients (13.8%) had positive brain pathology, with 39 total intracranial findings identified. Of 75 dementia PET/MRIs, 10 subjects had crossed cerebellar diaschisis; of these 6 with frontotemporal dementia, 3 with corticobasal degeneration and 1 Alzheimer's disease. For 29 parkinsonism patients with DBS, average SAR deposition for MPRAGE was 0.109±0.021, with no adverse effects during or after imaging.

Conclusions: Our study results highlight the potential of hybrid PET/MRI in advanced clinical neuroimaging, with a special emphasis on patients with neurocognitive disorders.

3.6. SAŽETAK

Nove primjene hibridne PET/MR metode u neurokognitivnim poremećajima

Uvod: Hibridni PET/MR je nova slikovna metoda koja nudi značajnu prednost u odnosu na PET/CT u evaluaciji neurokognitivnih poremećaja. Posebice, strukturalna MR komponenta nudi izvrsnu kontrastnost mekotkivnih struktura, izostanak izlaganja ionizirajućem zračenju te više informacija vezano za intrinzična svojstva tkiva u usporedbi s CT-om, poboljšavajući anatomsku lokalizaciju i povećavajući dijagnostičku preciznost.

Metode: Proveli smo tri retrospektivne studije analizirajući: a) dodatnu vrijednost uključivanja čitavog mozga prigodom snimanja FDG PET/MR tijela; b) FDG PET/MR mozga za vizualnu detekciju križane cerebelarne diashize u bolesnika s demencijom te c) optimizirani minimalni specifični udio apsorpcije (*specific absorption rate*, SAR) MR kod visoko-rezolucijskih snimanja pacijenata s Parkinsonovom bolešću koji imaju ugrađene elektrode za duboku stimulaciju mozga (DSM).

Rezultati: Od 269 bolesnika uključenih u analizu FDG PET/MR cijelog tijela, 37 bolesnika (13,8%) je imalo patološke promjene mozga, dok je ukupno 39 bolesnika imalo intrakranijalnu patologiju. Od 75 bolesnika s demencijom podvrgnutih PET/MR, 10 osoba je imalo križanu cerebelarnu diashizu, od kojih je 6 imalo frontotemporalnu demenciju, 3 kortikobazalnu degeneraciju i jedna osoba Alzheimerovu bolest. Za 29 osoba oboljelih od Parkinsonove bolesti s DSM, prosječan SAR depozit na MPRAGE iznosio je 0.109±0.021, bez nuspojava tijekom ili nakon snimanja.

Zaključak: Rezultati naših istraživanja ukazuju na izuzetne mogućnosti hibridnih PET/MR metoda u naprednim kliničkim neurooslikavanjima, osobito u bolesnika s neurokognitivnim poremećajima.

3.7. REFERENCES

1. Paudyal B, Paudyal P, Oriuchi N, Tsushima Y, Nakajima T, Endo K. Clinical implication of glucose transport and metabolism evaluated by 18F-FDG PET in hepatocellular carcinoma. Int J Oncol. 2008;33(5):1047-54. PMID: 18949368.
2. Maher MM, Kalra MK, Singh A, Blake MA, Aquino SL, Fischman AJ, Mueller PR. "Hot" spots in hybrid positron emission tomography/computed tomography scanning of the abdomen: protocols, indications, interpretation, responsibilities, and reimbursements. Curr Probl Diagn Radiol. 2006;35(2):35-54. doi: 10.1067/j.cpradiol.2005.12.002. PMID: 16517288.
3. Gorospe L, Raman S, Echeveste J, Avril N, Herrero Y, Herna Ndez S. Whole-body PET/CT: spectrum of physiological variants, artifacts and interpretative pitfalls in cancer patients. Nucl Med Commun. 2005;26(8):671-87. doi: 10.1097/01.mnm.0000171779.65284.eb. PMID: 16000985.
4. Matthews R, Choi M. Clinical Utility of Positron Emission Tomography Magnetic Resonance Imaging (PET-MRI) in Gastrointestinal Cancers. Diagnostics (Basel). 2016;6(3):35. doi: 10.3390/diagnostics6030035. PMID: 27618106.
5. Rosenkrantz, AB, Friedman K, Chandarana H, Melsaether A, Moy L, Ding YS, Jhaveri, K, Beltran L, Jain, R. Current status of hybrid PET/MRI in oncologic imaging. Am AJR Am J Roentgenol. 2016;206(1):162-72. doi: 10.2214/AJR.15.14968. PMID: 26491894.
6. Niederkohr RD, Rosenberg J, Shabo G, Quon A. Clinical value of including the head and lower extremities in 18F-FDG PET/CT imaging for patients with malignant melanoma. Nucl Med Commun. 2007;28(9):688-95. doi: 10.1097/MNM.0b013e32827420cc. PMID: 17667747.
7. Deck MD, Henschke C, Lee BC, Zimmerman RD, Hyman RA, Edwards J, Saint Louis LA, Cahill PT, Stein H, Whalen JP. Computed tomography versus magnetic resonance imaging of the brain. A collaborative interinstitutional study. Clin Imaging. 1989;13(1):2-15. doi: 10.1016/0899-7071(89)90120-4. PMID: 2743188.
8. Pantano P, Baron JC, Samson Y, Bousser MG, Derouesne C, Comar D. Crossed cerebellar diaschisis. Further studies. Brain. 1986;109 (Pt 4):677-94. doi: 10.1093/brain/109.4.677. PMID: 3488093.
9. Akiyama H, Harrop R, McGeer PL, Peppard R, McGeer EG. Crossed cerebellar and uncrossed basal ganglia and thalamic diaschisis in Alzheimer's disease. Neurology. 1989;39(4):541-8. doi: 10.1212/wnl.39.4.541. PMID: 2784550.
10. Sui R, Zhang L. Cerebellar dysfunction may play an important role in vascular dementia. Med Hypotheses. 2012;78(1):162-5. doi: 10.1016/j.mehy.2011.10.017. PMID: 22075237.
11. Al-Faham Z, Zein RK, Wong CY. 18F-FDG PET assessment of Lewy body dementia with cerebellar diaschisis. J Nucl Med Technol. 2014;42(4):306-7. doi: 10.2967/jnmt.114.139295. PMID: 25190733.
12. Nutt JG, Anderson VC, Peacock JH, Hammerstad JP, Burchiel KJ. DBS and diathermy interaction induces severe CNS damage. Neurology. 2001;56(10):1384-6. doi: 10.1212/wnl.56.10.1384. PMID: 11376192.
13. Henderson JM, Tkach J, Phillips M, Baker K, Shellock FG, Rezai AR. Permanent neurological deficit related to magnetic resonance imaging in a patient with implanted deep brain stimulation electrodes for Parkinson's disease: case report.

Neurosurgery. 2005;57(5):E1063; discussion E1063. doi: 10.1227/01.neu.0000180810.16964.3e. PMID: 16284543.
14. Spiegel J, Fuss G, Backens M, Reith W, Magnus T, Becker G, Moringlane JR, Dillmann U. Transient dystonia following magnetic resonance imaging in a patient with deep brain stimulation electrodes for the treatment of Parkinson disease. Case report. J Neurosurg. 2003;99(4):772-4. doi: 10.3171/jns.2003.99.4.0772. PMID: 14567615.
15. Larson PS, Richardson RM, Starr PA, Martin AJ. Magnetic resonance imaging of implanted deep brain stimulators: experience in a large series. Stereotact Funct Neurosurg. 2008;86(2):92-100. doi: 10.1159/000112430. PMID: 18073522.
16. Sarkar SN, Papavassiliou E, Hackney DB, Alsop DC, Shih LC, Madhuranthakam AJ, Busse RF, La Ruche S, Bhadelia RA. Three-dimensional brain MRI for DBS patients within ultra-low radiofrequency power limits. Mov Disord. 2014;29(4):546-9. doi: 10.1002/mds.25808. PMID: 24442797.
17. Chhabra V, Sung E, Mewes K, Bakay RA, Abosch A, Gross RE. Safety of magnetic resonance imaging of deep brain stimulator systems: a serial imaging and clinical retrospective study. J Neurosurg. 2010;112(3):497-502. doi: 10.3171/2009.7.JNS09572. PMID: 19681685.
18. Fraix V, Chabardes S, Krainik A, Seigneuret E, Grand S, Le Bas JF, Krack P, Benabid AL, Pollak P. Effects of magnetic resonance imaging in patients with implanted deep brain stimulation systems. J Neurosurg. 2010;113(6):1242-5. doi: 10.3171/2010.1.JNS09951. PMID: 20187699.
19. Tagliati M, Jankovic J, Pagan F, Susatia F, Isaias IU, Okun MS; National Parkinson Foundation DBS Working Group. Safety of MRI in patients with implanted deep brain stimulation devices. Neuroimage. 2009;47 Suppl 2:T53-7. doi: 10.1016/j.neuroimage.2009.04.044. PMID: 19376247.
20. Rezai AR, Baker KB, Tkach JA, Phillips M, Hrdlicka G, Sharan AD, Nyenhuis J, Ruggieri P, Shellock FG, Henderson J. Is magnetic resonance imaging safe for patients with neurostimulation systems used for deep brain stimulation? Neurosurgery. 2005;57(5):1056-62; discussion 1056-62. doi: 10.1227/01.neu.0000186935.87971.2a. PMID: 16284576.

4. RESUME

ANA M. FRANCESCHI, M.D.

WORK
Lenox Hill Hospital
4F
Department of Radiology
7024
New York, NY 10075
Phone: 212.434.2900
Fax: 212.434.2945
Email: afranceschi@northwell.edu

HOME
40 East 65th Street, Apt.

New York, NY, 10065-

Phone: 631.880.8686

Citizenship: American, Croatian (EU)
Languages: English, Croatian (native)
German (conversational)

LICENSURE
ECFMG Certificate **No. 0-783-600-0**
USMLE Step 1 (May 23rd, 2011): **262/99**
Step 2 CS (December 22nd, 2010): **Pass**
Step 2 CK (December 9th, 2010): **254/99**
Step 3 (June 6th and 7th, 2012): **246/90**

ABR ID#70811 (Core Exam 2016): Pass
DR Certifying Exam 2018: Pass
Neuroradiology CAQ 2019: Pass
NYS Medical License No. 288673
AU: NYS Radioactive Materials License (RML) #5255
DEA No. FF7933408
NPI No. 1922361666

POSITIONS & APPOINTMENT
July 2019 – present
Assistant Professor - Neuroradiology, Department of Radiology, Donald and Barbara Zucker School of Medicine at Hofstra/Northwell, Manhasset, NY, USA

July 2018 – June 2019
Assistant Professor - Neuroradiology, Department of Radiology, Stony Brook University School of Medicine, Stony Brook, NY, USA

July 2013 – June 2014
Assistant Instructor, Department of Radiology, Stony Brook University School of Medicine, Stony Brook, NY, USA

EDUCATION & TRAINING

July 2017 – June 2018
Neuroradiology Fellowship, New York University School of Medicine, New York, NY, USA

July 2016 – June 2017
Hybrid Imaging: Concentration in PET/MRI, New York University School of Medicine, New York, NY, USA

July 2014 – June 2017
Radiology Residency, New York University School of Medicine, New York, NY, USA

July 2013 – June 2014
Radiology Residency, Stony Brook University Medical Center, Stony Brook, NY, USA

July 2012 – June 2013
Internship, MetroWest Medical Center / Tufts University School of Medicine, Framingham, MA, USA

July 2010 – June 2012
Research Fellowship, Department of Radiology, Massachusetts General Hospital / Harvard Medical School,
Boston, MA, USA

July 2004 – June 2010
Doctor of Medicine, University of Zagreb School of Medicine, Zagreb, Croatia (GPA 4.95 on a 2.0-5.0 scale)

RESEARCH EXPERIENCE

April 2014
Research Scholar, Neuroradiology Section, Department of Radiology, University of North Carolina at Chapel Hill School of Medicine, Chapel Hill, NC, USA

February 2013 and November 2013
Research Scholar, Neuroradiology Section, Department of Radiology, University of North Carolina at Chapel Hill School of Medicine, Chapel Hill, NC, USA

June 2011 – September 2011
Research Assistant, Ultra-high Resolution Volume CT Laboratory, Department of Radiology, Massachusetts General Hospital / Harvard Medical School, Boston, MA, USA

June 2005 – July 2010
Research Assistant, Croatian Institute for Brain Research, University of Zagreb School of Medicine, Zagreb, Croatia

CLINICAL EXPERIENCE

June 2010
Elective Course, Neuroradiology, Department of Radiology, Memorial Sloan-Kettering Cancer Center, New York, NY, USA

May 2010
Sub-internship, Clinical Medicine and Oncology, Department of Medicine, Memorial Sloan-Kettering Cancer Center, New York, NY, USA

April 2010
Sub-internship, Critical Care Medicine, Department of Anesthesiology and Critical Care Medicine, Memorial Sloan-Kettering Cancer Center, New York, NY, USA

August 2009 – September 2009
Clinical Observership, Department of Radiology, Memorial Sloan-Kettering Cancer Center, New York, NY, USA

GRANT FUNDING

- **Foundation of the American Society of Neuroradiology Boerger Research Fund for Alzheimer's Disease and Neurocognitive Disorders (Franceschi PI)**
  June 2021 – July 2022
  Principal Investigator
  Funding Amount: $75,000

"[^{18}F] PI-2620 in Primary Progressive Aphasia"
Aim of this study is to characterize the biodistribution of abnormal tau accumulation in the three
subtypes of primary progressive aphasia using the novel second generation tracer PI-2620 and correlate these findings with clinical disease severity and neurodegeneration.

- **NIH R01 AG049953 (Clouston PI)**
  May 2015 – January 2026
  Co-investigator, 5-10% effort
  Funding Amount: $437,371

"A Life Course Approach to Integrating Trauma and Cognitive Aging: A Cohort of 9/11 Responders"
Study examining PTSD and World Trade Center (WTC) exposures as risk factors for cognitive dysfunction and decline alongside changes in ß-amyloid, tau, and neurodegeneration utilizing simultaneous PET/MRI in a prospective cohort of 9-11 responders.

- **ACR Innovation Fund (Bruno PI)**
  February 2019 – January 2020
  Co-investigator, 2-3% effort
  Funding Amount: $94,122

"Enhancing the Effectiveness of Clinical Decision Support by Understanding the Drivers of Clinician Resistance"
Project designed to understand and overcome pervasive cultural, organizational and individual drivers of physician resistance to acceptance and utilization of point-of-care clinical decision support (CDS) using ACR resources (ACR Care Select Imaging and R-SCAN), online interactive modules, surveys, focus groups and structured interviews in

multiple practice settings across the nation.

HONORS &AWARDS

- ASNR Education Exhibit Awards Summa Cum Laude – May 2021
- AJNR Reviewer Recognition – December 2017
- Minnies Scientific Paper of the Year Semifinalist – August 2017
- RSNA Student Travel Stipend – November 2016
- JMRI Certificate of Appreciation – May 2016
- AJNR Reviewer Recognition – December 2015
- UUP Individual Development Award – May 2014
- Best of AHA Specialty Conferences: ISC 2012 – June 2012
- Excellence in Pathophysiology Award – February 2007
- Academic Scholarship of the City of Zagreb – October 2006
- National Academic Scholarship of Croatia – October 2005
- Dean's Award for Excellence – December 2005

SPECIAL RECOGNITION

- AJR InBrief newsletter "Added Value of Including Entire Brain on Body Imaging with FDG PET/MRI" - July 2018
- Health Imaging newsletter "PET/MRI body imaging with full head scan identifies severe brain abnormalities" - May 2018
- Radiology Business newsletter "PET/MRI with full head scan catches more brain abnormalities than standard protocol" - May 2018
- SNMMI SmartBrief Top Story newsletter "FDG-PET/MRI with head scan detects additional abnormalities" - May 2018
- SNMMI SmartBrief Top Story newsletter "FDG-PET/MRI head scans detect incidental brain findings in cancer" - December 2016
- AuntMinnie.com RSNA 2016 News - Top 10 list newsletter "PET/MRI head scans reveal important incidental findings" - November 2016
- AuntMinnie.com RSNA Preview for Molecular Imaging newsletter "A 'heads-up' PET/MRI strategy recommended for cancer patients" - November 2016
- ARRS InPractice Insight Monthly newsletter "Utility of Susceptibility-weighted Imaging for Brain Metastases from Melanoma and Breast Cancer"- April 2014

INVITED LECTURES

- Grand Rounds, Department of Radiology, Dartmouth-Hitchcock Medical Center, Lebanon, NH, USA – November 2021
- Faculty Speaker, 4th Croatian Neuroradiological Meeting with International Participation, Srebreno, Mlini, Croatia – October 2021
- Guest Professor, Department of Radiology, University Hospital Split, School of Medicine at the University of Split, Split, Croatia – September 2021
- Grand Rounds, Department of Radiology, MetroHealth Medical Center, Case Western Reserve University School of Medicine, Cleveland, OH, USA – August 2021
- Faculty Speaker, American Society of Neuroradiology Alzheimer's Webinar Series, Virtual Platform – August 2021
- Guest Speaker, Neuroimaging in Health and Disease Seminar, Mallinckrodt Institute of Radiology, Washington University School of Medicine in St. Louis, MO, USA – August 2021

- Guest Speaker, Department of Radiology, Division of Nuclear Medicine and Molecular Imaging, The Johns Hopkins School of Medicine, Baltimore, MD, USA – June 2021
- Faculty Speaker, Society of Nuclear Medicine and Molecular Imaging, Virtual Platform – June 2021
- Guest Speaker, Neuropsychology Section, Department of Neurology, Donald and Barbara Zucker School of Medicine at Hofstra/Northwell, Manhasset, NY, USA – June 2021
- Grand Rounds, Department of Radiology and Biomedical Imaging, Yale School of Medicine, New Haven, CT, USA – May 2021
- Grand Rounds, Department of Radiology, University of Iowa Carver College of Medicine, Iowa City, IA, USA – April 2021
- Faculty Speaker, American Society of Functional Neuroradiology Presents Neuro PET-MR, Virtual Platform – April 2021
- Grand Rounds, Department of Neurosciences, New York-Presbyterian Brooklyn Methodist Hospital, Brooklyn, NY, USA – March 2021
- Guest Speaker, Neuropsychology Section, Department of Neurology, Donald and Barbara Zucker School of Medicine at Hofstra/Northwell, Manhasset, NY, USA – February 2021
- Grand Rounds, Department of Neurology, Donald and Barbara Zucker School of Medicine at Hofstra/Northwell, Manhasset, NY, USA – January 2021
- Grand Rounds, Department of Radiology, University of North Carolina at Chapel Hill School of Medicine, Chapel Hill, NC, USA – November 2020
- Guest Professor, Neuropsychology Section, Department of Neurology, Stony Brook University School of Medicine, Stony Brook, NY, USA – August 2020
- Faculty Speaker, Eastern Neuroradiological Society, Virtual Platform – August 2020
- Visiting Professor, Department of Radiology, Penn State Health Milton S. Hershey Medical Center, Hershey, PA, USA – August 2020
- Grand Rounds, Department of Radiology, University of Iowa Carver College of Medicine, Iowa City, IA, USA – August 2020
- Visiting Professor, Department of Radiology, Penn State Health Milton S. Hershey Medical Center, Hershey, PA, USA – July 2020
- Grand Rounds, Department of Radiology, University of Connecticut School of Medicine, Farmington, CT, USA – July 2020
- Grand Rounds, Division of Nuclear Medicine, Department of Radiology, Mount Sinai Icahn School of Medicine, New York, NY, USA – July 2020
- Guest Speaker, Memory and Movement Disorders conference, Division of Molecular Imaging and Therapeutics, Department of Radiology, Weill Cornell Medicine, New York, NY, USA – January 2020
- Guest Professor, Neuropsychology Section, Department of Neurology, Stony Brook University School of Medicine, Stony Brook, NY, USA – October 2019
- Faculty Speaker, American Society of Functional Neuroradiology, San Francisco, CA, USA – September 2022
- Guest Professor, Department of Radiology, University Hospital Dubrava, School of Medicine at the University of Zagreb, Zagreb, Croatia – June 2019
- Honorary Lecture, International Symposium program of the American Society of Neuroradiology (ASNR) and the Annual International Diagnostic Imaging Conference, National Congress of the Association of Radiologists of Ukraine

(ARU), Kyiv, Ukraine – March 2019
- Fellow Grand Rounds, Neuroradiology, Department of Radiology, New York University School of Medicine, New York, NY, USA – February 2018
- Guest Speaker, Department of Radiology, Stony Brook University Medical Center, Stony Brook, NY, USA – November 2017
- Fellow Grand Rounds, Neuroradiology, Department of Radiology, New York University School of Medicine, New York, NY, USA – September 2017
- Guest Speaker, International Rad-Path Correlation Conference, New York University School of Medicine, New York, NY, USA – August 2017
- Guest Professor, Department of Biomedical Imaging and Image-guided Therapy, Medical University of Vienna, Vienna General Hospital, Austria – November 2015
- Guest Speaker, Center for Understanding Biology using Imaging Technology (CUBIT), Stony Brook University School of Medicine, Stony Brook, NY, USA – May 2014

PROFESSIONAL ACTIVITIES

- Member, Data and Safety Monitoring Board, National Institutes of Health - National Institute of Neurological Disorders and Stroke, September 2021 - present
- Chair, Biogen-sponsored SNMMI 2021 Brain PET Imaging Symposium, June 2021
- Northwell Dementia Steering Committee, Donald and Barbara Zucker School of Medicine at Hofstra/Northwell, Manhasset, NY, May 2021 - present
- International Collaborations Committee, ASNR American Society of Neuroradiology, May 2021 - present
- Course Director, Dementia Board - Continuing Medical Education (CME) Course, Donald and Barbara Zucker School of Medicine at Hofstra/Northwell, Manhasset, NY, February 2021 - present
- Reviewer, MOME – Molecular Medicine, December 2020 - present
- Editorial Board, World Journal of Nuclear Medicine, July 2020 – present
- Editorial Board, AJNR American Journal of Neuroradiology, July 2020 - present
- Reviewer, WJNM – World Journal of Nuclear Medicine, July 2020 - present
- Research Committee, ASNR American Society of Neuroradiology, June 2020 - present
- Admissions Committee, Donald and Barbara Zucker School of Medicine at Hofstra/Northwell, Manhasset, NY, May 2020 - present
- Research Committee, ASFNR American Society of Functional Neuroradiology, November 2019 - present
- Abstract Review Committee, ASNR American Society of Neuroradiology, August 2019 - present
- Functional/Non-anatomic Imaging Scientific Subcommittee, XXII Symposium Neuroradiologicum, April 2019 - present
- Education Exhibit Awards Committee: Molecular Imaging, RSNA Radiological Society of North America, April 2019 - present
- Abstract Review Subcommittee for Neuroradiology, ARRS American Roentgen Ray Society, August 2018 - January 2020
- Admissions Committee, Medical Scientist Training Program (MD/PhD, MSTP), Stony Brook University Renaissance School of Medicine, Stony Brook, NY, USA, July 2018 - June 2019
- Teaching Atlas of PET/MR Neuroimaging, Department of Radiology,

Neuroradiology section, New York University School of Medicine, New York, NY, USA, June 2018
- Monthly Column, Healio HemOnc Today: Imaging Analysis, April 2017 - May 2019
- Reviewer, JMRI – Journal of Magnetic Resonance Imaging, May 2015 - present
- Reviewer, AJNR – American Journal of Neuroradiology, May 2015 - present
- House Staff Patient Safety Council Committee, New York University School of Medicine, New York, NY, August 2014 - June 2015
- Graduate Medical Education Committee, Stony Brook University Medical Center, Stony Brook, NY, September 2013 - June 2014
- Patient Education Committee, Tufts University School of Medicine - MetroWest Medical Center, Framingham, MA, August 2012 - June 2013

SOCIETY MEMBERSHIP

- WARMTH – World Association of Radiopharmaceutical and Molecular Therapy, Oct 2020 – present
- ASFNR – American Society of Functional Neuroradiology, May 2019 – present
- ACR – American College of Radiology, September 2013 – present
- ASNR – American Society of Neuroradiology, July 2013 – present
- ASHNR – American Society of Head and Neck Radiology, July 2013 – present
- ENRS – Eastern Neuroradiological Society, July 2013 – present
- ARRS –American Roentgen Ray Society, July 2013 –present
- RSNA – Radiological Society of North America, June 2011 – present
- SNMMI – Society of Nuclear Medicine and Molecular Imaging, June 2011 – present
- AMA – American Medical Association, August 2011 – present

PUBLISHED WORK

EDITOR (TEXTBOOK)

1. **Franceschi AM**, Franceschi D, Editors. Hybrid PET/MR Neuroimaging: A Comprehensive Approach. Springer Nature. (in press)

BOOK CHAPTERS

1. Sosa MS, **Franceschi AM**, Huang C. Quantitative PET Analysis. In: Franceschi **AM**, Franceschi D, Editors. Hybrid PET/MR Neuroimaging: A Comprehensive Approach. Springer Nature. (in press)

2. Roytman M, Gordon ML, **Franceschi AM**. Alzheimer's Disease. In: Franceschi AM, Franceschi D, Editors. Hybrid PET/MR Neuroimaging: A Comprehensive Approach. Springer Nature. (in press)

3. Gordon ML, **Franceschi AM**. Semantic Variant Primary Progressive Aphasia. In: Franceschi **AM**, Franceschi D, Editors. Hybrid PET/MR Neuroimaging: A Comprehensive Approach. Springer Nature. (in press)

4. Roytman M, Gordon ML, **Franceschi AM**. Agrammatic Variant Primary Progressive Aphasia. In: Franceschi AM, Franceschi D, Editors. Hybrid PET/MR Neuroimaging:

A Comprehensive Approach. Springer Nature. (in press)

5. Niethammer M, **Franceschi AM**. Parkinson's Disease. In: Franceschi AM, Franceschi D, Editors. Hybrid PET/MR Neuroimaging: A Comprehensive Approach. Springer Nature. (in press)

6. Jain V, **Franceschi AM**. Orbital Pathology. In: Franceschi AM, Franceschi D, Editors. Hybrid PET/MR Neuroimaging: A Comprehensive Approach. Springer Nature. (in press)

7. Jain V, Ahmed O, Agarwal M, **Franceschi AM**. Salivary Gland Pathology In: Franceschi AM, Franceschi D, Editors. Hybrid PET/MR Neuroimaging: A Comprehensive Approach. Springer Nature. (in press)

8. Clifton M, Naser-Tavakolian K, **Franceschi AM**. Crossed Cerebellar Diaschisis. In: Franceschi AM, Franceschi D, Editors. Hybrid PET/MR Neuroimaging: A Comprehensive Approach. Springer Nature. (in press)

9. **Franceschi AM**, Bangiyev L. Normal Pressure Hydrocephalus. In: Gupta R, Matthews R, Bangiyev L, Franceschi D, Schweitzer M, editors. PET/MR Imaging: A Case-Based Approach. Springer International Publishing, 2018. Print ISBN: 978-3-319-65105-7. Online ISBN: 978-3-319-65106-4. DOI: 10.1007/978-3-319-65106-4.

10. **Franceschi AM**. Frontotemporal Dementia. In: Gupta R, Matthews R, Bangiyev L, Franceschi D, Schweitzer M, editors. PET/MR Imaging: A Case-Based Approach. Springer International Publishing, 2018. Print ISBN: 978-3-319-65105-7. Online ISBN: 978-3-319-65106-4. DOI: 10.1007/978-3-319-65106-4.

11. **Franceschi AM**, Matthews R. Dural Metastases. In: Gupta R, Matthews R, Bangiyev L, Franceschi D, Schweitzer M, editors. PET/MR Imaging: A Case-Based Approach. Springer International Publishing, 2018. Print ISBN: 978-3-319-65105-7. Online ISBN: 978-3-319-65106-4. DOI: 10.1007/978-3-319-65106-4.

12. **Franceschi AM**, Hoch MJ, Shepherd TM. Dementia with Lewy Body. In: Gupta R, Matthews R, Bangiyev L, Franceschi D, Schweitzer M, editors. PET/MR Imaging: A Case-Based Approach. Springer International Publishing, 2018. Print ISBN: 978-3-319-65105-7. Online ISBN: 978-3-319-65106-4. DOI: 10.1007/978-3-319-65106-4.

13. **Franceschi AM**, Hoch MJ, Shepherd TM. Creutzfeldt-Jakob Disease. In: Gupta R, Matthews R, Bangiyev L, Franceschi D, Schweitzer M, editors. PET/MR Imaging: A Case-Based Approach. Springer International Publishing, 2018. Print ISBN: 978-3-319-65105-7. Online ISBN: 978-3-319-65106-4. DOI: 10.1007/978-3-319-65106-4.

14. Hoch MJ, **Franceschi AM**, Shepherd TM. Posterior Cortical Atrophy. In: Gupta R, Matthews R, Bangiyev L, Franceschi D, Schweitzer M, editors. PET/MR Imaging: A Case-Based Approach. Springer International Publishing, 2018. Print ISBN: 978-3-319-65105-7. Online ISBN: 978-3-319-65106-4. DOI: 10.1007/978-3-319-65106-4.

15. **Franceschi AM**, Matthews R. Amyloid Plaques in Alzheimer's Disease. In: Gupta R, Matthews R, Bangiyev L, Franceschi D, Schweitzer M, editors. PET/MR Imaging: A

Case-Based Approach. Springer International Publishing, 2018. Print ISBN: 978-3-319-65105-7. Online ISBN: 978-3-319-65106-4. DOI: 10.1007/978-3-319-65106-4.

16. Hoch MJ, **Franceschi AM**, Shepherd TM. Crossed Cerebellar Diaschisis. In: Gupta R, Matthews R, Bangiyev L, Franceschi D, Schweitzer M, editors. PET/MR Imaging: A Case-Based Approach. Springer International Publishing, 2018. Print ISBN: 978-3-319-65105-7. Online ISBN: 978-3-319-65106-4. DOI: 10.1007/978-3-319-65106-4.

17. Franceschi AM, Hoch MJ, Shepherd TM. Mesial Temporal Lobe Sclerosis. In: Gupta R, Matthews R, Bangiyev L, Franceschi D, Schweitzer M, editors. PET/MR Imaging: A Case-Based Approach. Springer International Publishing, 2018. Print ISBN: 978-3-319-65105-7. Online ISBN: 978-3-319-65106-4. DOI: 10.1007/978-3-319-65106-4.

18. Hoch MJ, **Franceschi AM**, Shepherd TM. Oligodendroglioma. In: Gupta R, Matthews R, Bangiyev L, Franceschi D, Schweitzer M, editors. PET/MR Imaging: A Case-Based Approach. Springer International Publishing, 2018. Print ISBN: 978-3-319-65105-7. Online ISBN: 978-3-319-65106-4. DOI: 10.1007/978-3-319-65106-4.

19. Franceschi AM, Hoch MJ, Shepherd TM. Alzheimer's Disease. In: Gupta R, Matthews R, Bangiyev L, Franceschi D, Schweitzer M, editors. PET/MR Imaging: A Case-Based Approach. Springer International Publishing, 2018. Print ISBN: 978-3-319-65105-7. Online ISBN: 978-3-319-65106-4. DOI: 10.1007/978-3-319-65106-4.

20. Franceschi AM. Warthin Tumor. In: Gupta R, Matthews R, Bangiyev L, Franceschi D, Schweitzer M, editors. PET/MR Imaging: A Case-Based Approach. Springer International Publishing, 2018. Print ISBN: 978-3-319-65105-7. Online ISBN: 978-3-319-65106-4. DOI: 10.1007/978-3-319-65106-4.

21. Franceschi AM, Bangiyev L. Recurrent Salivary Gland Cancer. In: Gupta R, Matthews R, Bangiyev L, Franceschi D, Schweitzer M, editors. PET/MR Imaging: A Case-Based Approach. Springer International Publishing, 2018. Print ISBN: 978-3-319-65105-7. Online ISBN: 978-3-319-65106-4. DOI: 10.1007/978-3-319-65106-4.

22. Franceschi AM, Matthews R. Recurrent Prostate Cancer with Fluciclovine. In: Gupta R, Matthews R, Bangiyev L, Franceschi D, Schweitzer M, editors. PET/MR Imaging: A Case-Based Approach. Springer International Publishing, 2018. Print ISBN: 978-3-319-65105-7. Online ISBN: 978-3-319-65106-4. DOI: 10.1007/978-3-319-65106-4.

23. Franceschi AM, Matthews R. Prostate Cancer with F-18 Sodium Fluoride. In: Gupta R, Matthews R, Bangiyev L, Franceschi D, Schweitzer M, editors. PET/MR Imaging: A Case-Based Approach. Springer International Publishing, 2018. Print ISBN: 978-3-319-65105-7. Online ISBN: 978-3-319-65106-4. DOI: 10.1007/978-3-319-65106-4.

24. Kallianos K, **Franceschi AM**, Carr JR, Mehan WA, Johnson JM. CT of the Carotid Arteries. In: Trivedi R, Saba L, Suri JS, editors. 3D Imaging Technologies in Atherosclerosis. Springer Science+Business Media LLC New York, 2015. ISBN: 978-1-4899-7617-8. ISBN (eBook): 978-1-4899-7618-5. DOI: 10.1007/978-1-4899-7618-5.

25. Franceschi AM, Johnson JM. Bisphosphonates. In: Ginat DT, Small JE, Schaefer

PW, editors. Neuroimaging Pharmacopeia. Springer International Publishing Switzerland, 2015. ISBN: 978-3-319-12714-9. DOI: 10.1007/978-3-319-12715-6.

26. Franceschi AM, Pina S, Castillo M. Parkinson's Disease: Clinical and Imaging Features. In: Saba L, editor. Imaging of Neurodegenerative Disorders. Oxford University Press New York, 2015. ISBN: 978-0-19-967161-8. DOI: 10.1093/med/9780199671618.001.0001.

PUBLICATIONS

1. Pederson C, Aboian M, McConathy JE, Daldrum-Link H, **Franceschi AM.** PET/MRI in Pediatric Neuroimaging: Primer for Clinical Practice. Am J Neuroradiol. (in press)

2. Roytman M, Chiang GC, Gordon ML, **Franceschi AM**. Multi-modality Imaging in Primary Progressive Aphasia. AJNR Am J Neuroradiol. (in press)

3. Bruno MA, Fotos JS, Pitot M, **Franceschi AM**, Neutze JA, Willis MH, Wasserman E, Snyder BL, Cruciata G, Stuckey S, Wintermark M. What Factors Drive Resistance to Clinical Decision Support? Finding Inspiration in Radiology 3.0^{TM}. Journal of the American College of Radiology (in press)

4. Kritikos M, **Franceschi AM**, Vaska P, Clouston SAP, Huang C, Salerno M, Deri Y, Tang C, Pellechia A, Santiago-Michels S, Sano M, Bromet EJ, Lucini RG, Gandy S Luft BJ. Assessment of Alzheimer's Disease Imaging Biomarkers in World Trade Center Responders with Cognitive Impairment at Midlife. World Journal of Nuclear Medicine. (in press)

5. **Franceschi AM**, Matthews R, Ahmed O, Mourtzikos K, Bajc M, Franceschi D. Extensive Non-Segmental Pulmonary Perfusion Defects on SPECT/CT: An Early Sign of COVID-19 Infection. World Journal of Nuclear Medicine. (in press)

6. **Franceschi AM**, Naser-Tavakolian K, Clifton M, Bangiyev L, Cruciata G, Clouston S, Franceschi D. Metabolic positron-emission tomography/magnetic resonance imaging in primary progressive aphasia and frontotemporal lobar degeneration subtypes: Reassessment of expected [^{18}F]-fluorodeoxyglucose uptake patterns. World J Nucl Med 2021;20:294-304. doi: 10.4103/wjnm. WJNM_137_20

7. Saramago I, **Franceschi AM**. Olfactory Dysfunction in Neurodegenerative Disease. Top Magn Reson Imaging. 2021;30(3):167-172. doi: 10.1097/RMR.0000000000000271. PMID: 34096900.

8. **Franceschi AM**, Clifton M, Naser-Tavakolian K, Ahmed O, Cruciata G, Bangiyev L, Clouston S, Franceschi D. [18F] FDG PET/MRI Assessment of Hypometabolism Patterns in Clinical Phenotypes of Suspected Corticobasal Degeneration Syndromes. World J Nucl Med. 2020;20(2):176-184. doi: 10.4103/wjnm.WJNM_62_20. PMID: 34321971.

9. **Franceschi AM**, Naser-Tavakolian K, Clifton M, Ahmed O, Stoffers K, Bangiyev L, Cruciata G, Clouston S, Franceschi D. Hybrid imaging in dementia: A semi-quantitative (18F)-fluorodeoxyglucose positron emission tomography/magnetic resonance imaging approach in clinical practice. World J Nucl Med. 2020;20(1):23-31. doi: 10.4103/wjnm.WJNM_27_20. PMID: 33850486;

10. **Franceschi AM**, Clifton M, Naser-Tavakolian K, Ahmed O, Bangiyev L, Clouston S, Franceschi D. Visual Detection of Crossed Cerebellar Diaschisis in Dementia Patients Utilizing FDG PET/MRI. AJR Am J Roentgenol. 2021;216(1):165-171. doi: 10.2214/AJR.19.22617. PMID: 33170738

11. **Franceschi AM**, Clifton M, Ahmed O, Matthews R, Franceschi D. Incidental PET/CT Findings of Suspected COVID-19 in a Region of High Prevalence. Cureus. 12(8): e9716. doi:10.7759/cureus.9716. PMID: 32944437.

12. **Franceschi AM**, Arora R, Wilson R, Giliberto L, Libman RB, Castillo M. Neurovascular Complications in COVID-19 Infection: Case Series. AJNR Am J Neuroradiol. 2020;41(9):1632-1640. doi: 10.3174/ajnr.A6655. PMID: 32527844.

13. **Franceschi AM**, Ahmed O, Giliberto L, Castillo M. Hemorrhagic Posterior Reversible Encephalopathy Syndrome as a Manifestation of COVID-19 Infection. AJNR Am J Neuroradiol. 2020;41(7):1173-1176. doi: 10.3174/ajnr.A6595. PMID: 32439646.

14. Wintermark M, Willis MH, Hom J, Franceschi AM, Fotos JS, Mosher T, Cruciata G, Reuss T, Horton R, Fredericks N, Burleson J, Haines B, Bruno M. Everything Every Radiologist Always Wanted (and Needs) to Know About Clinical Decision Support. J Am Coll Radiol. 2020;17(5):568-573. doi: 10.1016/j.jacr.2020.03.016. PMID: 32370997.

15. Huang M, Naser-Tavakolian K, Clifton M, **Franceschi AM**, Kim DT, Zhang JZ, Schweitzer ME. Gender Differences in Article Citations by Authors from American Institutions in Major Radiology Journals. Cureus. 2019;11(8):e5313. doi: 10.7759/cureus.5313. PMID: 31592368.

16. Raad RA, Lala S, Allen JC, Babb J, Mitchell CW, **Franceschi AM**, Yohay K, Friedman KP. Comparison of hybrid 18F-fluorodeoxyglucose positron emission tomography/magnetic resonance imaging and positron emission tomography/computed tomography for evaluation of peripheral nerve sheath tumors in patients with neurofibromatosis type 1. World J Nucl Med. 2018;17(4):241-248. doi: 10.4103/wjnm.WJNM_71_17. PMID: 30505221.

17. **Franceschi AM**, Raad RA, Abballe V, Nelson A, Jackson K, Babb J, Vahle T, Fenchel M, Zhan Y, Valadez Hermosillo G, Shepherd TM, Friedman KP. Visual detection of regional brain hypometabolism in cognitively impaired patients is independent of positron emission tomography-magnetic resonance attenuation correction method. World J Nucl Med. 2018 ;17(3):188-194. doi: 10.4103/wjnm.WJNM_61_17. PMID: 30034284.

18. **Franceschi AM**, Matthews R, Bangiyev L, Relan N, Chaudhry A, Franceschi D. Added Value of Including Entire Brain on Body Imaging With FDG PET/MRI. AJR Am J Roentgenol. 2018;211(1):176-184. doi: 10.2214/AJR.17.18858. PMID: 29792727.

19. Patel SH, Poisson LM, Brat DJ, Zhou Y, Cooper L, Snuderl M, Thomas C, **Franceschi AM**, Griffith B, Flanders A, Golfinos JG, Chi AS, Jain R. T2-FLAIR

Mismatch, an Imaging Biomarker for IDH and 1p/19q Status in Lower-grade Gliomas: A TCGA/TCIA Project. Clin Cancer Res. 2017;23(20):6078-6085. doi: 10.1158/1078-0432.CCR-17-0560. PMID: 28751449.

20. **Franceschi AM**, Rosenkrantz AB. Patterns of Recent National Institutes of Health (NIH) Funding to Diagnostic Radiology Departments: Analysis Using the NIH RePORTER System. Acad Radiol. 2017;24(9):1162-1168. doi: 10.1016/j.acra.2017.02.018. PMID: 28528855.

21. Miskin N, Patel H, **Franceschi AM**, Ades-Aron B, Le A, Damadian BE, Stanton C, Serulle Y, Golomb J, Gonen O, Rusinek H, George AE; Alzheimer's Disease Neuroimaging Initiative. Diagnosis of Normal-Pressure Hydrocephalus: Use of Traditional Measures in the Era of Volumetric MR Imaging. Radiology. 2017;285(1):197-205. doi: 10.1148/radiol.2017161216. PMID: 28498794.

22. **Franceschi AM**, Moschos SJ, Anders CK, Glaubiger S, Collichio FA, Lee CB, Castillo M, Lee YZ. Use of Susceptibility-Weighted Imaging (SWI) in the Detection of Brain Hemorrhagic Metastases from Breast Cancer and Melanoma. J Comput Assist Tomogr. 2016;40(5):803-5. doi: 10.1097/RCT.0000000000000420. PMID: 27636126.

23. **Franceschi AM**, Wiggins GC, Mogilner AY, Shepherd TM, Chung S, Lui YW. Optimized, Minimal Specific Absorption Rate MRI for High-Resolution Imaging in Patients with Implanted Deep Brain Stimulation Electrodes. AJNR Am J Neuroradiol. 2016;37(11):1996-2000. doi: 10.3174/ajnr.A4865. PMID: 27418467.

24. Timpone VM, Lev MH, Kamalian, S, Morais LT, **Franceschi AM**, Souza L, Schaefer PW. Percentage insula ribbon infarction of >50% identifies patients likely to have poor clinical outcome despite small DWI infarct volume. AJNR Am J Neuroradiol. 2015;36(1):40-5. doi: 10.3174/ajnr.A4091. PMID: 25190204.

25. Shapiro PA, Sloan RP, Deochand C, **Franceschi AM**, DeLorenzo C, Mann JJ, Parsey RV. Quantifying serotonin transporters by PET with [11C]-DASB before and after interferon-α treatment. Synapse. 2014;68(11):548-55. doi: 10.1002/syn.21766. Epub 2014 Aug 4. PMID: 25043294.

26. Johnson JM, **Franceschi AM**, Reed MS, Primm JC, Herschorn SD. Axillary Lymph Node Calcification: A Review of Local and Systemic Disease Processes. Contemporary Diagnostic Radiology. 2014;37(13):1-6.

27. Kamalian S, Kemmling A, Borgie RC, Morais LT, Payabvash S, **Franceschi AM**, Kamalian S, Yoo AJ, Furie KL, Lev MH. Admission insular infarction >25% is the strongest predictor of large mismatch loss in proximal middle cerebral artery stroke. Stroke. 2013;44(11):3084-9. doi: 10.1161/STROKEAHA.113.002260. Epub 2013 Aug 29. PMID: 23988643.

28. **Franceschi AM**, Matthews R, Mankes S, Safaie E, Franceschi D. Four chamber FDG uptake in the heart: an indirect sign of pulmonary embolism. Clin Nucl Med. 2012;37(7):687-91. doi: 10.1097/RLU.0b013e31824c5e64. PMID: 22691515.

29. **Franceschi AM**, Matthews R. Diagnostic Imaging: Musculoskeletal– Non-Traumatic Disease. Book review. J Nucl Med. 2012;53:658-659. doi: 10.2967/jnumed.111.098236.

ON-LINE EDUCATIONAL CASES

1. **Franceschi AM**, Cooper BT, Zagzag D, Howard J, Purswani JM, Ghesani M, Sahasrabundhe NA. Periventricular Germinoma with Leptomeningeal Dissemination: A Case Report. HemOnc Today: Imaging Analysis. May 25th, 2019. URL: http://www.healio.com/hematology-oncology

2. **Franceschi AM**, Purswani MJ, Ghesani M. Clinical Presentation Suggests Spinal Neoplasm, But Is It Really a Tumor? HemOnc Today: Imaging Analysis. September 25th, 2018. URL: http://www.healio.com/hematology-oncology

3. **Franceschi AM**, Fatterpekar G, Ghesani M. Brain PET/MR: Differentiating Recurrent Metastasis from Radiation Necrosis. HemOnc Today: Imaging Analysis. June 25th, 2018. URL: http://www.healio.com/hematology-oncology

4. **Franceschi AM**, Ghesani M. Multi-modality Imaging of SNUC: Sinonasal Undifferentiated Carcinoma. HemOnc Today: Imaging Analysis. April 25th, 2018. URL: http://www.healio.com/hematology-oncology

5. **Franceschi AM**, Ghesani M. Carotid Space Lesions: Added Value of ^{68}Gallium-DOTATE PET/MR Imaging. HemOnc Today: Imaging Analysis. February 25th, 2018. URL: http://www.healio.com/hematology-oncology

6. **Franceschi AM**, Zan E, Ghesani M. Initial Assessment of Nasopharyngeal Carcinoma: Added Value of PET/MRI. HemOnc Today: Imaging Analysis. December 25th, 2017. URL: http://www.healio.com/hematology-oncology

7. **Franceschi AM**, Ghesani M. Metastatic Neuroendocrine Tumor to the Interatrial Septum: Differentiating Lipomatous Hypertrophy from Metastatic Disease. HemOnc Today: Imaging Analysis. November 25th, 2017. URL: http://www.healio.com/hematology-oncology

8. **Franceschi AM**, Ghesani M. Skeletal Metastases in Breast Carcinoma: Classic Patterns of Treatment Response. HemOnc Today: Imaging Analysis. August 25th, 2017. URL: http://www.healio.com/hematology-oncology

9. **Franceschi AM**, Ghesani M. Uterine Carcinosarcoma: Liver Metastasis from Patient's Known Malignant Mixed Mullerian Tumor. HemOnc Today: Imaging Analysis. May 25th, 2017. URL: http://www.healio.com/hematology-oncology

10. **Franceschi AM**, Ghesani M. Assessment of Cervical Lymphadenopathy in the Setting of Malignancy. HemOnc Today: Imaging Analysis. April 10th, 2017. URL: http://www.healio.com/hematology-oncology

11. **Franceschi AM**, Shroyer R, Bangiyev L. Post-ictal Cerebral CTP Abnormalities. American Journal of Neuroradiology - Classic Case. April 6th, 2015. URL: http://www.ajnr.org/site/imgquiz/04062015qz.xhtml

12. **Franceschi AM**, Silva Priegue N, Castillo M. Radiation Necrosis with Delayed Cyst Formation. American Journal of Neuroradiology - Case of the Week. December 22nd, 2014. URL: http://www.ajnr.org/site/home/cow/12222014.xhtml

13. **Franceschi AM**, Johnson JM, Lightner JE, Filippi CG. Squamous Cell Carcinoma. American Journal of Neuroradiology - Case of the Week. December 11th, 2014. URL: http://www.ajnr.org/site/home/cow/12112014.xhtml

14. **Franceschi AM**, Mak W, Balsam D. Bile Aspiration Pneumonia in High Small Bowel Atresia. American College of Radiology - Case in Point. November 6th, 2014. URL: https://3s.acr.org/CIP/CaseView.aspx?CaseId=vQDnw01F5Z4%3d

15. Silva Priegue N, **Franceschi AM**, Castillo M. Cleidocranial Dysplasia (CCD). American Journal of Neuroradiology - Classic Case. June 24th, 2013. URL: http://www.ajnr.org/site/imgquiz/06242013qz.xhtml

PRESENTATIONS & ABSTRACTS

1. Petrover DR, Giliberto L, Clouston SAP, Gordon ML, **Franceschi AM**. [^{18}F]-Florbetaben PET/CT Clinical Interpretation: Visual Assessment and Semiquantitative Analysis. Accepted for presentation at the 107th Scientific Assembly and Annual Meeting of the Radiological Society of North America, Chicago, IL, November 2021.

2. Petrover DR, Giliberto L, Clouston SAP, Gordon ML, **Franceschi AM**. Semiquantitative Approach to Amyloid PET Interpretation in Clinical Practice. Proceedings of the 68th Annual Meeting of the Society of Nuclear Medicine and Molecular Imaging, Virtual Meeting, June 2021.

3. Pedersen C, Messina S, Daldrup-Link H, **Franceschi AM**, Aboian MS. PET/MRI in Pediatric Imaging: Primer for Implementation in Clinical Practice and Research. Accepted for presentation at the 59th Annual Meeting of the American Society of Neuroradiology, Virtual Meeting, May 2021.

4. **Franceschi AM**, Arora R, Wilson R, Ahmed O, Giliberto L, Libman RB, Castillo M. Neurovascular Complications in COVID-19 Infection. Accepted for presentation at the 59th Annual Meeting of the American Society of Neuroradiology, Virtual Meeting, May 2021.

5. **Franceschi AM**, Wilson R, Giliberto L, Libman RB, Castillo M. Neuro-Thrombembolic Complications in COVID-19 Infection. Proceedings of the 106th Scientific Assembly and Annual Meeting of the Radiological Society of North America, Virtual Meeting, November 2020.

6. Srivastava P, Hsu P, Matthews R, Franceschi D, **Franceschi AM**, Duong T, Bangiyev L. Utilizing PET/MRI to Determine Cerebellar Volume Asymmetry in Crossed Cerebellar Diaschisis Patients with Dementia. Proceedings of the 106th Scientific Assembly and Annual Meeting of the Radiological Society of North America, Virtual Meeting, November 2020.

7. Srivastava P, Hsu P, Matthews R, Franceschi D, **Franceschi AM**, Duong T, Bangiyev L. Utilizing PET-MRI to Evaluate Microstructural Changes in Cerebral-Cerebellar Pathways in Cross Cerebellar Diaschisis in Patients with Dementia. Proceedings of the 106th Scientific Assembly and Annual Meeting of the Radiological Society of North America, Virtual Meeting, November 2020.

8. **Franceschi AM**, Naser-Tavakolian K, Clifton M, Cruciata G, Bangiyev L, Clouston S, Franceschi D. [F18]-FDG PET/MRI in Primary Progressive Aphasia and Frontotemporal Lobar Degeneration (FTLD) Subtypes: Asymmetry of Hypometabolism Patterns. Proceedings of the 106th Scientific Assembly and Annual Meeting of the Radiological Society of North America, Virtual Meeting, November 2020.

9. **Franceschi AM**, Kritikos M, Cruciata G, Clouston SAP, Vaska P, Huang C, Horton M, Tang C, Salerno M, Deri Y, Carr M, Santiago-Michels S, Pellechia A, Gandy S, Sano M, Bromet EJ, Lucini R, Luft BJ. Neuritic Plaques and Neurofibrillary Tangles in a Positron Emission Tomography Feasibility Study for Alzheimer's Disease in World Trade Center Cognitively Impaired Responders. Proceedings of the 67th Annual Meeting of the Society of Nuclear Medicine and Molecular Imaging, Virtual Meeting, June 2020. J Nucl Med 2020 61:1573 J Nucl Med May 1, 2020 vol. 61 no. supplement 1 1573.

10. **Franceschi AM**, Cruciata G, Naser-Tavakolian K, Clifton M, Bangiyev L, Clouston S, Franceschi D. Metabolic PET/MRI in Primary Progressive Aphasia and FTD Subtypes: Reassessment of Expected FDG Uptake Patterns. Proceedings of the 58thAnnual Meeting of the American Society of Neuroradiology, Virtual Meeting, June 2020.

11. **Franceschi AM**, Clifton M, Kritikos M, Naser-Tavakolian K, Cruciata G, Bangiyev L, Salerno M, Deri Y, Parsey R, Vaska P, Franceschi D, Clouston S. Neuritic Plaques and Neurofibrillary Tangles: Integrated 3T PET/MRI PET-MRI Feasibility Study of World Trade Center Cognitively Impaired Responders. Proceedings of the 58thAnnual Meeting of the American Society of Neuroradiology, Virtual Meeting, June 2020.

12. Naser-Tavakolian K, Clifton M, **Franceschi AM**, Batista E, Salerno MJ, Cruciata G, Wengler K, Ouellette DJ, Wei S, Cruickshank B, Komatsu DE, Franceschi D, Bangiyev L, Spuhler K, Huang C, Oseni J, Thomas EB, Schweitzer M, Dams-O'Connor K, Penna J, He X, Vaska P. Utilizing Hybrid PET/MR Imaging to Understand Acute Sports Concussion. Proceedings of the 58thAnnual Meeting of the American Society of Neuroradiology, Virtual Meeting, June 2020

13. **Franceschi AM** Cruciata G, McMahon B, Garber B, Wintermak M, Bruno M. PAMA legislation: A CMS Perspective on Clinical Decision Support Systems. Proceedings of the 58thAnnual Meeting of the American Society of Neuroradiology, Virtual Meeting, June 2020.

14. Ahmed O, Naser-Tavakolian K, Clifton M, van Staalduinen E, Hussaini O, Khan A, Li H, **Franceschi AM**, Duong T, Bangiyev L. Utility of MRI Texture Analysis Assessment to Predict Meningioma Grade. Proceedings of the 58thAnnual Meeting of the American Society of Neuroradiology, Virtual Meeting, June 2020.

15. Ahmed O, Naser-Tavakolian K, Clifton M, van Staalduinen E, Hussaini O, Khan A, Li H, **Franceschi AM**, Duong T, Bangiyev L. Meningioma-Brain Adherence Assessment Using MRI Texture Analysis. Proceedings of the 58th Annual Meeting of the American Society of Neuroradiology, Virtual Meeting, June 2020.

16. Ahmed O, Naser-Tavakolian K, Clifton M, Cruciata G, Bangiyev L, Franceschi D, **Franceschi AM**. Qualitative [18F] FDG PET/MRI Assessment of Hypometabolism Patterns in Suspected Corticobasal Degeneration Syndromes. Proceedings of the 105th Scientific Assembly and Annual Meeting of the Radiological Society of North America, Chicago, IL, November 2019.

17. Naser-Tavakolian K, Clifton M, Batista E, Ahmed O, Franceschi D, Cruciata G, Bangiyev L, **Franceschi AM**. Hybrid PET-MR Imaging in Neurodegenerative disorders: Are Age-Matched Controls Needed to Evaluate FDG Hypometabolism Patterns? Proceedings of the 105th Scientific Assembly and Annual Meeting of the Radiological Society of North America, Chicago, IL, November 2019.

18. Naser-Tavakolian K, Clifton M, Batista E, Ahmed O, McPhee C, Hutnik R, Kung P, Cruciata G, Bangiyev L, Franceschi D, **Franceschi AM**. FDG PET/MRI analysis in Neurodegenerative Disorders: How Strong is the Correlation between Volumetric Analysis and Hypometabolism? Proceedings of the 105th Scientific Assembly and Annual Meeting of the Radiological Society of North America, Chicago, IL, November 2019.

19. Lucchini R, Horton M, Vaska P, Tang C, **Franceschi AM**, Deri Y, Gandy S, Sano M, Bromet E, Clouston SAP, Luft BJ. Neuritic Plaques Detected in a Series of World Trade Center Responders with Cognitive Impairment: An Amyloid PET/MRI Study. Proceedings of the 17th Biannual Meeting of the International Neurotoxicology Association, Dusseldorf, Germany, October 2019.

20. Salerno M, **Franceschi AM**, Clifton M, Naser-Tavakolian K, Wengler K, Ouellette D, Wei S, Cruickshank B, Komatsu D, Franceschi D, Bangiyev L, Huang C, Oseni J, Thomas E, Schweitzer M, Dams-O'Connor K, Penna J, He Xiang Vaska P. Neurometabolic Disruption Following Sports Concussion Using PET/MRI. Proceedings of the 66th Annual Meeting of the Society of Nuclear Medicine and Molecular Imaging, Anaheim, CA, June 2019. J Nucl Med May 1, 2019 vol. 60 no. supplement 1 391.

21. Naser-Tavakolian K, Clifton M, Batista E, Ahmed O, Franceschi D, Cruciata G, Bangiyev L, Bluestone A, **Franceschi AM**. Hybrid PET/MR Imaging in Dementia: Is There a Difference Comparing Patterns of FDG Hypometabolism to Age-Matched versus Non-Age Matched Controls? Proceedings of the 66th Annual Meeting of the Society of Nuclear Medicine and Molecular Imaging, Anaheim, CA, June 2019. J Nucl Med May 1, 2019 vol. 60 no. supplement 1 1454

22. Frey MK, Sawged Z, **Franceschi AM**, Friedman KP, Lutz K, Curtin JP, Blank SV, Pothuri B. Multi-parametric FDG PET/MRI As an Early Predictor of Response to Neoadjuvant Chemotherapy in Patients with Epithelial Ovarian Cancer. Proceedings of the Annual Meeting of the Society of Clinical Oncology, Chicago, IL, May 2019.

Journal of Clinical Oncology 2019 37:15_suppl, 5569-5569. DOI: 10.1200/JCO.2019.37.15_suppl.5569.

23. Naser-Tavakolian K, Clifton M, Khan A, Franceschi D, Cruciata G, Bangiyev L, **Franceschi AM**. Hybrid Imaging in Dementia: Semi-quantitative PET/MRI Approach. Proceedings of the 57thAnnual Meeting of the American Society of Neuroradiology, Boston, MA, May 2019.

24. Clifton M, Naser-Tavakolian K, Clouston S, Franceschi D, Cruciata G, Bangiyev L, Vaska P, Diminich E, Deri Y, **Franceschi AM**. PET Taupathology: Novel Direction of PET/MRI imaging. Proceedings of the 57thAnnual Meeting of the American Society of Neuroradiology, Boston, MA, May 2019.

25. Clifton M, Naser-Tavakolian K, Salerno M, Wengler K, Ouellette D, Wei S, Cruickshank B, Schweitzer M, Franceschi D, Cruciata G, Bangiyev L, Vaska P, **Franceschi AM**. Temporal Hypometabolism in Athletes with Head Trauma: A Pilot FDG PET/MRI Study. Proceedings of the 57thAnnual Meeting of the American Society of Neuroradiology, Boston, MA, May 2019.

26. Choi YS, Beomseok S, Chang JH, Lee SK, **Franceschi AM**, Patel SH, Chi AS, Jain R. "T2 FLAIR Mismatch" Sign and Radiomics in Lower Grade Gliomas. Proceedings of the the 57thAnnual Meeting of the American Society of Neuroradiology, Boston, MA, May 2019.

27. Van Staalduinen E, Khan A, **Franceschi AM**, Matthews R, Bangiyev L. Differentiating Metastatic and False-positive Lymph Nodes in Patients with Oropharyngeal Squamous Cell Carcinoma Using MR Texture Analysis. Proceedings of the 119th ARRS American Roentgen Ray Society Annual Meeting, Honolulu, HI, May 2019.

28. **Franceschi AM**, Franceschi D, Matthews R, Cruciata G, Bangiyev L. Cerebral Amyloid Angiopathy: PET/MRI Findings. Proceedings of the 119th ARRS American Roentgen Ray Society Annual Meeting, Honolulu, HI, May 2019.

29. **Franceschi AM**, Bangiyev L, Cruciata G, Matthews R, Franceschi D. Hybrid Imaging in Neuroradiology: Added Value of PET/MRI. Proceedings of the 119th ARRS American Roentgen Ray Society Annual Meeting, Honolulu, HI, May 2019.

30. **Franceschi AM**, Pothuri B, Frey M, Chandarana H, Babb J, Jackson K, Friedman K. Multi-parametric FDG PET/MRI as an Early Predictor of Response to Neoadjuvant Chemotherapy in Patients with Epithelial Ovarian Cancer. Proceedings of the 65th Annual Meeting of the Society of Nuclear Medicine and Molecular Imaging, Philadelphia, PA, June 2018.

31. Lu N, Ades-Aron B, Griffin M, Lotan E, **Franceschi AM**, Rusinek H, Golomb J, George A. High Volume Lumbar Puncture (HVLP) as a Predictor of Shunt Response in Normal Pressure Hydrocephalus: MRI features of HVLP Responders compared to Non-Responders. Proceedings of the 56thAnnual Meeting of the American Society of Neuroradiology, Vancouver, BC, Canada, June 2018.

32. Kim DT, Huang M, Zhang, Z, **Franceschi AM**, Schweitzer ME. Gender Differences

in Article Citations by American Authors in Major Radiology Journals. Proceedings of the 66th Association of University Radiologists Annual Meeting, Orlando FL, May 2018.

33. Franceschi AM, Vinayak S, Makhdomi K, Kajani M, Talib Z, Ghesani M. International Rad-Path Correlation Conference: A Multi-Institutional Experience. Proceedings of the 118th ARRS American Roentgen Ray Society Annual Meeting, Washington, DC, April 2018.

34. Franceschi AM, DeSantis M, Safaie E, Matthews R. Utility of PET/MRI in Cirrhotic and Metastatic Cancer with Liver Imaging Reporting and Data System. Proceedings of the 118th ARRS American Roentgen Ray Society Annual Meeting, Washington, DC, April 2018.

35. Franceschi AM, Pothuri B, Frey M, Chandarana H, Babb J, Jackson K, Friedman K. FDG PET/MRI as an Early Predictor of Response to Neoadjuvant Chemotherapy in Patients with Epithelial Ovarian Cancer. Proceedings of the New York University Radiology Resident Research Symposium, New York, NY, June 2017.

36. Franceschi AM, DeSantis M, Safaie E, Matthews R. Application of Liver Imaging Reporting and Data System (LI-RADS) in FDG PET-MRI for Cirrhotic and Metastatic Cancer Patients. Proceedings of the 64th Annual Meeting of the Society of Nuclear Medicine and Molecular Imaging, Denver, CO, June 2017. J Nucl Med May 1, 2017 vol. 58 no. supplement 1 425.

37. Franceschi AM, Raad R, Abballe V, Faul D, Friedman K. Interpretation of Brain PET/MR is Independent of Attenuation Correction Method. Proceedings of the 117th ARRS American Roentgen Ray Society Annual Meeting, New Orleans, LA, May 2017.

38. Franceschi AM, Rosenkrantz AB. Trends in National Institutes of Health (NIH) Funding to Diagnostic Radiology Departments. Proceedings of the 117th ARRS American Roentgen Ray Society Annual Meeting, New Orleans, LA, May 2017.

39. Franceschi AM, Claire P, DeSantis M. Liver Imaging Reporting and Data System (LIRADS) use for Comprehensive Management at VA Hospitals. Proceedings of the 117th ARRS American Roentgen Ray Society Annual Meeting, New Orleans, LA, May 2017.

40. Franceschi AM, Matthews R, Bangiyev L, Chaudhry A, Relan N, Franceschi D. Brain Pathology Initially Identified on Whole Body FDG PET-MRI. Proceedings of the 55thAnnual Meeting of the American Society of Neuroradiology, Long Beach, CA, April 2017.

41. Kim D, Huang M, **Franceschi AM**, Schweitzer M. Impact of Research Articles in Major Radiology Journals by American Female Authors: A 30-Year Analysis. Proceedings of the 11th Annual Women in Medicine Research Day, Stony Brook University School of Medicine, Stony Brook, NY, March 2017.

42. Franceschi AM, Matthews R, Bangiyev L, Chaudhry A, Relan N, Franceschi D. Incidental Brain Pathology on Whole Body FDG PET-MRI. Proceedings of the 102nd

Scientific Assembly and Annual Meeting of the Radiological Society of North America, Chicago, IL, November 2016.

43. Franceschi AM, DeSantis M, Dalessandro T, Dolan CE. Comparison of Microwave Absorption of [18F]-FDG and Spherical Nanocarbon to Assist in Thermal Ablation for Cancer Therapy. Proceedings of the 102nd Scientific Assembly and Annual Meeting of the Radiological Society of North America, Chicago, IL, November 2016.

44. Franceschi AM, Raad R, Abballe V, Nelson A, Jackson K, Babb J, Koesters T, Fenchel M, Zhan Y, Hermosillo G, Shepherd T, Friedman K. Clinical Visual Readings of Brain Region-Specific Hypometabolism in Cognitive Impairment Patients Is Independent of Attenuation Correction Method for Integrated PET/MR. Proceedings of the 63rd Annual Meeting of the Society of Nuclear Medicine and Molecular Imaging, San Diego, CA, June 2016. J Nucl Med 2016 57:1977.

45. Franceschi AM, Matthews R, Bangiyev L, Relan N, Chaudhry A, Franceschi D. Brain Findings on FDG PET-MRI Body Sequences That Include the Head. Proceedings of the 63rd Annual Meeting of the Society of Nuclear Medicine and Molecular Imaging, San Diego, CA, June 2016. J Nucl Med 2016 57:597.

46. Franceschi AM, Matthews R, Chimpiri AR, Relan N, Yaddanapudi K, Franceschi D. Simultaneously Acquired FDG PET-MR Body Imaging in the Detection of Breast Cancer Metastases. Proceedings of the 63rd Annual Meeting of the Society of Nuclear Medicine and Molecular Imaging, San Diego, CA, June 2016. J Nucl Med 2016 57:620.

47. Franceschi AM, Wiggins GC, Mogilner AY, Shepherd TM, Chung S, Lui YW. Practical Low SAR Protocol at 1.5T using Two Magnet Systems for Patients Undergoing Staged DBS Insertion. Proceedings of the 54thAnnual Meeting of the American Society of Neuroradiology, Washington, DC, May 2016.

48. Littig I, Fatterpekar G, Snuderl M, **Franceschi AM**, Davis A. Anaplastic Astrocytoma versus Glioblastoma Histological Grading with MRI DSC Perfusion Technique: Cerebral Blood Volume versus Cerebral Blood Flow Utilizing Standard, Time Insensitive and Bayesian Deconvolution Methods. Proceedings of the 54thAnnual Meeting of the American Society of Neuroradiology, Washington, DC, May 2016.

49. Patel S, Poisson LM, **Franceschi AM**, Griffith B, Jain R. T2-FLAIR mismatch, a potential imaging biomarker for IDH mutant status in lower grade gliomas: A TCGA/TCIA Project. Proceedings of the 54thAnnual Meeting of the American Society of Neuroradiology, Washington, DC, May 2016.

50. Franceschi AM, Matthews R, Chimpiri AR, Safaie E, Yaddanapudi K, Franceschi D. Assessing Breast Cancer with Dedicated FDG PET-MRI. Proceedings of the 116th ARRS American Roentgen Ray Society Annual Meeting, Los Angeles, CA, April 2016.

51. Safaie E, Matthews R, You K, Yaddanapudi K, **Franceschi AM**, Bergamaschi, R. Incidental FDG uptake in Rectal Cancer PET-CT. Proceedings of the 116th ARRS American Roentgen Ray Society Annual Meeting, Los Angeles, CA, April 2016.

52. Franceschi AM, DeSantis M, Minkoff LA, Greenhalgh JF, Green CA, Bowne WB, Dolan CE. MR Imaging during Thermal Ablation of Breast Tumor. Proceedings of the 116th ARRS American Roentgen Ray Society Annual Meeting, Los Angeles, CA, April 2016.

53. Franceschi AM, Matthews R, Bangiyev L, Franceschi D. Postablation Radioiodine Scintigraphy SPECT/CT: Functional and Anatomic Correlation. Proceedings of the 101st Scientific Assembly and Annual Meeting of the Radiological Society of North America, Chicago, IL, December 2015.

54. DeSantis M, **Franceschi AM**, Bowne WB, Dalessandro T, Gross J, Suprenant VJ, Kumar A, Ferretti JA, Dolan CE. MRI Image Guided Nanocarbon-Assisted Microwave Therapy (NAMT) Causing Cytotoxic Thermal Ablation of MK1 Breast Tumor Cells in SCID Mice. Proceedings of the 101st Scientific Assembly and Annual Meeting of the Radiological Society of North America, Chicago, IL, December 2015.

55. Franceschi AM, Friedman K, Ghesani M. Inguinal Hernia Repair Mimicking Malignancy On PET/CT: Mesh Is Cool, but the Plug Lights Up. Proceedings of the 62nd Annual Meeting of the Society of Nuclear Medicine and Molecular Imaging, Baltimore, MD, June 2015. J Nucl Med 2015 56:1426.

56. Franceschi AM, Matthews R, Relan NK, Safaie E, Franceschi D. Diagnostic Value of Bilateral Hip Bone Mineral Density (BMD) Using Dual Energy X-ray Absorptiometry (DXA) for Osteoporosis Screening. Proceedings of the 62nd Annual Meeting of the Society of Nuclear Medicine and Molecular Imaging, Baltimore, MD, June 2015. J Nucl Med 2015 56:1687.

57. Franceschi AM, Matthews R, Samara G, Marzouk M, Yaddanapudi K, Franceschi D. Localizing Parathyroid Adenoma with Tc-99m Sestamibi Comparing Planar Imaging, Single Photon Emission Computed Tomography (SPECT), and SPECT Combined With High Quality Computed Tomography (SPECT-CT). Proceedings of the 62nd Annual Meeting of the Society of Nuclear Medicine and Molecular Imaging, Baltimore, MD, June 2015. J Nucl Med 2015 56:203.

58. Franceschi AM, Wiggins GC, Mogilner AY, Lui YW. Optimized, Minimal SAR MRI for High-resolution Imaging in Patients with Implanted Deep Brain Stimulation Electrodes. Proceedings of the 53rdAnnual Meeting of the American Society of Neuroradiology, Chicago, IL, April 2015.

59. Stanton C, **Franceschi AM**, Miskin N, Damadian B, Golomb J, Gonen O, Rusinek H, George A. MRI Differentiation of Shunt Responsive Normal Pressure Hydrocephalus, Alzheimer Disease and Normal Aging: Comparison of Morphometric and Categorical Assessments to Automated Volumetric Segmentation. Proceedings of the 53rdAnnual Meeting of the American Society of Neuroradiology, Chicago, IL, April 2015.

60. Franceschi AM, Shapiro PA, Sloan RP, Deochand C, DeLorenzo C, Mann JJ, Parsey RV. Quantifying Serotonin Transporters by PET with [11C]-DASB Before and After Interferon-αTreatment. Proceedings of the 115th ARRS American Roentgen Ray Society Annual Meeting, Toronto, ON, Canada, April 2015.

61. Franceschi AM, Matthews R, Benveniste HD, Reland N, Safaie E, Franceschi D. Global Brain Brain Hypometabolism on FDG PET-CT in Advanced Metastatic Melanoma. Proceedings of the 115th ARRS American Roentgen Ray Society Annual Meeting, Toronto, ON, Canada, April 2015.

62. Franceschi AM, DeSantis M, Bowne WB, Ferretti JA, Dalessandro T, Gross J, Suprenant VJ, Kumar A, Zimmerman TE, Dolan CE. Evaluation of In-situ Nanocarbon-Assisted Microwave Therapy (NAMT) Causing Cytotoxic Thermal Ablation of Human Prostate Tumor Cells in Nude Mice. Proceedings of the 100th Scientific Assembly and Annual Meeting of the Radiological Society of North America, Chicago, IL, December 2014.

63. Franceschi AM, Bangiyev L, Weiss T, Matthews R, Safaie E, Franceschi D. Characterization of Central Neck Activity on Postablation Radioiodine Scintigraphy. Proceedings of the 27thAnnual Congress of the European Association of Nuclear Medicine, Gothenburg, Sweden, October 2014. Eur J Nucl Med Mol Imaging (2014) 41 (Suppl 2):S461. DOI: 10.1007/s00259-014-2901-9.

64. Franceschi AM, Matthews R, Reland N, Safaie E, Benveniste HD, Franceschi D. FDG Brain Metabolism on PET-CT Scans in Patients with Large Tumors. Proceedings of the 61st Annual Meeting of the Society of Nuclear Medicine and Molecular Imaging, St. Louis, MO, June 2014. J Nucl Med May 2014 55:1632.

65. DeSantis M, Bowne WB, Ferretti JA, **Franceschi AM**. Long-term Evaluation of Mouse Toxicity Using Application of Spherical Nanocarbon Injected into Known Human Prostatic Carcinoma in Nude Mouse with Microwave-assisted Therapy. Proceedings of the 61st Annual Meeting of the Society of Nuclear Medicine and Molecular Imaging, St. Louis, MO, June 2014. J Nucl Med May 2014 55:1515.

66. Franceschi AM, Moschos SJ, Ramalho J, Anders CK, Castillo M, Lee YZ. SWI Micro-hemorrhages Do Not Represent Metastases in Patients with Primary Breast Cancer or Melanoma. Proceedings of the 52ndAnnual Meeting of the American Society of Neuroradiology, Montreal, QC, Canada, May 2014.

67. Bazyar S, Ramalho J, **Franceschi AM**, Lee YZ. Comparison of Cerebral Blood Volume and Plasma Volume in Untreated Intracranial Lesions. Proceedings of the 52ndAnnual Meeting of the American Society of Neuroradiology, Montreal, QC, Canada, May 2014.

68. Kamalian S, Morais L, Yoo AJ, **Franceschi AM**, Kamalian S, Hirsch JA, Schwamm LH, Lev MH. Susceptibility Clot Width >5 mm Is a Highly Sensitive Marker for Development of Parenchymal Hematoma Following Intra-arterial Clot Retrieval in Acute Stroke. Proceedings of the 52ndAnnual Meeting of the American Society of Neuroradiology, Montreal, QC, Canada, May 2014.

69. Franceschi AM, Glaubiger S, Snavely A, Lee C, Anders CK, Castillo M, Moschos SJ, Lee YZ. Susceptibility-Weighted Imaging of Melanoma and Brain Metastases from Breast Cancer: Correlation With Tumor Volumes, Biological Features, and Patient Outcome. Proceedings of the 114th ARRS American Roentgen Ray Annual Meeting,

San Diego, CA, May 2014.

70. Franceschi D, Matthews R, Brunetti V, **Franceschi AM**, Safaie E, Carcamo CJ, Relan NK. FDG PET/CT Imaging in Diabetic Foot Infections. Proceedings of the 26th Annual Congress of the European Association of Nuclear Medicine, Lyon, France, October 2013. Eur J Nucl Med Mol Imaging. Oct 2013;40 (Suppl 2):S124. DOI: 10.1007/s00259-013-2535-3.

71. Franceschi D, Matthews R, Brunetti V, **Franceschi AM**, Safaie E, Relan NK. Value of FDG PET/CT in Diagnosis of Osteomyelitis in Diabetic Patients with Chronic Foot Infections. Proceedings of the 60th Annual Meeting of the Society of Nuclear Medicine and Molecular Imaging, Vancouver, BC, Canada, June 2013. J Nucl Med May 2013 54:1951.

72. Morais LT, Kamalian S, Borgie RC, Payabvash S, **Franceschi AM**, Schaefer P, Yoo AJ, Lev MH. Anterior Insula Infarction > 50% May Identify Proximal Occlusive Stroke Patients Likely to Benefit from Robust Revascularization. Proceedings of the 51st Annual Meeting of the American Society of Neuroradiology, San Diego, CA, May 2013.

73. **Franceschi AM**, Johnson JM, Sippo DA, Leightner JE, Primm JC, Herschorn SD. Axillary Lymph Node Calcification: A Review of Local and Systemic Disease Processes. Proceedings of the 98th Scientific Assembly and Annual Meeting of the Radiological Society of North America, Chicago, IL, November 2012.

74. **Franceschi AM**, Johnson JM, Ginat D, Fillipi CG. Exophitic Head and Neck Masses in Oculocutaneous Albinism. Proceedings of the 46th Annual Meeting of the American Society of Head and Neck Radiology, Miami Beach, FL, October 2012.

75. Johnson JM, Cohen AB, Moonis G, **Franceschi AM**, Toocheck D, Fillipi CG. Multimodality Imaging of Optic Neuropathies. Proceedings of the 46th Annual Meeting of the American Society of Head and Neck Radiology, Miami Beach, FL, October 2012.

76. **Franceschi AM**, Chaudhry ZA, Yoo AJ, Kamalian S, Hirsch JA, Schwamm LH, Lev MH. Degree of Clot-related Susceptibility Artifact Is an Independent Risk Factor for Parenchymal Hematoma Following Intra-arterial Therapy. Proceedings of the 50th Annual Meeting of the American Society of Neuroradiology, New York, NY, April 2012.

77. Johnson JM, **Franceschi AM**, Yoo AJ, Romero J. Utility of CT Angiography in Primary Angiitis of the Central Nervous System. Proceedings of the 50th Annual Meeting of the American Society of Neuroradiology, New York, NY, April 2012.

78. **Franceschi AM**, Chaudhry ZA, Yoo AJ, Kamalian S, Hirsch JA, Schwamm LH, Lev MH. Degree of Clot-related Susceptibility Artifact Is an Independent Risk Factor for Parenchymal Hematoma After Intra-arterial Therapy. Proceedings of the AHA International Stroke Conference 2012, New Orleans, LA, February 2012. Stroke, February 2012;43:A74.

79. Souza LCS, Lev MH, **Franceschi AM**, Hi J, Gonzalez RG, Schaefer PW. Thresholded CTP Maps Can Accurately Determine Infarct Core When DWI Is Unavailable and Have Similar Specificity in Identifying Patients Unlikely to Benefit from Thrombolysis. Proceedings of the 97th Scientific Assembly and Annual Meeting of the Radiological Society of North America, Chicago, IL, November 2011.

80. **Franceschi AM**, Chaudhry ZA, Kamalian S, Yoo AJ, Hirsch JA, Schwamm LH, Lev MH. Degree of Clot-related Susceptibility Artifact Is an Independent Risk Factor for Parenchymal Hematoma Following Mechanical Thrombectomy. Presented at the Massachusetts General Hospital Clinical Research Day 2011, Boston, MA, October 2011.

81. Kamalian S, Rapalino O, Kamalian S, **Franceschi AM**, Lev MH, Pomerantz SR. Cranial Computed Tomography with Adaptive Statistical Iterative Reconstruction (ASIR): Improved Image Quality with Concomitant Radiation Dose Reduction. Proceedings of the 1st Annual Symposium on Radiation Safety in CT: Basic Concepts and Recent Advances, Boston, MA, September 2011.

82. Souza LCS, **Franceschi AM**, Gonzalez RG, Lev MH, Schaefer PW. Thresholded CTP Maps Can Accurately Determine Infarct Core When DWI Is Unavailable and Have Similar Specificity in Identifying Patients Unlikely to Benefit from Thrombolysis. Proceedings of the 49th Annual Meeting of the American Society of Neuroradiology, Seattle, WA, June 2011.

5. COPY OF PUBLICATIONS

1. **Franceschi AM**, Matthews R, Bangiyev L, Relan N, Chaudhry A, Franceschi D. Added Value of Including Entire Brain on FDG PET/MRI Body Imaging. AJR Am J Roentgenol. 2018;24:1-9. doi: 10.2214/AJR.17.18858. PMID: 29792727.

2. **Franceschi AM**, Clifton M, Naser-Tavakolian K, Ahmed O, Bangiyev L, Clouston S, Franceschi D. FDG PET/MRI for Visual Detection of Crossed Cerebellar Diaschisis in Patients With Dementia. AJR Am J Roentgenol. 2021;216(1):165-171. doi: 10.2214/AJR.19.22617. PMID: 33170738

3. **Franceschi AM**, Wiggins GC, Mogilner AY, Shepherd TM, Chung S, Lui YW. Optimized, Minimal Specific Absorption Rate MRI for High-Resolution Imaging in Patients with Implanted Deep Brain Stimulation Electrodes. AJNR Am J Neuroradiol. 2016;37(11):1996-2000. doi: 10.3174/ajnr.A4865. PMID: 27418467

Added Value of Including Entire Brain on Body Imaging With FDG PET/MRI

Ana M. Franceschi[1]
Robert Matthews[2]
Lev Bangiyev[2]
Nand Relan[2]
Ammar Chaudhry[2]
Dinko Franceschi[2]

OBJECTIVE. FDG PET/MRI examination of the body is routinely performed from the skull base to the mid thigh. Many types of brain abnormalities potentially could be detected on PET/MRI if the head was included. The objective of this study was therefore to identify and characterize brain findings incidentally detected on PET/MRI of the body with the head included.

MATERIALS AND METHODS. We retrospectively identified 269 patients with FDG PET/MRI whole-body scans that included the head. PET/MR images of the brain were reviewed by a nuclear medicine physician and neuroradiologist, first individually and then concurrently. Both PET and MRI findings were identified, including abnormal FDG uptake, standardized uptake value, lesion size, and MRI signal characteristics. For each patient, relevant medical history and prior imaging were reviewed.

RESULTS. Of the 269 subjects, 173 were women and 96 were men (mean age, 57.4 years). Only the initial PET/MR image of each patient was reviewed. A total of 37 of the 269 patients (13.8%) had abnormal brain findings noted on the PET/MRI whole-body scan. Sixteen patients (5.9%) had vascular disease, nine patients (3.3%) had posttherapy changes, and two (0.7%) had benign cystic lesions in the brain. Twelve patients (4.5%) had serious nonvascular brain abnormalities, including cerebral metastasis in five patients and pituitary adenomas in two patients. Only nine subjects (3.3%) had a new neurologic or cognitive symptom suggestive of a brain abnormality.

CONCLUSION. Routine body imaging with FDG PET/MRI of the area from the skull base to the mid thigh may miss important brain abnormalities when the head is not included. The additional brain abnormalities identified on whole-body imaging may provide added clinical value to the management of oncology patients.

Keywords: brain, FDG, incidental findings, oncology, PET/MRI

doi.org/10.2214/AJR.17.18858

Received August 2, 2017; accepted after revision December 11, 2017.

Based on a presentation at the Radiological Society of North America (RSNA) 2016 annual meeting, Chicago, IL. Aunt Minnie 2017 Semifinal Candidate for Scientific Paper of the Year (for an RSNA abstract).

Supported by Student Travel Stipend Award given to presentation at RSNA 2016 annual meeting.

[1]Department of Radiology, New York University Medical Center, New York, NY.

[2]Department of Radiology, Stony Brook University School of Medicine, 101 Nicolls Rd, HSC Level 4, Rm 120, Stony Brook, NY 11794-8434. Address correspondence to R. Matthews (robert.matthews@stonybrook.edu).

AJR 2018; 211:1–9

0361–803X/18/2111–1

PET is a well-established modality for the evaluation of oncology patients. The most common radiotracer used in the workup of malignant tumors is the glucose analog ^{18}F-FDG, which is a positron emitter with a 110-minute half-life [1]. However, the use of PET alone has several limitations, including low spatial resolution and difficulty localizing and characterizing foci of increased uptake in the setting of normal physiologic uptake in different organs. Although PET detects sites of malignancy and metastatic spread, other pathologic processes, such as inflammation and infection can also have prominent increased FDG uptake [2]. CT was added to PET to aid in the interpretation of whole-body PET, greatly improving sensitivity and specificity. PET/CT does have some drawbacks, including a higher level of radiation exposure and a lack of anatomic definition that is related to the inherent low-tissue resolution of CT when imaging the head and neck, pelvis, liver, and bone marrow [3].

More recently, PET/MRI has emerged as another hybrid imaging modality used in the detection of malignancy. This hybrid scanner combines the molecular and functional tissue characterization of PET with the superior tissue resolution of MRI without added radiation. The addition of MRI was particularly useful for assessing neoplastic diseases in the brain, head and neck, musculoskeletal system, abdominal organs (especially the liver), and pelvis [4]. Because of the complexities of MRI, different protocols are established for imaging different parts of the body, with much variation existing between institutions and scanner manufacturers. MRI also requires organ-specific radiofrequency coils used for the transmission and receipt of signal [5].

For the typical oncology patient, routine FDG PET/CT covers the area from the skull

base to the mid thigh; however, for patients with malignant melanoma and some other malignancies, the imaging area is increased to include the area from the top of the head to the feet. The routine protocol was established to limit scanning times and to reduce the amount of radiation exposure [6]. Brain metastases are difficult to diagnose by both PET and CT, especially without the use of dedicated PET/CT brain protocols and IV contrast administration, so imaging of the entire brain during PET/CT has not been considered valuable. On the contrary, with the introduction of the PET/MRI scanner, both benign and malignant brain abnormalities can be detected by the MRI portion of the scanner, even though they typically would not be conspicuous with the use of PET/CT, even with the use of dedicated brain protocols [7].

At our imaging center, we routinely include the entire head in clinical body imaging with PET/MRI. Therefore, our aim in the present study is to identify and characterize FDG PET and MRI brain findings detected in the portion of the study that included the head.

Materials and Methods

Patients

In this institutionally approved and HIPAA-compliant retrospective study, we identified 269 adult patients (age, 18 years or older) who were referred from September 2013 until December 2016 for clinically indicated FDG PET/MRI examination of the area from the base of skull to the mid thigh that included the entire head. For all 269 patients, we included only the first PET/MRI scan obtained if more than one study was available. We excluded all patients younger than 18 years old, pregnant women, and patients with a fasting blood glucose level greater than 150 mg/dL; we also excluded all patients with PET/MRI body scans that did not include the entire brain, PET/MRI scans with dedicated brain sequences, PET/MRI scans with technical issues such as missing sequences, or non-FDG PET scans.

Image Acquisition

PET/MRI studies were performed using a 3-T scanner (Biograph mMR, Siemens Healthcare). The PET detector is composed of lutetium oxyorthosilicate scintillation crystals attached to avalanche photodiodes replacing typical photomultiplier tubes used in PET/CT. Each block detector consists of 64 crystal elements, and each crystal measures 4 × 4 × 20 mm. In each ring, there are 56 block detectors, and a total of 64 detector element rings are arranged along the *z*-axis. The MRI unit is equipped with a 3-T magnet.

PET and MRI data were acquired simultaneously with the use of body radiofrequency coils. A dual-echo T1-weighted gradient-recalled echo sequence was performed from the skull vertex to the mid thighs to acquire the MR attenuation correction map based on a Dixon segmentation. The PET data were reconstructed using an iterative 3D ordinary Poisson ordered subsets expectation-maximization algorithm at four iterations and 21 subsets with a 4-mm gaussian postreconstruction image filter. The transaxial image matrix size was 172 × 172 × 515 with a transaxial FOV of 59.4 × 59.4 cm and an axial FOV of 25.8 × 25.8 cm. The voxel size for the PET images was 4.17 × 4.17 × 2.03 mm.

All patients fasted for a minimum of 4 hours before receiving IV administration of approximately 10 mCi (370 MBq) of FDG, with the dose modified according to the patient's body weight. Before injection, the blood glucose level was measured to be 150 mg/dL or lower. After radiotracer injection, the patient was placed in a quiet, warm room and was told not to talk or move excessively. Simultaneous PET and MRI examinations were performed approximately 1 hour after administration of FDG.

For diagnostic MRI body sequences, we performed T1-weighted radial volumetric interpolated breath-hold examination with fat suppression or T1-weighted volumetric interpolated breath-hold examination with fat suppression in the axial orientation, followed by T2-weighted HASTE without fat suppression in the axial plane, T2-weighted turbo spin-echo in the coronal plane, and either DWI with apparent diffusion coefficient maps in the axial plane or a short T1-weighted inversion recovery sequence of the spine in the sagittal plane.

Image Analysis

All PET/MR images of the head were reviewed first individually and then concurrently by a board-

TABLE 1: Demographic and Clinical Characteristics of Patients Who Underwent Body PET/MRI Including the Head

Characteristic	All Patients (*n* = 269)	Patients With Brain Abnormality (*n* = 37)
Age (y)		
Mean ± standard error	57.4 ± 1.1	
Range	18–89	
Sex, no. of patients		
Male	96	14 (14.6)
Female	173	23 (13.3)
Pathologic abnormality distribution		
Cancers		
Breast	72	13
Lymphoma	50	5
Cervical	31	2
Gyneco-urologic	16	1
Colorectal	16	1
Head and neck	12	3
Sarcoma	9	0
Pancreatic	8	0
Lung	6	2
Multiple myeloma	5	1
Other cancers	25	2
Noncancer abnormalities		
Paraneoplastic syndrome	6	6
Adenopathy or soft-tissue mass	6	0
Lung nodules	4	1
Monoclonal gammopathy	2	0
Vasculitis	1	0

Note—Except where otherwise indicated, data are number of patients or number (%) of patients.

TABLE 2: Number and Percentage of Pathologic Abnormalities Found in 269 Patients

Category of Brain Findings	No. of Abnormalities	Percentage of Abnormalities
Vascular	16	5.9
Posttherapy changes	9	3.3
Parenchymal metastases	5	1.9
Benign cystic lesions	2	0.7
Pituitary adenomas	2	0.7
Creutzfeldt-Jakob disease	1	0.4
Metabolic encephalopathy	1	0.4
Encephalitis	1	0.4
Primary CNS lymphoma	1	0.4
Leptomeningeal metastases	1	0.4
Total	39	14.5

certified nuclear medicine physician and a board-certified neuroradiologist. A MIM workstation (version 6.1, MIM Software) was used to perform visual assessment of PET/MRI images. Both PET and MRI findings were noted, including abnormal FDG uptake, standardized uptake value, lesion size, and MRI signal characteristics. Relevant medical history and prior imaging were reviewed.

Statistical Analysis

The *t* test was used for statistical analysis of the results. The final data are presented as mean (± standard error) values and corresponding *p* values that represent statistical significance.

Results

Of the 269 patients who underwent FDG PET/MRI body studies that included the entire head, 173 were women (64%) and 96 were men (36%) (mean age, 57.4 ± 1.1 years; age range, 18–89 years). A total of 250 studies were performed for cancer assessment (91 for staging and 159 for restaging). The cancers that were identified in 225 of these studies were breast cancer ($n = 72$), lymphoma ($n = 50$), cervical cancers ($n = 31$), other gynecourologic cancers ($n = 16$), colorectal cancers ($n = 16$), head and neck cancers ($n = 12$), sarcomas ($n = 9$), pancreatic cancers ($n = 8$), lung cancers ($n = 6$), and multiple myelomas ($n = 5$). According to the 25 other cancer assessment studies, fewer than five patients had each type of cancer. The other 19 indications included paraneoplastic syndrome ($n = 6$), adenopathy or a soft-tissue mass ($n = 6$), lung nodules ($n = 4$), monoclonal gammopathy ($n = 2$), and vasculitis ($n = 1$). Five of the 19 patients with these other indications later received a diagnosis of cancer, including three cases of lung nodules, one case of adenopathy, and one case of paraneoplastic syndrome (Table 1).

Of the 269 patients whose PET/MRI scans were included in the study, 37 patients (13.8%) had a brain abnormality detected on FDG PET/MRI body imaging sequences. For men, 14.6% (14/96) of the scans showed a positive brain finding, compared with 13.3% (23/173) of the scans for women, which was not significant between the two groups. Two patients had two brain abnormalities, with the first patient having brain metastases and a chronic infarct and the second patient having radiation changes and an intracranial aneurysm (Table 2). Sixteen subjects (5.9%; mean age, 71 ± 3.2 years) had vascular disease: eight of these patients had findings compatible with chronic microvascular changes, six patients had brain infarcts in various stages, one patient had a chronic subdural hematoma, and one patient had an intracranial aneurysm. Comparison of the age of patients in the group with vascular disease with that of the remaining 253 patients (mean age, 57 ± 1.0 years) was statistically significant ($p < 0.001$). In four patients, the presence of brain infarcts of various stages was known before imaging, whereas in two patients (a 78-year-old woman with lung nodules and a 38-year-old woman with cervical cancer) newly diagnosed cerebellar lacunar infarcts were identified on PET/MRI. A chronic subdural hematoma was also newly diagnosed on the basis of a PET/MRI study of a 79-year-old woman who was undergoing staging of colorectal cancer. Of note, the rate of detection of microvascular ischemic changes was likely lower than anticipated because of the suboptimal quality of T2-weighted body MRI sequences.

Nine subjects (3.3%) had posttherapy changes in the brain that were caused by chemotherapy ($n = 3$), craniotomy for a benign pathologic finding ($n = 3$), radiation therapy ($n = 2$), or both craniotomy and radiation therapy for cancer ($n = 1$). Two subjects had benign cystic lesions in the brain. Twelve subjects (4.5%) had a serious nonvascular brain abnormality, including five of the patients who underwent imaging for evaluation of paraneoplastic syndrome, which re-

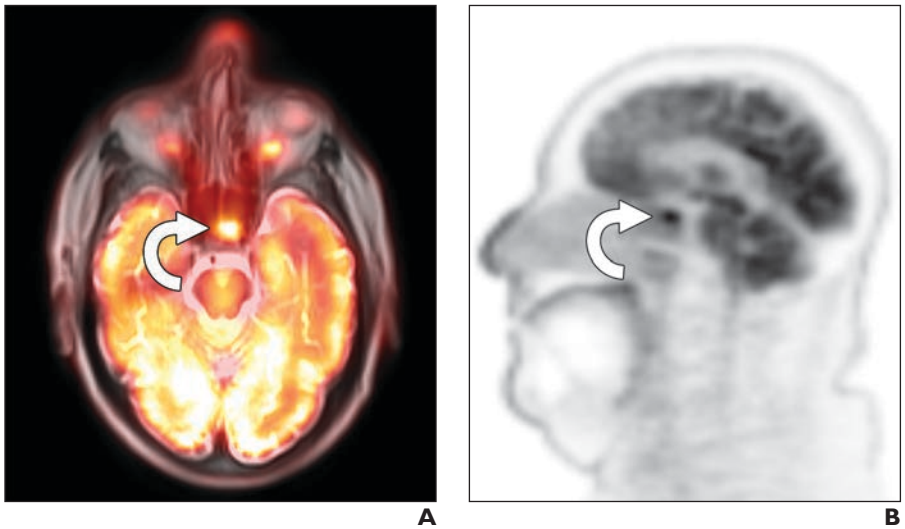

Fig. 1—79-year-old man with head and neck cancer.
A and **B,** PET/MRI axial fusion image with T1-weighted radial volumetric interpolated breath-hold examination fat suppression image (**A**) and PET sagittal image (**B**) show intense hypermetabolic focus representing pituitary adenoma (*arrows*).

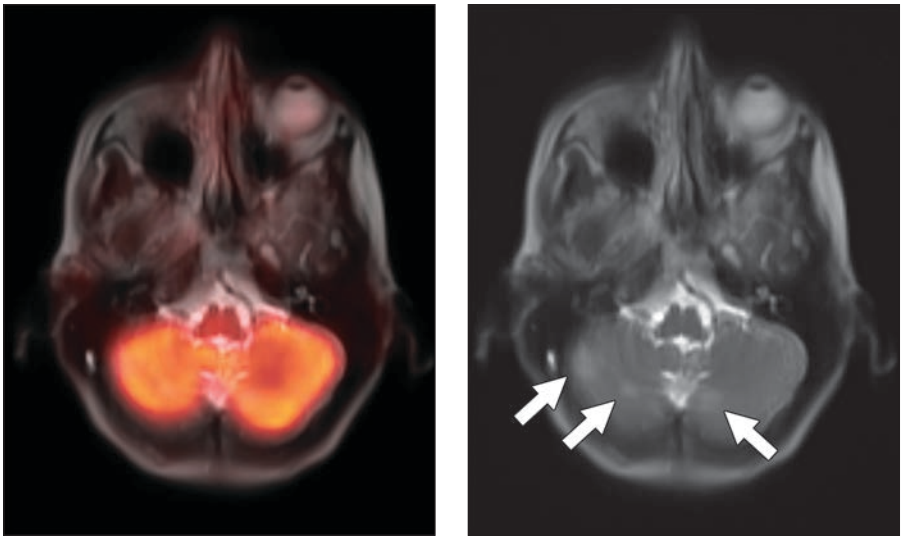

Fig. 2—54-year-old woman with breast cancer and no neurologic symptoms.
A, PET/MRI axial fusion image (**A**) shows no abnormal focal FDG uptake within cerebellum.
B, Axial T2-weighted HASTE MR image shows three new foci of hyperintensity within cerebellar hemispheres that were suspicious for metastases (*arrows*). Other suspicious cerebral lesions were seen. Follow-up dedicated brain MRI confirmed multiple cerebral metastases.

vealed leptomeningeal metastases, metabolic encephalopathy, Creutzfeldt-Jakob disease, primary cerebral lymphoma, and encephalitis. Five other patients had parenchymal cerebral metastases; two of these five patients received a diagnosis more than a year before undergoing PET/MRI examination, two patients were given a diagnosis 1–3 days before PET/MRI examination, and one patient had quiescent brain metastatic disease initially detected on the whole-body PET/MRI examination. In addition, two pituitary adenomas were newly diagnosed (Fig. 1). The mean age of the 12 patients with a serious nonvascular brain abnormality was 60.6 years.

Of the 269 patients evaluated, only nine patients (3.3%) had neurologic or cognitive symptoms suggestive of brain abnormality at the time of the examination. Of these patients, one patient had old craniotomy changes that did not explain the acute symptoms, whereas the others had either new or recently diagnosed brain abnormalities. Of the seven patients with malignant brain lesions, five had neurologic symptoms, including one new case of cerebral metastases found to be asymptomatic (Fig. 2). The patients with Creutzfeldt-Jakob disease, metabolic encephalopathy, and encephalitis had new symptoms for which they received treatment on the basis of PET/MRI findings noted in conjunction with dedicated brain MRI findings identified on the same day that the PET/MRI examination was performed. One patient had a recently identified subacute cerebral infarct that was originally thought to have been a malignant cerebral lesion on head CT; however, after PET/MRI, the lack of FDG uptake within the lesion forestalled a biopsy. In 4.1% of the patients, including whole-brain imaging resulted in either additional workup or a change in management (Table 3).

Perhaps the most significant example outlining the importance of including the head on routine whole-body PET/MRI was the case of a partially thrombosed, enlarging aneurysm that was detected in a 64-year-old woman with metastatic breast cancer. The patient had a history of whole-brain radiation therapy and was receiving systemic chemotherapy at the time of the whole-body PET/MRI examination. She had a known 1.0-cm aneurysm at the level of the left middle cerebral artery bifurcation. However, dedicated neuroradiologic review of PET/MRI sequences of the head and neck showed interval enlargement of the known aneurysm at the left middle cerebral artery bifurcation, along with an adjacent 2.2-cm rounded T1-hyperintense, T2-hypointense lesion with a peripheral rim of T2 hyperin-

TABLE 3: Summary of PET/MRI Brain Findings and Resulting Clinical Management

Patient Number	Age (y)	Sex	Study Indication	Neurologic Symptoms	Brain Finding	New Diagnosis	Clinical Management and Comments
1	71	M	Esophageal cancer	Asymptomatic	Chronic brain infarct	No	None
2	56	M	Paraneoplastic syndrome	Ataxic gait and disoriented	Leptomeningeal metastases	Yes	Intrathecal port for chemotherapy
3	87	F	Paraneoplastic syndrome	Confusion	Subacute cerebral infarct	Yes	Prevent biopsy; subacute infarct showed no activity
4	79	M	Colorectal cancer	Asymptomatic	Chronic subdural hematoma	Yes	None
5	63	M	Lymphoma	Tardive dyskinesia and neck twitching	Craniotomy	No	None
6	81	F	Breast cancer	Asymptomatic	Chronic microvascular disease	No	None
7	24	M	Lymphoma	Asymptomatic	Craniotomy	No	None
8	79	M	Head and neck cancer	Asymptomatic	Pituitary tumor	Yes	Neurosurgery consultation; no excision
9	55	M	Multiple myeloma	Asymptomatic	Chronic brain infarct	No	None
10	54	F	Breast cancer	Asymptomatic	Benign cystic lesion	No	None

(Table 3 continues on next page)

TABLE 3: Summary of PET/MRI Brain Findings and Resulting Clinical Management (continued)

Patient Number	Age (y)	Sex	Study Indication	Neurologic Symptoms	Brain Finding	New Diagnosis	Clinical Management and Comments
11	75	M	Lymphoma	Asymptomatic	Craniotomy with radiation changes	No	None
12	71	M	Head and neck cancer	Asymptomatic	Chronic microvascular disease	No	None
13	70	F	Breast cancer	Asymptomatic	Chemotherapy-related changes	No	None
14	76	M	Lymphoma	Asymptomatic	Chronic microvascular disease	No	None
15	47	F	Cancer of cervix	Asymptomatic	Craniotomy	No	None
16	82	F	Head and neck cancer	Asymptomatic	Chronic microvascular disease	No	None
17	55	F	Breast cancer	Asymptomatic	Chemotherapy-related changes	No	None
18	51	M	Paraneoplastic syndrome	Cognitive changes	Metabolic encephalopathy	Yes	Initiated glucosteroid therapy; brain MRI already scheduled
19	28	F	Breast cancer	Asymptomatic	Chemotherapy-related changes	No	None
20	56	F	Breast cancer	Asymptomatic	Benign cystic lesion	No	None
21	68	M	Paraneoplastic syndrome	Migraines and worsening balance	Creutzfeldt-Jakob disease	Yes	Immunoglobulin therapy; brain MRI already scheduled
22	78	M	Lung cancer	Asymptomatic	Radiation therapy changes	No	None
23	38	F	Cancer of cervix	Asymptomatic	Cerebellar lacunar infarct	Yes	None
24	85	F	Vulvar cancer	Asymptomatic	Chronic microvascular disease	No	None
25	51	F	Breast cancer	Asymptomatic	Pituitary tumor	Yes	None
26	68	F	Lymphoma	Asymptomatic	Chronic microvascular disease	No	None
27	64	F	Breast cancer	Asymptomatic	Brain parenchymal metastases	No	None; known lesions
28	65	F	Unknown primary	Word-finding difficulties	Brain parenchymal metastases	No	Resection of largest brain lesion; diagnosed 5 days earlier
29	78	F	Breast cancer	Asymptomatic	Chronic microvascular disease	No	None
30	53	M	Paraneoplastic syndrome	Right face numbness and dizziness	Primary cerebral lymphoma	Yes	Biopsy with treatment; prior misdiagnosis of multiple sclerosis
31	69	F	Lung cancer	Headaches and unusual behavior	Brain parenchymal metastases	No	None; known lesions
32	58	F	Breast cancer	Asymptomatic	Chronic microvascular disease	No	None
33	64	F	Breast cancer	Asymptomatic	Intracranial aneurysm and radiation changes	Yes	Coiling aneurysm; enlarging known lesion
34	54	F	Breast cancer	Asymptomatic	Brain parenchymal metastases	Yes	Dedicated brain MRI ordered; no additional therapy
35	78	F	Lung nodule	Asymptomatic	Cerebellar lacunar infarct	Yes	None
36	66	F	Breast cancer	Asymptomatic	Brain parenchymal metastases and brain infarct	No	Dedicated brain MRI ordered; no additional therapy
37	55	F	Paraneoplastic syndrome	Sensory and hearing loss	Encephalitis	Yes	Rituximab treatment; brain MRI already scheduled

tensity, which was concerning for subacute blood products within a pseudoaneurysm or walled-off intraparenchymal rupture of the aneurysm (Fig. 3). The patient underwent emergent neurosurgical evaluation as well as unenhanced head CT followed by CT angiography. The patient subsequently underwent successful balloon-and-stent–assisted coiling that resulted in complete occlusion of the enlarging aneurysm at the left middle cerebral artery bifurcation. Although this patient would have received routine brain imaging for evaluation of the aneurysm and metastatic brain disease, PET/MRI allowed intervention for this patient whose condition was asymptomatic before more serious effects occurred.

Of the 250 patients undergoing FDG PET/MRI of the body for staging or restaging of malignancy, 15 patients were undergoing dedicated brain MRI as part of routine cancer screening or for continued assessment of metastatic spread, including four of the six patients with lung cancer (67%) and 11 of the 72 patients with breast cancer (15.3%). The higher rate of brain imaging for patients with lung cancer reflects national cancer guidelines [8], whereas brain MRI is not routinely recommended for patients with breast cancer that is asymptomatic. However, a low threshold for ordering brain MRI is acceptable for patients with ErbB-2 (also known as HER2/neu)–positive advanced breast cancer because of the high incidence of brain metastases [9]. One patient with lymphoma underwent frequent brain MRI examinations to assess craniotomy changes, and another patient with multiple myeloma underwent frequent brain MRI examination to evaluate a chronic infarct.

When PET findings were compared with MRI findings, 38 of the 39 brain findings (97.4%) could be detected on the MR images alone. Eight of the 39 brain findings (20.5%) had abnormal areas of increased FDG uptake on PET images that indicated an underlying metabolic brain abnormality. Both pituitary adenomas had intense radiotracer uptake on PET images, whereas only one had a lesion detectable on the body MRI sequences. Three of the five cerebral metastases showed markedly increased FDG uptake, as did the case of primary cerebral lymphoma, whereas cases of leptomeningeal metastases showed only subtle abnormalities of PET that were difficult to detect without the fusion images. For the case of encephalitis, intense temporal lobe FDG uptake was seen. On PET images, two patients had cortical hypometabolism that was not related to posttherapy changes, including the patient with Creutzfeldt-Jakob disease, for whom markedly abnormal cortical and basal ganglia FDG uptake was seen on PET images, with increased signal observed on T2-weighted images within the basal ganglia. Also, the patient with metabolic encephalopathy had globally decreased cortical FDG uptake on PET images, with subcortical T2 hyperintensities seen on the corresponding MR images. The two patients with benign cystic brain lesions and the patient with the subdural hematoma had areas of absent FDG uptake that corresponded to their respective lesions on the PET portion of the study.

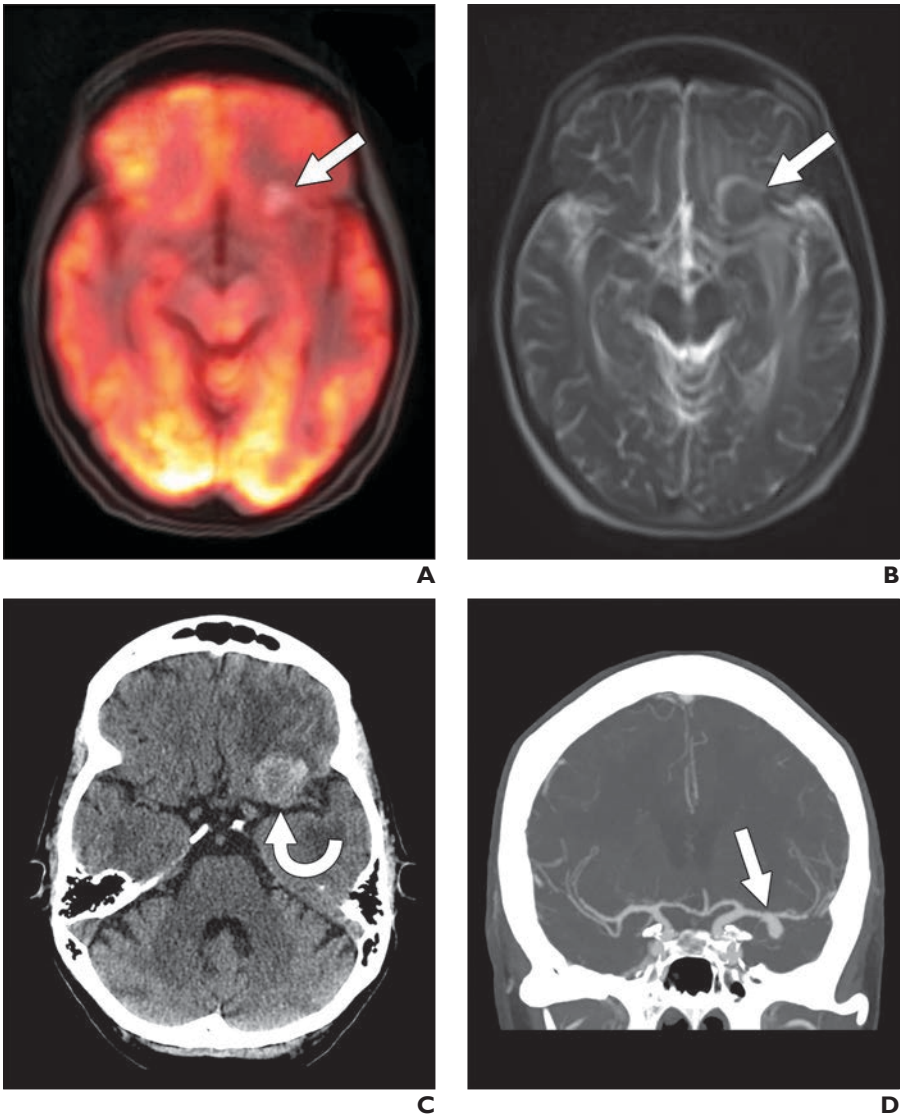

Fig. 3—64-year-old woman with metastatic breast cancer with history of brain metastases treated by whole-brain radiation therapy.
A, PET/MRI axial fusion image with T1-weighted radial volumetric interpolated breath-hold examination fat suppression shows new hyperintense lesion (*arrow*) in left frontal lobe region. No abnormal FDG activity is associated with this lesion.
B, Axial T2-weighted HASTE MR image shows 2.2-cm hypointense round lesion (*arrow*) with peripheral hyperintense rim that was concerning for subacute blood products. Cerebral edema from prior radiation therapy is also seen.
C, Axial unenhanced CT scan shows extraaxial hyperattenuated mass (*arrow*).
D, Coronal maximum-intensity-projection CT angiography image shows patent part of inferiorly oriented saccular aneurysm (*arrow*).

Discussion

On whole-body PET/CT and PET/MRI performed for oncologic evaluation, the patient is typically imaged from the base of the skull to the mid thigh. Only patients with ma-

lignant melanoma or cutaneous lymphoma are routinely imaged from the top of the head to the feet. Depending on the positioning of the patient and localization by the scout image, various portions of the brain may be included in the study because technologists use different anatomic landmarks for establishing the FOV and because head positioning may vary. Typically, only the bottom third of the brain is included on PET studies covering the base of the skull to the mid thigh.

For multiple reasons, the brain usually was not considered essential for inclusion on whole-body PET images. For example, the additional bed position required for the head added an extra 3–5 minutes of imaging time. Furthermore, the CT protocol used for oncologic PET/CT frequently involved a low dose and was not optimized for imaging the brain, compared with diagnostic head CT. The PET image acquisition time was also deemed inadequate for optimal brain viewing, including the detection of brain metastases [10].

With dedicated PET/MRI scanners, the patient receives no additional radiation other than the FDG dose. The only limiting factor is the time required to acquire additional images that include the brain. For the PET/MRI body imaging protocol, this may take only 3–5 minutes of additional time, depending on the protocol being used. Because of the limited number of sequences performed, the radiologist would require only 2–3 minutes to review the brain images. However, higher-resolution brain imaging, such as that used for dedicated brain MRI, would require 20–30 minutes of additional imaging time and 7–10 minutes for radiologist review.

The literature includes contradictory reports regarding inclusion of the whole brain as part of routine oncologic PET studies. For example, in a retrospective study of 1000 consecutive patients that included imaging of the top of the head with FDG PET/CT, Abdelmalik et al. [11] found that 102 patients (10.2%) had clinically significant findings above the base of the skull. Although 69% of these patients already had a known or suspected pathologic finding above the base of the skull, 31% of the patients had unsuspected abnormal findings, with most of the findings being brain metastases [11].

Contrary to the aforementioned findings, in a study by Tan and Chatterton [12], the value of an imaging protocol covering the area from the top of the head to the feet was compared with that of a protocol covering the area from the base of skull to the mid thigh in patients with malignant melanoma. Abnormal FDG uptake within the brain or scalp that might be suggestive of metastatic disease was seen on only 3% of the 398 PET/CT scans performed for 361 patients, with most scans showing disseminated metastatic disease. Only 1% of these patients had unexpected findings in the brain. Furthermore, none of the metastatic lesions were an isolated malignant deposit that would have changed patient management.

With the use of a routine body PET/CT protocol, Bochev et al. [13] studied 2502 patients with various cancers but no symptoms. MRI was used to confirm the presence of cerebral lesions. Bochev and colleagues found that 25 patients (1.0%) had brain metastases, with lung cancer occurring most often. The authors thought that the early and crucial information warranted the extra radiation dose and time associated with inclusion of the head in imaging [13]. The importance of finding brain metastases was also reflected in a recent study by Kung et al. [14], who reviewed 1876 patients who were undergoing PET/CT from the top of the head to the mid thigh. In that study, 71 patients (3.8%) were suspected of having brain metastases on the basis of PET/CT findings, and 40 patients (2.1%) were not previously known to have metastatic disease. Of the patients confirmed to have metastases, 94.1% had significant changes in clinical management, including whole-brain radiation therapy, craniotomy, and IV steroid treatment [14].

Although most articles evaluating incidental findings from PET/CT focus on PET abnormalities, several studies have also looked at the increased diagnostic accuracy of delineating structural findings on MRI sequences compared with CT images. In a study in which contrast-enhanced brain MRI was compared with dual-phase contrast-enhanced head CT, Davis et al. [15] found that the total number of lesions detected using MRI was much greater than that detected using CT (61 vs 37 lesions). In addition, PET/CT is not as sensitive for the detection of brain metastases when compared with dedicated brain MRI. For example, Kruger et al. [16] found the sensitivity of FDG PET/CT to be only 27% (specificity, 97.6%) when MRI was used as the reference standard. Rohren et al. [17] had better success, finding that FDG PET/CT had a sensitivity of 75% and a specificity 83% for the detection of cerebral metastases, with MRI as the reference standard.

Of the intracranial tumors found in the brain, metastases are by far the most common, with 15–40% of patients with cancer having brain metastases develop. However, most patients do not have symptoms, with only 8–10% of patients with cancer developing symptomatic brain lesions during their illness. The most common types of cancer that develop brain metastases are lung cancer (frequency, 40–50%), breast cancer (frequency, 15–25%), and malignant melanoma (frequency, 5–20%) [18, 19]. The distribution of brain metastases includes the cerebral hemispheres in 80% of cases and lesions in the cerebellum and the brainstem in 15% and 5% of cases, respectively. Common features of symptomatic brain metastases include headache, seizures, cognitive impairment, and neurologic deficits from brain tissue destruction or displacement, peritumoral edema, increased intracranial pressure, and vascular compromise [20].

In addition to brain parenchymal lesions, patients with systemic cancer often have other neurologic complications. Metabolic encephalopathy is a common cause of altered mental status. Patients may therefore present with stroke, hemorrhage, tumor vascular compression or invasion, tumor-induced coagulation disorders, radiation-induced brain injury, and chemotherapy-related neurologic side effects [21].

Incidental findings are not limited to patients with cancer. In a study of 2000 otherwise healthy subjects (mean age, 63.3 years) that evaluated the use of brain MRI, Vernooij et al. [22] found asymptomatic brain infarcts in 7.2% of subjects, cerebral aneurysms in 1.8%, and benign primary tumors (mainly meningiomas) in 1.6%. Similarly, Koppelmans et al. [23] assessed undetected brain abnormalities on MR images of 191 female long-term survivors of breast cancer. Of these subjects, 2.6% had aneurysms, 3.7% had meningiomas, and 1.6% had pituitary adenomas. Only pituitary adenomas had an incidence that was higher than that found in the general population [23]. Katzman et al. [24] performed brain MRI for 1000 volunteers without symptoms (age range, 3–83 years) and found incidental findings on the images of 18%, with 2.9% of all patients requiring a referral appointment. Findings included cysts, benign tumors, vascular abnormalities, and demyelinating disease, with microvascular disease and brain atrophy occurring in older patients.

In a study of 1006 patients that involved the use of brain MRI, Håberg et al. [25] found a much higher incidence of intracranial abnormalities (32.7%), 27.1% of which were incidental findings. The lesions included cysts (in 3.6% of patients), structural vascular abnormalities (1.9%), developmental variations (< 0.1%), excessive areas of signal hyperintensity in white matter (9.1%), tumors (1.4%), microhemorrhages (< 0.1%), infarctions (4.4%), and acquired brain abnormalities (1.0%), such as contusions or multiple sclerosis. Of the 1006 patients, 3.5% were referred for neurosurgical consultation, with 1.4% eventually undergoing an intracranial procedure [25]. Another study by Sandeman et al. [26] found that older patients had a higher rate of incidental brain findings, which included a higher incidence of prior infarcts or hemorrhage, areas of signal hyperintensity deep in the white matter, and cerebral atrophy.

In the present study, the shorter 5-minute acquisition time for PET/MRI limits the number and quality of MRI sequences that can potentially be performed, compared with the number and quality of those performed during a dedicated brain MRI study. In addition, dedicated PET of the brain involves a higher-resolution matrix (often 344 × 344 × 127) with a longer imaging time, which leads to better-quality images, when compared with the 172 × 172 × 515 matrix used in typical body PET acquisitions. For all the cerebral lesions identified on PET/MRI body sequences, there was a predominance of MRI findings over PET findings. In fact, for all the PET findings, with the exception of one pituitary adenoma, corresponding abnormalities were identified on body MRI sequences. Including brain MRI alone in the staging or restaging of cancer would identify most abnormalities without the need to perform the PET portion of the examination, although this would add an additional burden of time and cost to health care. The MRI findings were best identified on the T2-weighted HASTE sequence that had a slice thickness of 5 mm and was not optimized for evaluation of the brain parenchyma. The most clinically relevant findings were identified on both the PET and MRI portions of the examination. Of note, some incidental brain findings could be construed as either a benefit or a negative aspect of including the whole head on routine PET/MRI. Newly detected findings have the potential of increasing the cost of medical management without leading to patient benefit. One limitation of the present study is that there was a higher proportion of women included in the study, compared with men. In addition, the types of indications for obtaining whole-body PET/MRI studies, especially the types of cancers imaged, vary depending on the institution and referring clinicians involved. In the present study, a predominance of cervical cancer, breast cancer, and lymphoma was noted, which may not be reflective of cases at other institutions.

Conclusion

FDG PET/MRI is a new evolving modality that is most commonly used for staging and restaging of malignancy, as well as for other indications. The routine PET/MRI protocol that images the area from the skull base to the mid thigh may miss many important brain abnormalities that are easily detected with PET/MRI body sequences. These abnormalities could change patient management or alter patient prognosis. The amount of time required to include the entire head was only an additional 3–5 minutes of imaging time for the standard scan covering the skull base to the mid thigh, and the radiologist needed only 2–3 minutes to review the images. Dedicated brain radiofrequency coils were not required, and no additional radiation was accrued by its implementation. An FDG PET/MRI whole-body scan that includes the head provides added value to the management of these patients.

References

1. Paudyal B, Paudyal P, Oriuchi N, Tsushima Y, Nakajima T, Endo K. Clinical implication of glucose transport and metabolism evaluated by ^{18}F-FDG PET in hepatocellular carcinoma. *Int J Oncol* 2008; 33:1047–1054
2. Maher MM, Kalra MK, Singh A, et al. "Hot" spots in hybrid positron emission tomography/computed tomography scanning of the abdomen: protocols, indications, interpretation, responsibilities, and reimbursements. *Curr Probl Diagn Radiol* 2006; 35:35–54
3. Gorospe L, Raman S, Echeveste J, Avril N, Herrero Y, Herna Ndez S. Whole-body PET/CT: spectrum of physiological variants, artifacts and interpretative pitfalls in cancer patients. *Nucl Med Commun* 2005; 26:671–687
4. Matthews R, Choi M. Clinical utility of positron emission tomography magnetic resonance imaging (PET-MRI) in gastrointestinal cancers. *Diagnostics (Basel)* 2016; 6:E35
5. Rosenkrantz AB, Friedman K, Chandarana H, et al. Current status of hybrid PET/MRI in oncologic imaging. *AJR* 2016; 206:162–172
6. Niederkohr RD, Rosenberg J, Shabo G, Quon A. Clinical value of including the head and lower extremities in ^{18}F-FDG PET/CT imaging for patients with malignant melanoma. *Nucl Med Commun* 2007; 28:688–695
7. Deck MD, Henschke C, Lee BC, et al. Computed tomography versus magnetic resonance imaging of the brain: a collaborative interinstitutional study. *Clin Imaging* 1989; 13:2–15
8. Backhus LM, Farjah F, Varghese TK, et al. Appropriateness of imaging for lung cancer staging in a national cohort. *J Clin Oncol* 2014; 32:3428–3435
9. Ramakrishna N, Temin S, Chandarlapaty S, et al. Recommendations on disease management for patients with advanced human epidermal growth factor receptor 2-positive breast cancer and brain metastases: American Society of Clinical Oncology clinical practice guideline. *J Clin Oncol* 2014; 32:2100–2108
10. Hjorthaug K, Højbjerg JA, Knap MM, et al. Accuracy of ^{18}F-FDG PET-CT in triaging lung cancer patients with suspected brain metastases for MRI. *Nucl Med Commun* 2015; 36:1084–1090
11. Abdelmalik AG, Alenezi S, Muzaffar R, Osman MM. The incremental added value of including the head in ^{18}F-FDG PET/CT imaging for cancer patients. *Front Oncol* 2013; 3:71
12. Tan JC, Chatterton BE. Is there an added clinical value of "true" whole body ^{18}F-FDG PET/CT imaging in patients with malignant melanoma? *Hell J Nucl Med* 2012; 15:202–205
13. Bochev P, Klisarova A, Kaprelyan A, Chaushev B, Dancheva Z. Brain metastases detectability of routine whole body ^{18}F-FDG PET and low dose CT scanning in 2502 asymptomatic patients with solid extracranial tumors. *Hell J Nucl Med* 2012; 15:125–129
14. Kung BT, Auyong TK, Tong CM. Prevalence of detecting unknown cerebral metastases in fluorodeoxyglucose positron emission tomography/computed tomography and its potential clinical impact. *World J Nucl Med* 2014; 13:108–111
15. Davis PC, Hudgins PA, Peterman SB, Hoffman JC Jr. Diagnosis of cerebral metastases: double-dose delayed CT vs contrast-enhanced MR imaging. *AJNR* 1991; 12:293–300
16. Krüger S, Mottaghy FM, Buck AK, et al. Brain metastasis in lung cancer: comparison of cerebral MRI and ^{18}F-FDG-PET/CT for diagnosis in the initial staging. *Nuklearmedizin* 2011; 50:101–106
17. Rohren EM, Provenzale JM, Barboriak DP, Coleman RE. Screening for cerebral metastases with FDG PET in patients undergoing whole-body staging of non-central nervous system malignancy. *Radiology* 2003; 226:181–187

18. Barnholtz-Sloan JS, Sloan AE, Davis FG, Vigneau FD, Lai P, Sawaya RE. Incidence proportions of brain metastases in patients diagnosed (1973 to 2001) in the Metropolitan Detroit Cancer Surveillance System. *J Clin Oncol* 2004; 22:2865–2872
19. Schouten LJ, Rutten J, Huveneers HA, Twijnstra A. Incidence of brain metastases in a cohort of patients with carcinoma of the breast, colon, kidney, and lung and melanoma. *Cancer* 2002; 94:2698–2705
20. Eichler AF, Loeffler JS. Multidisciplinary management of brain metastases. *Oncologist* 2007; 12:884–898
21. Newton HB. Neurologic complications of systemic cancer. *Am Fam Physician* 1999; 59:878–886
22. Vernooij MW, Ikram MA, Tanghe HL, et al. Incidental findings on brain MRI in the general population. *N Engl J Med* 2007; 357:1821–1828
23. Koppelmans V, Schagen SB, Poels MM, et al. Incidental findings on brain magnetic resonance imaging in long-term survivors of breast cancer treated with adjuvant chemotherapy. *Eur J Cancer* 2011; 47:2531–2536
24. Katzman GL, Dagher AP, Patronas NJ. Incidental findings on brain magnetic resonance imaging from 1000 asymptomatic volunteers. *JAMA* 1999; 282:36–39
25. Håberg AK, Hammer TA, Kvistad KA, et al. Incidental intracranial findings and their clinical impact; the HUNT MRI Study in a general population of 1006 participants between 50-66 years. *PLoS One* 2016; 11:e0151080
26. Sandeman EM, Hernandez Mdel C, Morris Z, et al. Incidental findings on brain MR imaging in older community-dwelling subjects are common but serious medical consequences are rare: a cohort study. *PLoS One* 2013; 8:e71467

FDG PET/MRI for Visual Detection of Crossed Cerebellar Diaschisis in Patients With Dementia

Ana M. Franceschi, MD[1], Michael A. Clifton, MD, MSc[2], Kiyon Naser-Tavakolian, MD[2], Osama Ahmed, MD[2], Lev Bangiyev, DO[2], Sean Clouston, PhD[3], Dinko Franceschi, MD[2]

Nuclear Medicine · Original Research

Keywords

asymmetry, cerebellar diaschisis, dementia, PET/MRI

Submitted: Nov 25, 2019
Revision requested: Jan 2, 2020
Revision received: Feb 6, 2020
Accepted: Apr 25, 2020

The authors declare that they have no disclosures relevant to the subject matter of this article.

OBJECTIVE. Depressed regional metabolism and cerebellar blood flow may be caused by dysfunction in anatomically separate but functionally related regions, presumably related to disruption of the corticopontine-cerebellar pathway. The purpose of this study was to evaluate the prevalence of crossed cerebellar diaschisis (CCD) in patients undergoing ^{18}F-FDG PET/MRI for suspected neurodegenerative disease.

MATERIALS AND METHODS. In total, 75 patients (31 men, 44 women; mean age, 74 years) underwent hybrid FDG PET/MRI for clinical workup of neurodegenerative disease. Images were obtained with an integrated 3-T PET/MRI system. PET surface maps, fused T1-weighted magnetization-prepared rapid acquisition gradient echo and axial FLAIR/PET images were generated with postprocessing software. Two board-certified neuroradiologists and a nuclear medicine physician blinded to patient history evaluated for pattern of neurodegenerative disease and CCD.

RESULTS. Qualitative assessment showed that 10 of 75 (7.5%) patients had decreased FDG activity in the cerebellar hemisphere contralateral to the supratentorial cortical hypometabolism consistent with CCD. Six of the 10 patients had characteristic imaging findings of frontotemporal dementia (three behavioral variant frontotemporal dementia, two semantic primary progressive aphasia, and one logopenic primary progressive aphasia), three had suspected corticobasal degeneration, and one had Alzheimer dementia.

CONCLUSION. Our study results suggest that CCD occurs most commonly in frontotemporal dementia, particularly the behavioral variant, and in patients with corticobasal degeneration. Careful attention to cerebellar metabolism may assist in the clinical evaluation of patients with cognitive impairment undergoing FDG PET/MRI as part of their routine dementia workup.

Brain PET/MRI is a newer imaging modality that has advantages over PET/CT in the evaluation of patients with cognitive impairment who have suspected underlying dementia and neurodegenerative disease. Specifically, compared with CT, the structural MRI component has superior soft-tissue contrast, is free of radiation exposure, and yields more information about intrinsic tissue characteristics, improving anatomic accuracy. Furthermore, PET/MRI systems with simultaneous imaging capabilities allow PET and MRI acquisition in a single convenient session, affording precise image coregistration and improved anatomic localization. Additionally, hybrid imaging such as brain PET/MRI inherently promotes a more collaborative interpretation effort among radiologists, nuclear medicine physicians, and clinical subspecialists owing to the inherent complexity of the imaging modality and associated pathologic conditions. This collaboration encourages a multidisciplinary team approach to complex cases, especially those of patients with multiple comorbid conditions and complex differential diagnoses.

Crossed cerebellar diaschisis (CCD) is an imaging artifact present in patients with various supratentorial insults, including cerebral infracts, traumatic brain injury, and prior surgery. These insults may destroy the corticobulbar, corticopontine, or corticocerebellar fiber tracts. Subsequent transneural degeneration of the white matter tracts, specifically the corticocerebellar fibers, results in cerebellar parenchymal changes that are best visualized with functional PET and are typically occult on structural imaging studies [1–4].

[1]Department of Radiology, Neuroradiology Section, Donald and Barbara Zucker School of Medicine at Hofstra/Northwell Health, Manhasset, NY.

[2]Department of Radiology, SUNY Stony Brook, 101 Nicolas Rd, Stony Brook, NY, 11794. Address correspondence to M. A. Clifton (michael.clifton@stonybrookmedicine.edu).

[3]Department of Family, Population, and Preventive Medicine, SUNY Stony Brook, Stony Brook, NY.

doi.org/10.2214/AJR.19.22617
AJR 2021; 216:1–7
ISSN-L 0361–803X/21/2161–1

Traditionally, CCD was considered to be associated with a degree of hemiparesis at clinical examination. Pantano et al. [1], however, found that CCD may also be present in patients who do not have hemiparetic symptoms. Those authors suggested that destruction of the pyramidal tract alone is not sufficient for the development of CCD, nor, conversely, is it its sole clinical manifestation. Furthermore, in certain cases imaging findings of CCD were present on images hours after stroke and subsequently resolved, suggesting that with certain etiologic factors, there exists a window of reversibility for cerebellar diaschisis.

There are limited data on the prevalence of CCD in patients presenting with cognitive impairment due to suspected underlying dementia and neurodegenerative disease and the potential impact of CCD on progression of neurodegeneration and associated symptoms. In this study, we used hybrid ^{18}F-FDG PET/MRI of the brain to detect differences in cerebellar metabolism and patterns of asymmetric hypometabolism in the cerebral cortex in patients undergoing neuroimaging evaluation for clinically symptomatic cognitive impairment. We conducted a retrospective prevalence-based assessment for CCD. The results may further our understanding of the potential contribution of CCD to underlying neuronal demise in the various dementia subtypes.

Materials and Methods

This HIPAA-compliant retrospective study received local institutional review board approval. The requirement for written informed consent was waived because of the retrospective nature of this study.

Subjects

Among 175 patients initially identified, 75 patients (44 women, 31 men; mean age, 74 years) with clinically symptomatic neurodegenerative disorders were enrolled in our study from January 2015 to February 2019. All 75 subjects underwent FDG PET/MRI of the brain as part of their routine clinical workup for cognitive impairment and suspected neurodegenerative disease. The exclusion criteria were as follows: age younger than 18 years, clinical indication other than dementia, pregnancy, and fasting blood glucose level greater than 150 mg/dL. Additional technical exclusions were PET/MRI examination without dedicated brain sequences, deviation from standard protocol in image acquisition, and brain studies other than FDG PET/MRI.

Image Acquisition

Before imaging, an IV injection of approximately 5 mCi (185 MBq) of FDG was administered. After 40 minutes of uptake, the patient was positioned for brain imaging in a 3-T PET/MRI system (Biograph mMR, Siemens Healthcare) with a standard 12-channel head coil. A dual-echo T1-weighted gradient-recalled echo sequence was performed to acquire the MRI attenuation-correction map based on Dixon segmentation (air, fat, soft tissue, lungs). Emission data were collected for 20 minutes while dedicated brain MRI sequences were performed. PET data were reconstructed with an iterative 3D ordinary Poisson ordered subsets expectation maximization algorithm at three iterations and 21 subsets and with a 4-mm gaussian postreconstruction image filter. The PET image matrix size was 344 × 344 × 127 mm, and transaxial voxel dimensions were 1.04 × 1.04 mm with a thickness of 2.03 mm. Further postprocessing of PET images was performed with MIMneuro software (version 6.9.5, MIM Software).

MRI data included images from the skull vertex to the foramen magnum. Standard high-resolution 3D sagittal magnetization-prepared rapid acquisition gradient echo (MP-RAGE) and 3D FLAIR sequences were used to image the anatomic features of the brain. Afterward, routine diagnostic MRI sequences, including T2-weighted turbo spin-echo imaging in the axial and coronal planes, axial susceptibility-weighted imaging, diffusion-tensor imaging, axial proton density–weighted imaging, and DWI, were performed. Three-dimensional MP-RAGE image data were additionally postprocessed with NeuroQuant software (version 2019, CorTechs Laboratories) for semiquantitative volumetric analysis.

The sagittal 3D FLAIR fat-suppressed images were obtained with the following parameters: TR/TE, 5000/402; inversion time, 1800 ms; FOV, 250 × 250 mm; voxel size, 0.9 × 0.9 × 0.9 mm; slice thickness, 0.9 mm; acquisition time, 7 minutes. The 3D sagittal MP-RAGE sequence was performed with the following parameters: TR/TE, 1700/2.44; inversion time, 841 ms; FOV, 250 × 250 mm; voxel size, 1.0 × 1.0 × 1.0 mm; slice thickness, 1.0 mm; flip angle, 9°; acquisition time, 3 minutes 58 seconds. The MR-based attenuation-corrected PET sequence was performed with the following parameters: TR/TE 1, 3.6/1.23; TR/TE 2, 3.6/2.46; FOV, 500 × 500 mm; voxel size, 4.2 × 2.6 × 3.1 mm; slice thickness, 3.12 mm; flip angle, 10°; acquisition time, 19 seconds.

The diffusion-tensor imaging sequence was performed with the following parameters: TR/TE, 5600/90; FOV, 250 × 250 mm; voxel size, 2.0 × 2.0 × 4.0 mm; slice thickness, 4 mm; delay, 0 ms; acquisition time, 3 minutes 10 seconds.

Axial T2-weighted turbo spin-echo images were obtained with the following parameters: TR/TE, 4000/96.0; FOV, 230 × 230 mm; voxel size, 0.8 × 0.7 × 3.0 mm; slice thickness, 3.0 mm; delay, 0 ms; flip angle, 150°; acquisition time, 1 minute 12 seconds. The following parameters were used for coronal turbo spin-echo imaging: TR/TE, 4720/96.0; FOV, 230 × 230 mm; voxel size, 0.8 × 0.7 × 3.0 mm; slice thickness, 3.0 mm; delay, 0 ms; of flip angle, 150°; acquisition time, 1 minute 25 seconds.

Axial susceptibility-weighted imaging was performed at TR/TE, 26/20; FOV, 230 × 230 mm; voxel size, 0.8 × 0.7 × 1.3 mm; slice thickness, 1.3 mm; flip angle, 15°; acquisition time, 5 minutes 2 seconds. DW images were obtained at TR/TE, 7500/92.0; FOV, 240 × 240 mm; voxel size, 1.5 × 1.5 × 4.0 mm; slice thickness, 4.0 mm; delay, 0 ms; acquisition time, 2 minutes 8 seconds. Axial proton density–weighted images were obtained at TR/TE 1, 2800/10; TR/TE 2, 2800/93; FOV, 230 × 230 mm; voxel size, 0.9 × 0.9 × 3.0 mm; slice thickness, 3.0 mm; delay, 0 ms; flip angle, 150°; acquisition time, 2 minute 41 seconds.

Image Analysis

Two neuroradiology fellowship–trained board-certified radiologists with dedicated brain PET/MRI clinical and research experience independently reviewed the fused PET/MR images and classified each case according to subtype of neurodegenerative disease. Along with qualitative assessment, 3D MP-RAGE MR image data were additionally evaluated by means of quantitative volumetric analysis with NeuroQuant software (version 2019, CorTechs Laboratories). This U.S. Food and Drug Administration–cleared program is used to analyze intracranial volume and com-

pare these volumes with those in a normative database. The program compares lobar and sublobar cortical volumes with data in a standardized database, adjusted for age, sex, and volume status. Regions of parenchymal volume loss greater than 2 SD from that of healthy control subjects in the standardized atlas were flagged as abnormal. Quantitative percentages were assigned to lobar and sublobar areas to quantify the extent of parenchymal volume loss. The software provides semiquantitative data regarding the aforementioned variables and does not provide a dementia diagnosis.

One nuclear medicine physician with 25 years of experience in brain PET used MIMneuro 6.9.5 (MIM Software) to review the PET portion of the study with additional cortical surface map reconstructions (qualitative assessment) and semiquantitative *z*-score analysis of brain hypometabolism. This program runs a region-based analysis that calculates *z* scores (number of SD from the mean) and asymmetry measurements for individual brain regions defined by the single brain atlas and MIM probabilistic anatomic atlas to perform semiquantitative analysis of brain hypometabolism. According to the manufacturer, the single brain atlas and MIM probabilistic anatomic atlas are composed of 43 individuals (19 women, 24 men; age range, 41–80 years; mean, 63.8 ± 9.98 [SD] years). The distribution of the normal age-based atlas is as followed: six subjects 40–49 years old, eight subjects 50–59 years old, 14 subjects 60–69 years old, 14 subjects 70–79 years old, and one subject 80–89 years old. The automated z scores were calculated by comparing the patient to the selected age-matched set of healthy control subjects (within 5 years of the patient's age). The MIMneuro software performs semiquantitative *z*-score analysis of the aforementioned variables and does not provide a dementia diagnosis.

All three readers separately scored the supratentorial brain parenchymal FDG uptake as follows: symmetric, asymmetric left greater than right, and asymmetric right greater than left. After supratentorial analysis, cerebellar FDG uptake was also independently scored as symmetric versus asymmetric and specifically evaluated for the presence of CCD. Any discrepancy was resolved by secondary consensus review among the three readers. Interreader agreement was evaluated with Cohen kappa coefficient for readers 1 versus 2, readers 1 versus 3, and readers 2 versus 3.

Results

Qualitative assessment of images revealed that 19 subjects had imaging findings typical of frontotemporal dementia (FTD) (nine, behavioral variant FTD; six, semantic variant primary progressive aphasia (PPA); three, logopenic variant PPA; one, agrammatic variant PPA); 12 had Alzheimer disease; 10 had Lewy body dementia; 12 had corticobasal degeneration; and two had progressive supranuclear palsy. Characteristic structural and functional PET/MRI findings for each dementia subtype [5, 6] are outlined in Table 1. All three readers agreed on identification of 65 cases of symmetric cerebellar FDG uptake and 10 cases of cerebellar diaschisis. The Cohen kappa coefficient for interreader reliability indicated perfect agreement ($\kappa = 1$) for all combinations of readers (1 vs 2, 1 vs 3, and 2 vs 3).

Ten of 75 (7.5%) subjects also had hypometabolism within the cerebellar hemisphere contralateral to the side of supratentorial cortical hypometabolism, findings compatible with associated CCD. Initial interreader agreement on detection of CCD is depicted in Table 2. The results of assessment of interreader reliability for detection of asymmetric supratentorial hypometabolism are shown in Table 3.

The underlying neurodegenerative disorders in the 10 patients with CCD were distributed as follows: six, suspected FTD (specifically, three behavioral variant FTD; two, semantic PPA; one, logopenic PPA), three, corticobasal degeneration; one, Alzheimer disease. Figure 1 shows serial fused FDG PET and axial FLAIR MR images of a 73-year-old woman with metabolic and structural imaging find-

TABLE 1: Brain FDG PET Hypometabolism and Structural MRI Findings in Neurodegenerative Disorders

Dementia Subtype	Region of Hypometabolism According to FDG PET	Structural MRI Finding
Behavioral variant frontotemporal dementia	Frontal and anterior temporal lobe	Volume loss in the frontal and to a lesser degree temporal lobes
	Anterior cingulate gyrus	
Primary progressive aphasia		
Semantic variant	Asymmetric involvement of the temporal poles	Volume loss in temporal lobe (left greater than right, anterior greater than posterior)
	Predilection for the left temporal lobe or pole	Hippocampal atrophy (left greater than right)
Logopenic variant	Left lateral temporoparietal regions	Volume loss in left temporal and parietal lobes
	Supramarginal and angular gyri of parietal lobe and superior temporal gyrus	
Agrammatic variant	Predominant left posterior frontoinsular	Volume loss in the left posterior frontoinsular cortex
Alzheimer dementia	Bilateral parietotemporal (including precuneus)	Volume loss in parietotemporal (precuneus) and mesial temporal lobes
	Posterior cingulate gyrus	
	Mesial temporal lobe (hippocampus and entorhinal cortex)	

(Table 1 continues on next page)

TABLE 1: Brain FDG PET Hypometabolism and Structural MRI Findings in Neurodegenerative Disorders (continued)

Dementia Subtype	Region of Hypometabolism According to FDG PET	Structural MRI Finding
Lewy body dementia	Bilateral parietotemporal	Overlap with Alzheimer dementia with volume loss involving parietotemporal lobe
	With or without basal ganglia	Absent swallow tail sign (loss of expected hyperintensity in nigrosome 1 of substantia nigra) highly specific on susceptibility weighted imaging
	Symmetric mesial occipital lobe	
Corticobasal degeneration	Asymmetric frontal, parietotemporal, and occipital lobes of a single cerebral hemisphere	Pronounced asymmetric volume loss in posterior frontoparietal region of a single cerebral hemisphere
	Asymmetric subcortical structures (ipsilateral basal ganglia, thalamus)	Asymmetric ipsilateral primary sensorimotor cortex
	Asymmetric primary sensorimotor cortex	
Progressive supranuclear palsy	Paramedian frontal lobes	Midbrain atrophy
	Anterior cingulate gyrus	Possible absent swallow tail sign (seen in atypical parkinsonian syndromes)
	Basal ganglia and midbrain	

TABLE 2: Interreader Agreement on Detection of Asymmetric Supratentorial Hypometabolism

Outcome	Reader 1	Reader 2	Reader 3
No asymmetry in cortical FDG uptake	51	37	40
Left greater than right hypometabolism	20	33	30
Right greater than left hypometabolism	4	5	5

Note—Values are numbers of subjects.

TABLE 3: Interreader Reliability in Assessment of Hypometabolic Supratentorial Asymmetry

Comparison	Reader Agreement (%)	Cohen κ
Reader 1 vs reader 2	81.3	0.62
Reader 1 vs reader 3	85.3	0.70
Reader 2 vs reader 3	96.0	0.92

ings suggestive of underlying behavioral variant FTD with associated CCD. Specifically, the FDG distribution pattern was abnormal with substantially decreased radiotracer uptake primarily in the right frontal lobe and to a lesser degree in the right temporal lobe, including the anterior cingulate gyrus, with corresponding striking hypometabolism in the contralateral left cerebellar hemisphere. These findings were consistent with CCD.

Figure 2 shows serial fused FDG PET and axial FLAIR MR images of a 75-year-old man with metabolic and structural imaging findings suggestive of underlying corticobasal degeneration and associated CCD. Specifically, the FDG distribution pattern was abnormal with striking hemispheric asymmetry and decreased radiotracer uptake in nearly the entire left cerebral hemisphere. Marked hypometabolism was evident, particularly in the left frontoparietal region, including the sensorimotor cortex. Decreased uptake was also evident in the ipsilateral left basal ganglia and left thalamus. There was corresponding hypometabolism in the contralateral right cerebellar hemisphere. These findings were compatible with CCD.

Discussion

Recognizing that little is known about CCD in the context of geriatric cognitive impairment due to underlying neurodegenerative disease, we conducted a retrospective qualitative analysis of a large database of patients with various dementia subtypes to evaluate for the prevalence of CCD. Our results indicate that CCD is most commonly present in patients with behavioral variant FTD and to a lesser extent corticobasal degeneration. Our study addressed the potential of routine assessment of cerebellar metabolism patterns and asymmetry in supratentorial tracer uptake in the evaluation of patients with cognitive impairment undergoing hybrid FDG PET/MRI of the brain as part of the diagnosis of dementia.

Data in the literature on cerebellar FDG abnormalities in patients with neurodegenerative disease are limited. Akiyama et al. [2] were the first to evaluate for the presence of crossed cerebellar and uncrossed basal ganglia and thalamic diaschisis by means of FDG PET. Their study included 26 patients with clinically diagnosed and pathologically proven Alzheimer disease and nine age-matched control subjects. They calculated asymmetry indexes of cerebral metabolic rate for matched left-right ROIs and used them to determine the extent of diaschisis by means of correlative analyses. In the group with Alzheimer disease, cerebellar asymmetry indexes correlated negatively and thalamic asymmetry indexes positively with those of the cerebral hemisphere and frontal, temporal, parietal, and angular cortexes. Basal ganglia asymmetry indexes correlated positively with frontal cortical asymmetry index. The only significant correlation of asymmetry

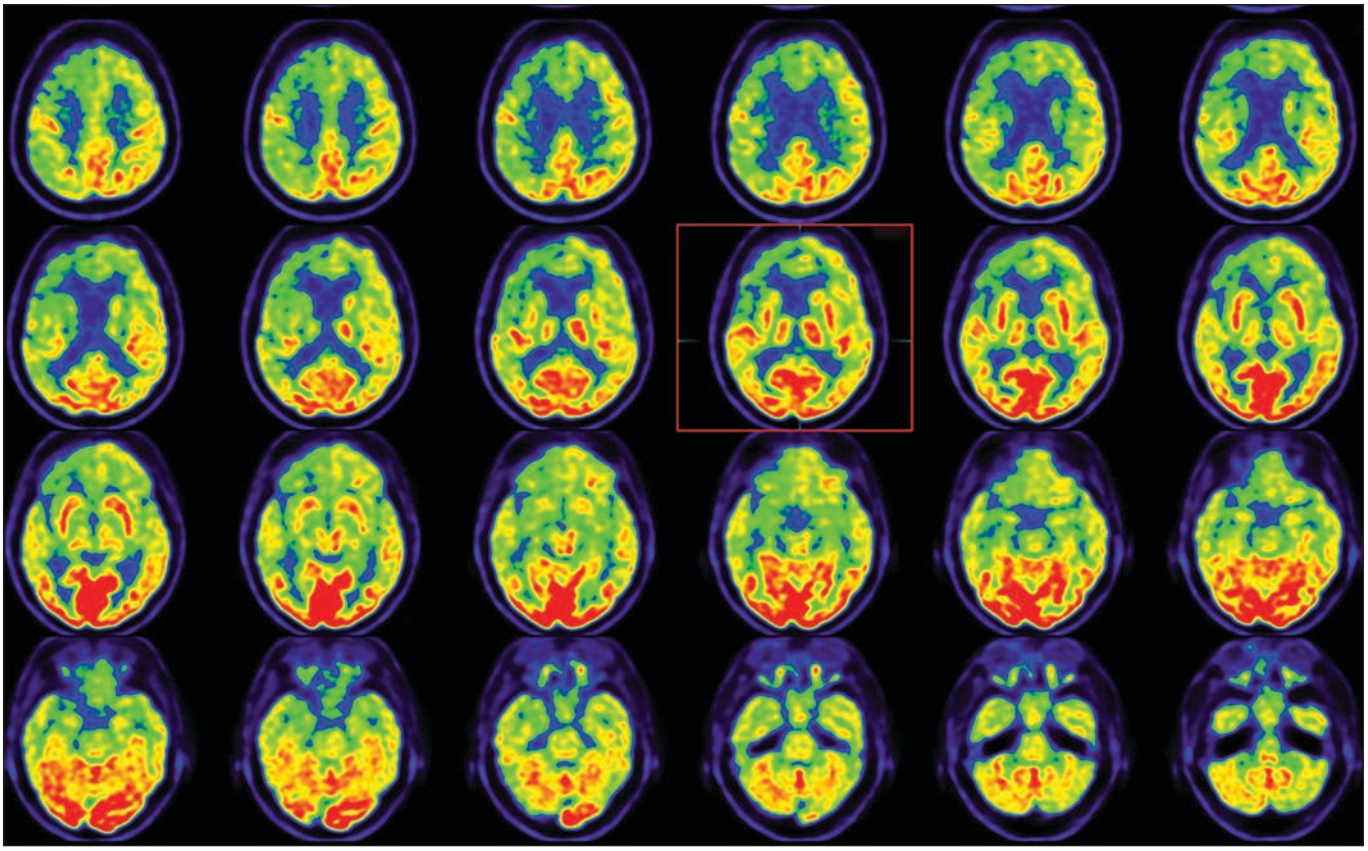

Fig. 1—73-year-old woman with behavioral variant frontotemporal dementia. Axial fusion PET and FLAIR MR images show abnormal FDG distribution and decreased radiotracer uptake primarily in right frontal lobe and striking hypometabolism in contralateral left cerebellar hemisphere. Findings are consistent with crossed cerebellar diaschisis. Red box indicates dominant clinical image with findings suggestive of behavioral variant frontotemporal dementia. There is marked asymmetrical hypometabolism within frontal and temporal lobes.

indexes for healthy subjects was between the thalamus and cerebral hemisphere.

Prior studies [1, 3] have shown that after stroke, the cerebellum undergoes reduction in metabolism and blood flow in the cerebellar hemisphere contralateral to the destructive cerebral lesion. Previous reports have also shown that electrical stimulation of the fastigial nucleus can improve symptoms of vascular dementia. Taken together, the empirical evidence seems to suggest that the cerebellum plays a role in the regulation of vascular dementia, and special attention should be paid to cerebellar FDG uptake patterns in these patients [3]. Additionally, a 2014 case report outlining the FDG hypometabolism pattern in a patient with Lewy body dementia [4] described marked hypometabolism in the occipital lobes (left greater than right) with associated decreased FDG uptake in the right cerebellar hemisphere, presumably related to disruption of the corticopontine-cerebellar pathway.

There are also few reports in the literature on hemispheric differences in FDG uptake patterns, specifically left versus right asymmetry in cortical metabolism in patients with neurodegenerative disease. Murayama et al. [7] reported on 36 patients with Alzheimer disease and amnestic mild cognitive impairment. The patients were divided into three groups according to FDG avidity (left-dominant hypometabolism, right-dominant hypometabolism, and nondominant hypometabolism) based on hemispheric asymmetries of decreases in cerebral metabolic rate of glucose consumption in the posterior cingulate cortex, precuneus, and parietotemporal cortex. The left-dominant hypometabolism group had significantly lower scores in verbal memory than the other two groups and also were more likely to have their condition diagnosed as Alzheimer dementia rather than amnestic mild cognitive impairment. Jeong et al. [8] used voxel-wise analysis with statistical parametric mapping to compare regional metabolic patterns on FDG PET of 29 patients with FTD and 11 healthy subjects. The hemispheric asymmetry of hypometabolism (more frequently lateralized to the left) was more common in patients with FTD, which may aid in differentiating FTD from Alzheimer disease and other causes of dementia if there is clinical uncertainty.

Several publications have also described hemispheric asymmetry patterns in various dementia syndromes based on results of structural volumetric analysis. For example, Whitwell et al. [9] reported on frontal lobe asymmetry in 80 patients with behavioral variant FTD and evaluated for associations between clinical, imaging, pathologic, and genetic features. Most of the patients (65%) had a symmetric pattern; 20%, asymmetric left; and 15%, asymmetric right. There were no significant clinical differences across groups, although a trend toward greater behavioral disinhibition was noted in patients with a right asymmetric pattern. Furthermore, genetic features differed across groups with sym-

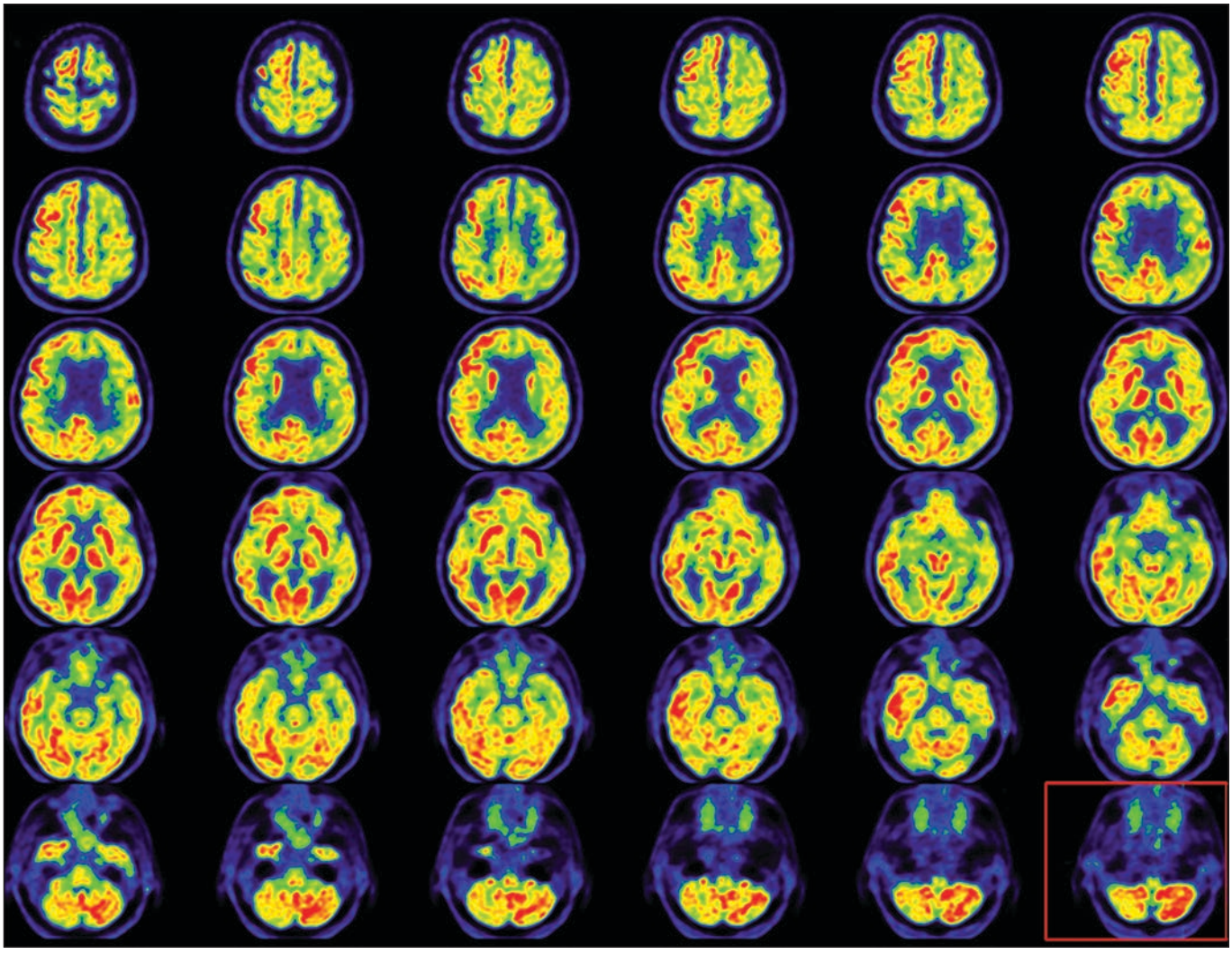

Fig. 2—75-year-old man with corticobasal degeneration. Axial fusion PET and FLAIR images show abnormal FDG distribution pattern, hemispheric asymmetry, and decreased radiotracer uptake in nearly entire left cerebral hemisphere. Marked hypometabolism is evident, particularly in left frontoparietal region, as is decreased uptake in ipsilateral left basal ganglia and left thalamus. Corresponding hypometabolism is present in contralateral right cerebellar hemisphere. Findings are compatible with crossed cerebellar diaschisis. Red box indicates dominant clinical image of marked hypometabolism in cerebellum. There is asymmetry of radiotracer uptake consistent with crossed cerebellar diaschisis.

metric frontal lobes associated with *C9ORF72* and tau mutations, and asymmetric frontal lobes were more commonly associated with progranulin mutations.

Thompson et al. [10] reported on behavioral-cognitive implications of left-right asymmetry of temporal lobe atrophy in 47 patients with semantic dementia. The frequency of several symptoms differed significantly between left and right temporal variants of the disease. Social awkwardness, job loss, loss of insight, and difficulty with person identification were more likely to be associated with major right temporal atrophy. Word-finding difficulties and reduced comprehension were more salient features of left-dominant temporal lobe atrophy. Both groups had deficits in semantic memory tests, but several items yielded greater impairment for patients with left-dominant temporal atrophy.

Finally, Rogalski et al. [11] reported on patterns of asymmetry in cortical decline as characterized by changes in cortical thickness and volume loss and neuropsychological performance in 26 patients who fulfilled criteria for logopenic (eight patients), agrammatic (10 patients), or semantic primary progressive aphasia (eight patients). Progression in cortical volume loss for each of the three subtypes showed left greater than right hemispheric asymmetry, and progression was greater within the language network, suggesting that preferential neurodegeneration of the left hemisphere language network is a common denominator for all three PPA subtypes.

In our study, the key finding in patients with cognitive impairment undergoing clinical FDG PET/MRI neuroimaging as part of their routine dementia workup is an expected association of asymmetric supratentorial hypometabolism in patients with CCD. This imaging finding has been well documented in patients with supratentorial cerebral infarcts, traumatic brain injury, and prior surgery. Our findings, however, indicate that CCD may often be present in patients presenting with underlying neurodegenerative disease.

The SUV ratio is a typical value used in PET to derive radioactivity concentration as a ratio of concentrated radioactivity versus whole body concentration [12]. Traditional SUV calculations include administered dose (megabecquerels) and body weight (kilograms) measurements, although some institutions have replaced body weight calculations with lean body weight or body surface area, but that remains institution specific [13].

Typical brain PET relies heavily on cerebellar uptake as the standardized reference region. Our results, however, suggest that abnormal cerebellar uptake patterns are present in 10% of patients with clinical dementia. This imaging finding is consistent with those of previous studies; however, we are practically intrigued by the prevalence of CCD in various neurodegenerative diseases. CCD as an imaging finding likely represents macroscopic tissue atrophy and subsequent degeneration of corticocerebellar tracts. As the supratentorial upper motor neurons undergo insult, the lower motor neurons lose their neurotropic effect on the cerebellum. Severing the upper motor neuron connection could lead to loss of neurotropic stimulation, loss of intracellular signaling to maintain neuronal function, and tissue atrophy [14]. This could manifest as asymmetric decreased SUV ratio within the cerebellum and subsequent development of CCD. Future work is needed to further characterize the intracellular signaling abnormalities and the extent to which CCD biases SUV ratio–based quantification in clinical neuroimaging studies.

Limitations

Although this study is the first, to our knowledge, to effectively examine findings of CCD in the context of neurodegenerative disorders in a clinical setting, limitations include a fairly heterogeneous dataset, retrospective nature, and limited availability of long-term patient follow-up to assess for morbidity and mortality, including potential clinical impact of CCD-type pathologic conditions. Our future work will focus on further elucidating the impact of cerebellar diaschisis and hemispheric asymmetry on clinical presentation, neurologic and neurocognitive assessment, and disease progression in patients with neurodegenerative disease, with a special focus on the FTD subtypes and patients with corticobasal degeneration.

Conclusion

Patients with cognitive impairment who undergo FDG PET/MRI of the brain as part of their clinical dementia workup need a focused assessment of the cerebellum for the presence of CCD, in particular when findings suggest an asymmetric supratentorial hypometabolism pattern. To elicit further clinical implications of these findings, follow-up PET/MRI neuroimaging is needed to fully characterize the progression of clinically symptomatic supratentorial neurodegenerative disorders with associated diaschisis.

References

1. Pantano P, Baron JC, Samson Y, Bousser MG, Derouesne C, Comar D. Crossed cerebellar diaschisis: further studies. *Brain* 1986; 109:677–694
2. Akiyama H, Harrop R, McGeer PL, Peppard R, McGeer EG. Crossed cerebellar and uncrossed basal ganglia and thalamic diaschisis in Alzheimer's disease. *Neurology* 1989; 39:541–548
3. Sui R, Zhang L. Cerebellar dysfunction may play an important role in vascular dementia. *Med Hypotheses* 2012; 78:162–165
4. Al-Faham Z, Zein RK, Wong CY. ^{18}F-FDG PET assessment of Lewy body dementia with cerebellar diaschisis. *J Nucl Med Technol* 2014; 42:306–307
5. Brown RK, Bohnen NI, Wong KK, Minoshima S, Frey KA. Brain PET in suspected dementia: patterns of altered FDG metabolism. *RadioGraphics* 2014; 34:684–701
6. Broski SM, Hunt CH, Johnson GB, Morreale RF, Lowe VJ, Peller PJ. Structural and functional imaging in parkinsonian syndromes. *RadioGraphics* 2014; 34:1273–1292
7. Murayama N, Ota K, Kasanuki K, et al. Cognitive dysfunction in patients with very mild Alzheimer's disease and amnestic mild cognitive impairment showing hemispheric asymmetries of hypometabolism on ^{18}F-FDG PET. *Int J Geriatr Psychiatry* 2016; 31:41–48
8. Jeong Y, Cho SS, Park JM, et al. ^{18}F-FDG PET findings in frontotemporal dementia: an SPM analysis of 29 patients. *J Nucl Med* 2005; 46:233–239
9. Whitwell JL, Xu J, Mandrekar J, et al. Frontal asymmetry in behavioral variant frontotemporal dementia: clinicoimaging and pathogenetic correlates. *Neurobiol Aging* 2013; 34:636–639
10. Thompson SA, Patterson K, Hodges JR. Left/right asymmetry of atrophy in semantic dementia: behavioral-cognitive implications. *Neurology* 2003; 61:1196–1203
11. Rogalski E, Cobia D, Martersteck A, et al. Asymmetry of cortical decline in subtypes of primary progressive aphasia. *Neurology* 2014; 83:1184–1191
12. Zasadny KR, Wahl RL. Standardized uptake values of normal tissues at PET with 2-[fluorine-18]-fluoro-2-deoxy-D-glucose: variations with body weight and a method for correction. *Radiology* 1993; 189:847–850
13. Oikonen V. Standardized uptake value (SUV). Turku PET Centre website. www.turkupetcentre.net/petanalysis/model_suv.html. November 11, 2008. Accessed August 26, 2020
14. Furmaga H, Carreno FR, Frazer A. Vagal nerve stimulation rapidly activates brain-derived neurotrophic factor receptor TrkB in rat brain. *PLoS One* 2012; 7:e34844

Published July 14, 2016 as 10.3174/ajnr.A4865

Optimized, Minimal Specific Absorption Rate MRI for High-Resolution Imaging in Patients with Implanted Deep Brain Stimulation Electrodes

A.M. Franceschi, G.C. Wiggins, A.Y. Mogilner, T. Shepherd, S. Chung, and Y.W. Lui

ABSTRACT

BACKGROUND AND PURPOSE: Obtaining high-resolution brain MR imaging in patients with a previously implanted deep brain stimulator has been challenging and avoided by many centers due to safety concerns relating to implantable devices. We present our experience with a practical clinical protocol at 1.5T by using 2 magnet systems capable of achieving presurgical quality imaging in patients undergoing bilateral, staged deep brain stimulator insertion.

MATERIALS AND METHODS: Protocol optimization was performed to minimize the specific absorption rate while providing image quality necessary for adequate surgical planning of the second electrode placement. We reviewed MR imaging studies performed with a minimal specific absorption rate protocol in patients with a deep brain stimulator in place at our institution between February 1, 2012, and August 1, 2015. Images were reviewed by a neuroradiologist and a functional neurosurgeon. Image quality was qualitatively graded, and the presence of artifacts was noted.

RESULTS: Twenty-nine patients (22 with Parkinson disease, 6 with dystonia, 1 with essential tremor) were imaged with at least 1 neuromodulation implant in situ. All patients were imaged under general anesthesia. There were 25 subthalamic and 4 globus pallidus implants. Nineteen patients were preoperative for the second stage of bilateral deep brain stimulator placement; 10 patients had bilateral electrodes in situ and were being imaged for other neurologic indications, including lead positioning. No adverse events occurred during or after imaging. Mild device-related local susceptibility artifacts were present in all studies, but they were not judged to affect overall image quality. Minimal aliasing artifacts were seen in 7, and moderate motion, in 4 cases on T1WI only. All preoperative studies were adequate for guidance of a second deep brain stimulator placement.

CONCLUSIONS: An optimized MR imaging protocol that minimizes the specific absorption rate can be used to safely obtain high-quality images in patients with previously implanted deep brain stimulators, and these images are adequate for surgical guidance.

ABBREVIATIONS: DBS = deep brain stimulator; RF = radiofrequency; SAR = specific absorption rate

Deep brain stimulation is an effective treatment for medically refractory movement disorders, including Parkinson disease, essential tremor, and dystonia. Imaging plays a critical role in stereotactic targeting and long-term assessment. Preoperative MR images routinely used for deep brain stimulator (DBS) placement guidance include a high-resolution T1-weighted sequence used to identify standard anatomic landmarks such as the anterior/posterior commissures and high-resolution T2-weighted MR imaging routinely used to target the subthalamic nucleus, the most common structure targeted in deep brain stimulation for Parkinson disease. For patient safety and to judge treatment efficacy, placing bilateral leads in staged unilateral procedures can be advantageous. Due to the precision required for stereotaxis and the size of the anatomic structures (Fig 1), immediate preoperative imaging is the standard of care. When staged procedures are used, this necessitates imaging with 1 electrode in place for subsequent placement of the second electrode. Additionally, electrode-in imaging may be required to assess lead placement. Manufacturer's guidelines for performing MR imaging with DBSs in situ are extremely conservative; this feature makes acquiring diagnostic and therapeutic imaging in these patients challenging.

The recommended head specific absorption rate (SAR) limit for Medtronic DBS systems (Medtronic, Minneapolis, Minnesota) has been 0.1 W/kg (compared with the usual normal mode,

Received November 18, 2015; accepted after revision May 4, 2016.

From the Departments of Radiology (A.M.F., G.C.W., T.S., S.C., Y.W.L.) and Neurosurgery (A.Y.M.), New York University School of Medicine, New York, New York.

Please address correspondence to Yvonne W. Lui, MD, Department of Neuroradiology, 660 First Ave, 2nd Floor, New York, NY 10016-6481; e-mail: Yvonne.lui@nyumc.org

http://dx.doi.org/10.3174/ajnr.A4865

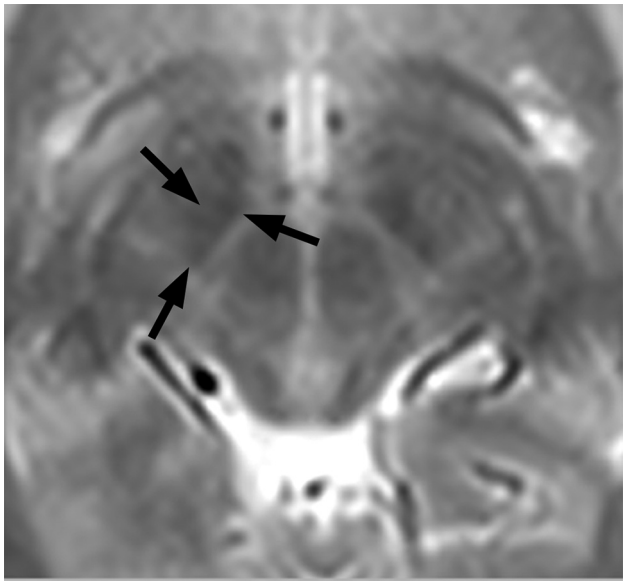

FIG 1. The smallest of the basal ganglia nuclei can be delineated on appropriate T2-weighted imaging through a region just cephalad to the midbrain. The subthalamic nucleus, a frequent target for deep brain stimulation, is outlined by *arrows* on the patient's right.

which calls for SAR < 3.2 W/kg). These devices are rated conditional at 1.5T. The main safety concern is heating the electrode due to energy deposition, and a few prior complications have been reported in the literature[1,2]; however, Larson et al[3] described 405 patients imaged with implanted DBS systems by using a variety of different scanning protocols, and their review suggests that a head SAR up to 3.0 W/kg may be applied without untoward incidents. Other potential interactions between MR imaging and implantable neuromodulators include magnetic field interactions, induced stimulation, effects on neurostimulator function, and artifacts from the device. In a single published article, Sarkar et al[4] reported being able to achieve diagnostic quality within the manufacturer's SAR limit with research 3D spin-echo sequences. The research sequences used in that study are not universally available, and the method they used most likely underestimated the loss of the signal-to-noise ratio. There is no clear consensus in the literature as to the optimal SAR and MR imaging parameters for safe imaging of patients with DBS electrodes.

The purpose of this study was to describe our experience with an MR imaging protocol by using product sequences, optimized for both therapeutic image quality in patients with implanted DBS electrodes and low SAR on 1.5T clinical scanners.

MATERIALS AND METHODS

The study was approved by the institutional review board, and the imaging protocol was approved by the institutional MR imaging safety committee.

Patients

Patients with neuromodulation devices, including Itrel II Model 7424, Soletra Model 7426, Kinetra Model 7428, Activa PC Model 37601, Activa RC Model 37612, Activa SC Model 37602, Activa SC Model 37603 (Medtronic), referred by the Center for Neuromodulation at the New York University Department of Neurosurgery for MR imaging, were included in this protocol. Patients with bilateral DBS devices all had separate pacemakers, separated by 6 cm.

Protocol Optimization

Axial T1-weighted magnetization prepared rapid acquisition of gradient echo is an intrinsically low-SAR sequence and requires little optimization. SAR-limited T2-weighted protocols were constructed by varying TRs, resolutions, flip angles, and radiofrequency (RF) pulse types. Use of the manufacturer-supplied low-SAR RF pulse reduced the SAR to 58% of the value with the default RF pulse. The target resolution to provide diagnostic information was 1 mm in-plane with a 2.5-mm section. The applied strategy was to keep TEs and flip angles constant and to reduce the SAR by lowering the number of RF pulses per unit of time in the sequence by increasing TRs and reducing the number of averages. It was not possible to meet the implant manufacturer's 0.1 W/kg SAR limit within reasonable scan times by this strategy. Therefore, the 0.1 W/kg SAR limit was only reached by additionally reducing the excitation flip angle and the phase resolution (to reduce encoding steps and thus reduce the number of RF pulses). Longer-than-normal scan times of up to 13 minutes were tolerated, given that patients were anesthetized. The SAR level associated with each sequence was determined by examining the scanner log files after running each sequence on a healthy volunteer and subsequently by monitoring the SAR levels recorded in the DICOM header for individual patient scans. Both sequences provided imaging through the ROI from the corpus callosum to the base of the pons.

Our initial tests showed that at SAR = 0.1 W/kg and 0.4 W/kg, the quality of the study was insufficient for stereotaxis. At an SAR of ~0.7 W/kg, we were able to achieve images adequate for intraoperative stereotaxis, and the images were reviewed by a neuromodulation neurosurgeon (A.Y.M.) and a neuroradiologist (Y.W.L.) for adequacy (Fig 2). Therefore, the following protocol was set up: MPRAGE obtained in the axial plane with the following parameters: TR = 1870 ms, TE = 4 ms, flip angle = 15°, number of signal averages = 1, FOV = 260 × 260 mm, matrix size = 256 × 256, section thickness = 1.5 mm, 176 sections; a T2-weighted sequence obtained in the axial plane with the following parameters: TR = 2500 ms, TE = 80–83 ms, flip angle = 150°, number of signal averages = 4, FOV = 260 × 260 mm, matrix size = 256 × 256, section thickness = 2.5 mm, low SAR RF pulse. Using these parameters, we recorded ~1.0 W/kg SAR or lower for our test images obtained on an Avanto 1.5T horizontal bore magnet (Siemens, Erlangen, Germany), with a circularly polarized transmit-receive head coil.

Of note, fast spin-echo inversion recovery sequences are routinely used to identify the globus pallidus internus, the primary surgical target used to treat dystonia, but are targeted less frequently than the subthalamic nucleus in Parkinson disease. Preliminary calculations revealed that it would not be possible to modify the sequence to create usable images with acceptable SARs. Surgical targeting for the GPi was thus performed on the T2 images.

Scanning and Patient Monitoring

Device impedance was checked by personnel from the Center for Neuromodulation before imaging preoperative patients. Patients

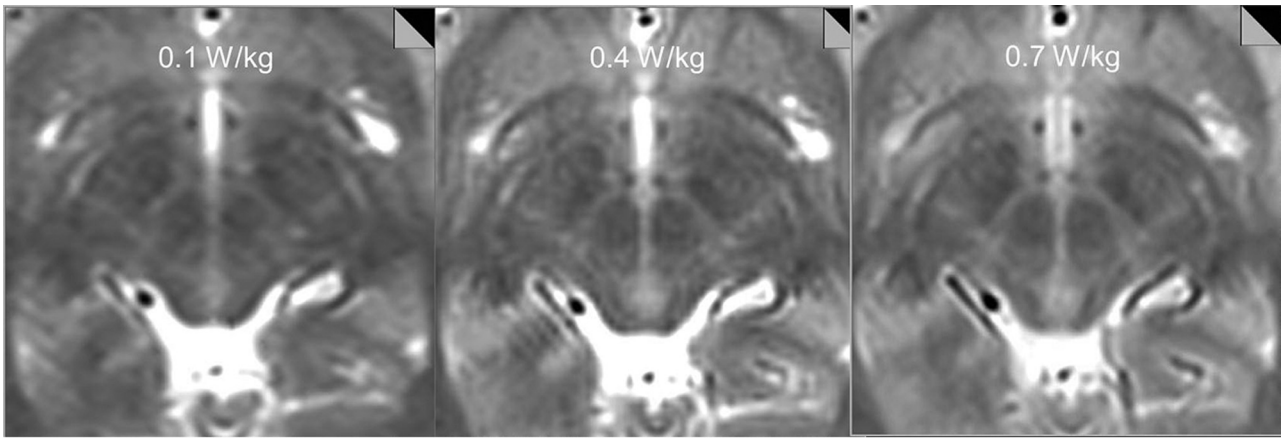

FIG 2. Tests on a volunteer subject show decreasing anatomic detail of the subthalamic region with decreasing SAR. T2-weighted images obtained with an SAR = 0.1 W/kg and 0.4 W/kg were deemed insufficient for stereotaxis by consensus view between the neuromodulation neurosurgeon and neuroradiologist, while images obtained with an SAR of 0.7 W/kg were adequate for intraoperative stereotaxis.

with abnormal impedance readings, broken leads, or electrodes not connected to the pacemaker were excluded because free wires are potentially more hazardous. DBS devices were deactivated before imaging by trained personnel. Imaging was performed by using either an Avanto or Aera 1.5T magnet (Siemens) with circularly polarized transmit-receive head coils, with the patient under general anesthesia to minimize motion in this patient cohort with primary movement disorders. Following imaging, devices were reprogrammed and inspected by trained neuromodulation staff. Patients were strictly monitored during and after MR imaging for complications.

Surgical Technique

MR imaging scans were all obtained 1–4 weeks before DBS surgery. The day of the operation, a stereotactic headframe (Leksell G frame; Elekta Instruments, Stockholm, Sweden) was affixed to the head with the patient under local anesthesia, and a high-resolution CT scan was performed (120 kV, 325 mAs, detector configuration of 128 at 0.6-mm collimation). The CT data were then fused via standard stereotactic neurosurgical software (Brainlab, Munich, Germany) to the MR imaging scans for surgical targeting.

Patients

We retrospectively reviewed the institutional data base of patients who underwent implantation of DBS electrodes between February 1, 2012, and August 1, 2015, by using the optimized low-SAR protocol. Patients who underwent clinical MR imaging performed at our institution with a DBS device in place during imaging were included. No specific exclusion criteria were applied. Chart review was performed to determine outcome, as measured by the rate of subsequent lead revision required relating directly to complications from MR imaging.

Image Analysis

All MR images were reviewed by a board-certified neuroradiologist (Y.W.L.) and a neurosurgeon specializing in neuromodulation (A.Y.M.). Images were aligned parallel to the anterior/posterior commissure plane. The subthalamic nucleus was assessed on the T2 images on an axial section 4 mm below the anterior/posterior commissure plane ($z = -4$). The globus pallidus was assessed on the axial T2 section containing the anterior/posterior commissures ($z = 0$). Overall image quality was graded as either acceptable or not acceptable for stereotactic surgical guidance on the basis of consensus review for the presurgical patients. The presence of device-related artifacts and any other artifacts was noted, and a comment was made about the impact on image quality. Data were extracted from the DICOM header for each patient scan regarding SAR deposition for each sequence. Comparison of SARs was made between magnets by using the Student *t* test with a significance level $\alpha = .05$.

RESULTS

Twenty-nine patients (23 male/6 female) were included. The mean age was 58 ± 14 years (range, 16–75 years). All subjects (22 with Parkinson disease, 6 with dystonia, 1 with essential tremor) had neuromodulation implants in situ (Activa PC Models No. 37601 and 37603; Medtronic). There were 25 subthalamic and 4 globus pallidus implants; 10 patients had bilateral electrodes. Of the 29 patients, 5 were scanned on the Aera system and 24, on the Avanto.

Average imaging time was 6 minutes 17 seconds for MPRAGE and 12 minutes 16 seconds for T2. The average SAR deposition for MPRAGE was 0.114 ± 0.021 for the Avanto system, 0.090 ± 0.001 for the Aera system, and 0.109 ± 0.021 overall. The average SAR deposition for the T2-weighted sequence was 1.037 ± 0.214 for the Avanto system, 0.828 ± 0.091 for the Aera system, and 0.987 ± 0.210 overall. SAR depositions for both MPRAGE and T2-weighted sequences were significantly lower on the Aera system ($P = .012$ and $P = .03$, respectively) (Fig 3). Four patients underwent MPRAGE imaging only, for reasons not specified on retrospective review.

All patients tolerated imaging well, with successful completion of MR imaging. No clinical adverse events were reported during or immediately after imaging. All images were deemed by consensus review to be adequate for surgical stereotaxis and were used for subsequent surgical guidance. At an average follow-up time of 553 days ~ 1.5 years (range, 2–1251 days; standard deviation, 374 days), there were no adverse patient outcomes and no cases re-

quiring lead replacement resulting directly from MR imaging complications.

Consensus review of imaging revealed mild device-related local susceptibility artifacts present in all studies that were judged not to affect overall image quality required for subsequent stereotaxis. Mild aliasing artifacts (seen only on T1-weighted images) were present in 6/29 (21%) cases, and apparent motion artifacts were seen in 4/29 (14%) cases, all seen on MPRAGE sequences (Fig 4). No such artifacts were present on T2-weighted images.

DISCUSSION

Our results demonstrate the effective use of an optimized imaging protocol balancing image quality and low SAR to scan patients with DBS implants for surgical planning. The T2-weighted images used applied an average SAR of 0.987 seconds, which, though still higher than the original manufacturer's recommendations, is lower than that published in the literature by using standard sequences and less than one-third the usual SAR when scanning in normal mode. The MPRAGE sequences used in this study were in the range of 0.1 W/kg SAR. Low SAR imaging is accomplished with longer imaging times, the use of a low SAR RF pulse, and adjustment of image resolution and was found to be well-tolerated by patients, without complications.

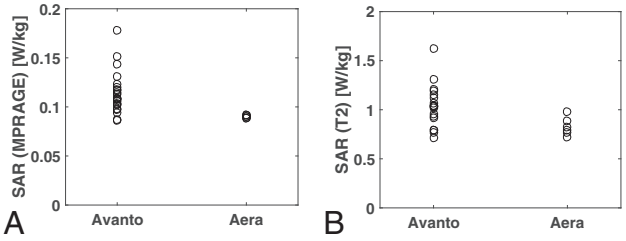

FIG 3. SAR deposition was significantly lower on the Aera system for both MPRAGE ($P = .01$) (*A*) and T2-weighted images ($P = .03$) (*B*). On the Aera system, all patients were imaged by using an SAR < 1 W/kg, and the SAR SD was small: ± 0.02 and ± 0.09 W/kg for MPRAGE and T2-weighted images, respectively.

Imaging patients with implantable devices is challenging because of potential safety concerns and artifacts arising from the device, such as local susceptibility effects and spatial distortion. While it is possible to image patients with Medtronic DBS devices,[5-7] there is limited published information describing appropriate SARs for preoperative planning. Rezai at al[8] summarized the major safety concerns of imaging patients with implanted devices, with one of the primary concerns being heating of electrodes due to energy deposition from the transmit RF field. Their in vitro tests showed changes in the temperature of an electrode tip of up to 25.3°C by using a transmit/receive body coil in contrast to a maximum change in temperature of 7.1°C by using a transmit-receive head coil. Irreversible lesions in brain tissue can occur at temperatures of 45°C and higher (ie, 8°C above normal body temperature). The degree of electrode heating depends on a number of factors, including routing of the leads, position and orientation of the device, type of coil used, whether leads are connected to the neurostimulator device, where the device is located relative to the isocenter of the MR imaging unit, and energy deposition during imaging or SAR. In the literature, there are 2 reported cases of complications from overheating of DBS electrodes.[1,2] In the first case, a body coil was used for excitation, and in the other, the patient had free, unconnected leads present. Additional transient adverse events such as dystonia have also been reported.[9]

Due to these potential adverse events, the device manufacturer (Medtronic) issued very conservative guidelines, most notably a head SAR limit of 0.1 W/kg (the usual limit is >30 times that at 3.2 W/kg). Despite a single report[4] of 6 subjects in whom quality MR images were obtained by using research sequences that were within the manufacturer's SAR limit, our tests concur with the more widespread experience that this power limitation is insufficient to produce therapeutic-quality T2-weighted images for surgical planning (Fig 2) with FDA-approved sequences. In December 2015, Medtronic issued updated guidelines in which they suggested switching to the use of B1 + root mean square to calculate RF power with a maximum of 2.0 μT, though they continue to recommend that if B1 + root mean square is not available, the maximum SAR remains 0.1 W/kg.

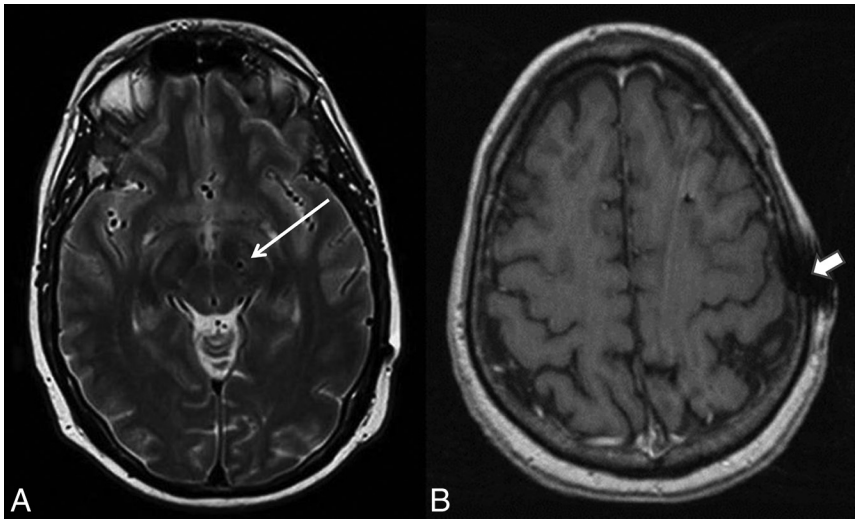

FIG 4. *A*, Susceptibility from the electrode was very minimal within the adjacent brain parenchyma on T2-weighted images (*arrow*). *B*, Device-related local susceptibility in the scalp at the site of electrode entry was seen in most cases on the MPRAGE sequence and was not thought to affect image quality. Additionally, a minority of cases showed artifacts likely attributable to stimulated echoes arising from peripheral fat on MPRAGE images only (*arrowhead*). Overall, all images were judged to be adequate for presurgical guidance.

Relatively low SAR imaging is accomplished with longer imaging times, use of a low SAR RF pulse, and adjustment of image resolution and is well-tolerated by patients, without complications. We found artifacts to be minimal and more prominent on MPRAGE. Susceptibility effects in the brain parenchyma from the lead itself were minor. Potential room for improvement in image quality may be obtained by shortening the TE (from 104 to below 90 TE) and reducing the

bandwidth (from 195 to 160 Hz/pixel). Limiting section coverage to only the electrode target region would allow more averaging and higher resolution for the same SAR level.

Our results indicate significantly lower SAR for both pulse sequences on the Aera scanner compared with the Avanto scanner with a lower SD of SAR values, which could be due to a variety of factors including coil selection. The 2 magnet systems have a number of differences, including bore diameter, software version, and coil. In our clinical practice, specifications for the Aera and Avanto magnet systems are as follows: D13, 70 cm diameter bore, circularly polarized send/receive Aera head coil with integrated preamplifier: 315 × 475 × 360 mm (length × width × height) and B17, 60 cm diameter bore, circularly polarized Avanto head coil with 2 integrated preamplifiers: 480 × 330 × 270 mm (length × width× height), respectively. SAR levels reported by different scanners can also vary for the same actual delivered energy, and this has motivated the manufacturer's recent shift to using B1 + root mean square as the safety metric for DBS implants. Different magnets and magnet systems can affect SAR and individualized phantom scanning, and testing should be performed before clinical implementation.

The primary indication for our subjects was presurgical targeting and electrode placement/location confirmation. One limitation of this protocol is that it may not be suitable for other indications such as assessing new or additional pathology. In fact, the protocol does not include whole-brain coverage, which would result in higher SAR. Furthermore, all of our scans were obtained with the patient under general anesthesia, thereby allowing slightly longer scan time without motion. Scan time would certainly be a limitation for awake subjects.

CONCLUSIONS

Here we introduce a practical, low-SAR MR imaging protocol that can effectively and safely obtain high-quality and high-resolution preoperative images for DBS surgical guidance in patients with a previously implanted electrode. In our multiyear experience with an average T2 head SAR of 0.987 W/kg, there are no recorded adverse events to date. Optimized coil design, such as the incorporation of a multi-element receive array in a geometry that still allows the use of the stereotactic frame, could improve image quality without increasing the SAR.

Disclosures: Graham C. Wiggins—*UNRELATED*: *Grants/Grants Pending*: National Institutes of Health/National Institute of Biomedical Imaging and Bioengineering grant No. P41 EB017183, *Comments*: The Center for Advanced Imaging Innovation and Research (CAI^{2}R, www.cai2r.net) at New York University School of Medicine is supported by National Institutes of Health/National Institute of Biomedical Imaging and Bioengineering grant No. P41 EB017183. Alon Y. Mogilner—*UNRELATED*: *Consultancy*: Medtronic Neurological; *Fees for Participation in Review Activities such as Data Monitoring Boards, Statistical Analysis, Endpoint Committees, and the Like*: Medtronic Neurological. Timothy Shepherd—*UNRELATED*: *Grants/Grants Pending*: National Institutes of Health National Institute of Aging (NIH 1K23 AG048622-01),* *Comments*: Alzheimer disease research. This work does not relate to the article in any way; *Patents (planned, pending or issued)*: Velona Technologies,* *Comments*: I have several recent provisional and full patents. 1) Three of these relate to medical devices for image-guided procedures. I am also in the process of cofounding a start-up company, Velona Technologies, with the goal of bringing these products to market. This work does not relate to the article in any way. 2) An additional patent is related to using multiparametric MRI for evaluating gamma knife radiosurgery treatment responses. This work does not relate to the article in any way; *Other*: Brainlab contract,* *Comments*: Through the above patent related to using multiparametric MRI for evaluating gamma knife radiosurgery treatment responses, I am the Principal Investigator on a 2-year industry-funded project ("contract") from Brainlab to study the clinical uses of multiple MRI parameters for predicting and evaluating tumor response to gamma knife therapies. This work does not relate to the article in any way. Yvonne W. Lui—*UNRELATED*: *Grants/Grants Pending*: National Institutes of Health R01.* *Money paid to the institution.

REFERENCES

1. Nutt JG, Anderson VC, Peacock JH, et al. **DBS and diathermy interaction induces severe CNS damage.** *Neurology* 2001;56:1384–86 CrossRef Medline
2. Henderson JM, Tkach J, Phillips M, et al. **Permanent neurological deficit related to magnetic resonance imaging in a patient with implanted deep brain stimulation electrodes for Parkinson's disease: case report.** *Neurosurgery* 2005;57:E1063; discussion E1063 CrossRef Medline
3. Larson PS, Richardson RM, Starr PA, et al. **Magnetic resonance imaging of implanted deep brain stimulators: experience in a large series.** *Stereotact Funct Neurosurg* 2008;86:92–100 Medline
4. Sarkar SN, Papavassiliou E, Hackney DB, et al. **Three-dimensional brain MRI for DBS patients within ultra-low radiofrequency power limits.** *Mov Disord* 2014;29:546–49 CrossRef Medline
5. Chhabra V, Sung E, Mewes K, et al. **Safety of magnetic resonance imaging of deep brain stimulator systems: a serial imaging and clinical retrospective study.** *J Neurosurg* 2010;112:497–502 CrossRef Medline
6. Fraix V, Chabardes S, Krainik A, et al. **Effects of magnetic resonance imaging in patients with implanted deep brain stimulation systems.** *J Neurosurg* 2010;113:1242–45 CrossRef Medline
7. Tagliati M, Jankovic J, Pagan F, et al; National Parkinson Foundation DBS Working Group. **Safety of MRI in patients with implanted deep brain stimulation devices.** *Neuroimage* 2009;47(suppl 2):T53–57 CrossRef Medline
8. Rezai AR, Baker KB, Tkach JA, et al. **Is magnetic resonance imaging safe for patients with neurostimulation systems used for deep brain stimulation?** *Neurosurgery* 2005;57:1056–62; discussion 1056–62 CrossRef Medline
9. Spiegel J, Fuss G, Backens M, et al. **Transient dystonia following magnetic resonance imaging in a patient with deep brain stimulation electrodes for the treatment of Parkinson disease: case report.** *J Neurosurg* 2003;99:772–74 CrossRef Medline